# Paleoenvironmental changes across the Late Cambrian–Early Ordovician in western Newfoundland

By

© Luyi Wang

A thesis submitted to the

School of graduate studies

In Partial fulfillment of the requirements of the degree of

Master of Science

Department of Earth Science

Memorial University of Newfoundland

March 2019

St. John's, Newfoundland

# ABSTRACT

The Martin Point section (western Newfoundland, Canada) spans the uppermost Cambrian Broom Point and Martin Point members of the Green Point Formation (upper Furongian). The investigated interval (~ 90 m) consists of rhythmites of thinly-bedded marine carbonates (lime mudstones) alternating with green and black shale and thin conglomerate beds. Samples were extracted from the micritic carbonates and their preservation was petrographically and geochemically examined. The $\delta^{13}C_{org}$ profile exhibits a positive shift (~ 2 ‰) associated with the globally well documented negative $\delta^{13}C_{carb}$ excursion at the HERB (Hellnmaria – Red Tops Boundary) and correlates with similar distinct shifts in the Al, Si, and ΣREE components, thus suggesting contributions from detrital organic matter relatively depleted in $^{12}C$ likely induced by an eustatic sea-level drop and enhanced terrigenous inputs. Similarly, the $\delta^{15}N_{org}$ variations are consistent with the proposed sea-level drop. This is also correlated with positive shifts on the Fe and Mn profiles reflecting overprinting of terrigenous inputs rather than reflecting the fluctuations in redox conditions.

## Acknowledgments

Firstly, I would like to thank my supervisor Dr. Karem Azmy for giving me the chance to come to Memorial University of Newfoundland, work on a project I felt very attractive and the help he gave me during the whole process. I also want to thank The Dr. Svend Stouge for his help in the field.

Secondly, I would like to thank my parents, for the encouragement and support that they gave me to study in a foreign country. I am thankful to everything they have done to help me.

Lastly, I also express my gratitude to the Petroleum Exploration Enhancement Program (PEEP) for their funding to Prof. Azmy.

# Table of contents

# LIST OF FIGURES

# LIST OF TABLES

# CO-AUTHORSHIP STATEMENT

The thesis is constructed in a manuscript format and consisted of 5 chapters. A paper regarding the research results was published on the Geological Journal (Wang, L., Azmy, K., 2019. Paleoenvironmental changes in slope carbonates across the Late Cambrian–Early Ordovician in western Newfoundland).

Chapter 1 reviews the Geologic settings, defines the proxies of paleoenvironment, and outlines the main objectives of the study. Chapters 2 through 5 represent a research paper, and include analytical methods, results, discussion and conclusions.

The mainframe of the thesis research was designed primarily by Prof. Karem Azmy. As the primary author, I was responsible for all aspects of the research project, reviewing the literature, formulating the research questions, performing the laboratory work, analyzing and interpreting the data, and preparing the manuscripts. Meanwhile, the co-author (Prof. Karem Azmy) guided the research progress, gave the main advices for analyzing and interpreting the data, and corrected the paper published on the Geological Journal.

# Chapter 1

# Introduction

The geochemistry of well-preserved carbonates has been a useful tool for better understanding the paleoenvironmental conditions that prevailed during the Earth's history (e.g., Wignall and Twitchett, 1996; Veizer et al., 1999; Halverson et al., 2005; Śilwiński et al., 2010). Therefore, primary/near-primary (affected by insignificant alteration) signatures are essential factors for paleoenvironmental reconstruction, especially with no or poor occurrences of fossils.

Global sea-level variations during the latest Cambrian not only influenced seawater redox conditions and primary productivity (e.g., Landing, 2012; Terfelt et al., 2012; Landing, 2013; Terfelt et al., 2014; Azmy et al., 2015), but also altered continental inputs and, subsequently, the composition of trace elements in marine deposits, which are reflected in changes in P, Si, Al, U, Ni, and REE (e.g., Wignall and Twitchett, 1996; Murphy et al., 2000; Arnaboldi and Meyers, 2007; Wignall et al., 2007; Piper and Calvert, 2009). An increase of oxygen level in seawater is associated with oxidation of organic matter and consequently variations in the C ratio in carbon content, in total organic content (TOC) contents as well as the C- and N- isotope compositions of the organic matter (e.g., Quan et al., 2008; Kump et al., 2011). Changes in redox conditions can also be reflected in marine carbonate by the uranium concentrations and Ce/Ce* anomalies of marine carbonates (e.g., Towe, 1991; Bau and Dulski, 1996; Ling et al., 2011; Nakada et al., 2013; Azmy et al., 2015). The investigated interval of Martin Point consists of slope rhythmite deposits composed of alternating thinly-bedded lime

mudstones and shales that were deposited under dysoxic (suboxic) conditions (e.g., James and Stevens, 1986; Landing et al., 2002; Landing, 2013; Azmy et al., 2015, 2018a).

### 1.1 Geological Setting

The Upper Cambrian to Lower Ordovician carbonates of the Martin Point Member constitute the lower part of the Green Point Formation, a part of the Cow Head Group, in western Newfoundland (within the northeast Canadian Appalachians) where they were deposited in a distal slope setting on the eastern Laurentian Margin (Fig. 1.1; James et al., 1989). The investigated sedimentary rocks consist mainly of mixed siliciclastic-carbonate slope deposits and alternate with deep-water non-carbonaceous to carbonaceous organic-rich green, grey and black shales, siltstones, parted and ribbon limestones and breccias derived from debris flows (James et al., 1989). The succession reflects the sedimentary response to eustatic sea-level fluctuations in the Cambrian, which were affected by transgressive-regressive events known as Cambrian grand cycles (Lavoie et al., 2012). The Laurentian plate was formed by active rifting around ca. 570 Ma that produced a wide Iapetus Ocean, rifting continued along the Iapetan margin from 540 – 535 Ma into the late early Cambrian (ca. 520 Ma) and locally into the Middle Cambrian (Cawood et al., 2001; Landing, 2012, 2013; Landing and Webster, 2018), resulting in the development of the Laurentian platform covered by clastic sediments (James et al., 1989). During the late Cambrian, a major sea-level rise resulted in thick transgressive carbonate deposits (Wilson et al., 1992; Landing, 2007) that were swept off the shelf to form the on-slope Cow Head Group. The depositional environment on the Laurentian platform experienced a high- to low-energy condition from the Late Cambrian to the Early Ordovician (Knight et al., 2007; Lavoie et al., 2013). The outcrops of the

Green Point Formation are extensive along western Newfoundland and well exposed at Martin Point but also occur at Western Brook Pond and St. Pauls Inlet (Fig. 1.1; Schuchert and Dunbar, 1934). Earlier studies (e.g., Azmy et al., 2014, 2015; Azmy, 2018 a, b) showed a high degree of petrographic and geochemical preservation of the carbonates, which was supported by a multi-technique approach that examined the patterns and relations among many proxies such as Sr, Mn, Ni, $\delta^{13}C$, $\delta^{18}O$ and Th/U.

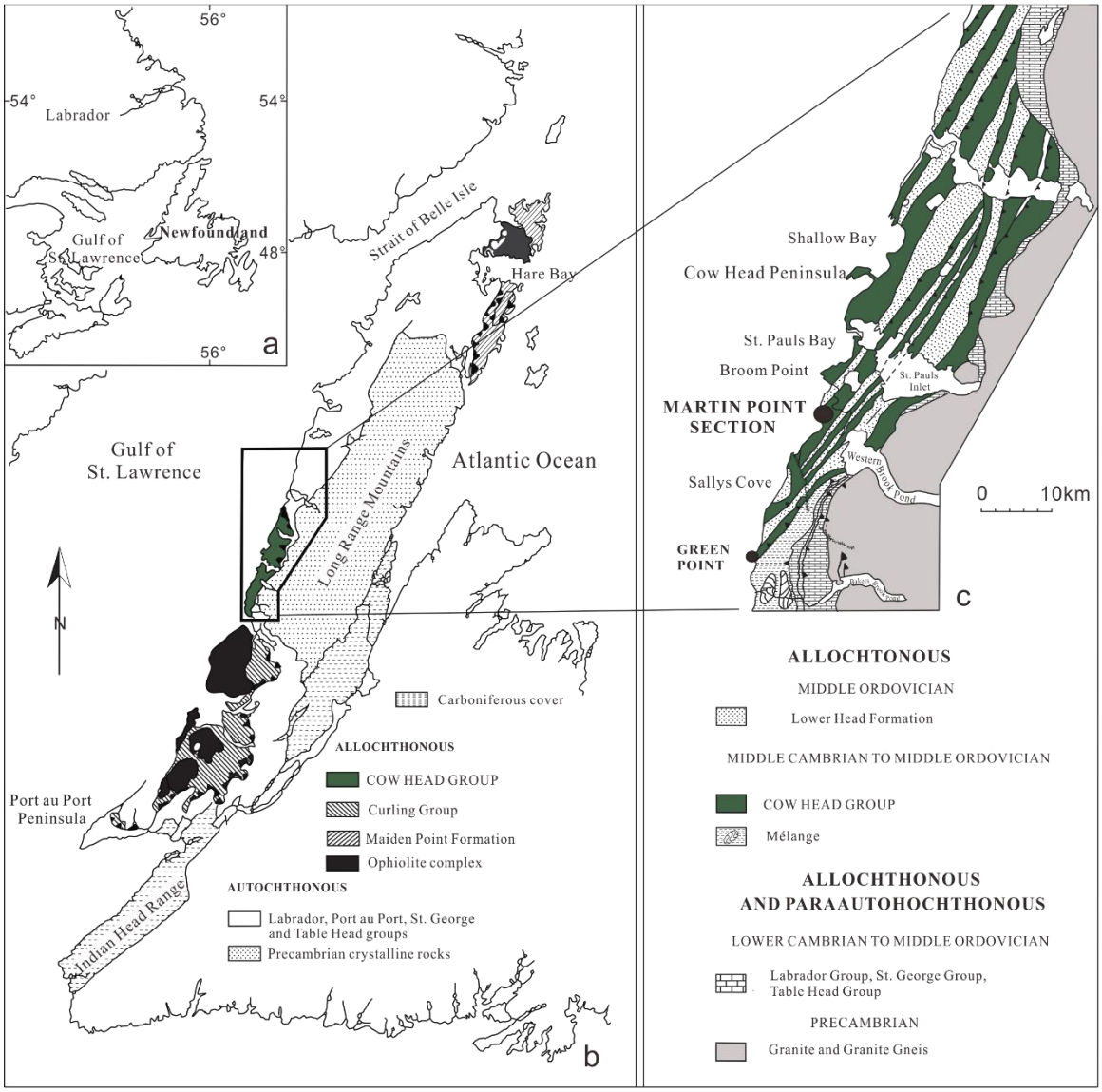


**Figure 1.1** Map of the research area showing the surface geology and the location of the Martin Point section (49° 40′ 51″ N; 57° 57′ 36″ W) in western Newfoundland, Canada. (modified from Cooper et al. 2001).

## 1.2 Stratigraphy

### 1.2.1 Lithostratigraphy

James and Stevens (1986) have discussed in detail the lithostratigraphy of the investigated Martin Point section (Fig. 1.2), which is a part of the Green Point Formation of the Cow Head Group. The Green Point Formation is dominated by varying proportions of non-calcareous to calcareous green/black shales with ribbon limestone and scarce conglomerate beds. The entire succession of Green Point Formation was overturned and slightly faulted by later tectonic activity (James and Stevens, 1986), which induced the formation of wrinkled limestone fabrics.

The Green Point Formation includes the Upper Cambrian Martin Point Member and the overlying lowermost Ordovician Broom Point Member. The Martin Point Member consists of 80 – 100 m of rhythmites of thinly-bedded green and black shale, interspersed with thin siltstone and calcareous sandstone bed, alternating ribbon limestone (micritic to near-micritic) and thin conglomerate interbeds may also occasionally occur. The limestone beds are isolated and up to 20 cm thick. The conglomerate beds consist of shallow-water carbonate clasts that were transported into deeper-water environments along the slope of the Laurentian margin (James and Stevens, 1986). The Ordovician Broom Point Member is ~ 80 m thick and dominated by ribbon to parted limestone with few siltstone, sandstone, conglomerate and red shale intervals. The limestones of the Broom Point Member are thicker and better developed than those in the Martin Point Member and composed of mostly lime mudstone with fine-grained peloidal

calcarenite. Some of the limestone has been replaced by brown weathering nodular to bedded chert (James and Stevens, 1986).

### 1.2.2 Biostratigraphy

The faunal occurrences in the Martin Point section are limited compared to their counterparts of the same age in other sections. The investigated section has conodont Zones (Fig. 1.2) that include, in ascending order, the *Proconodontus muelleri*, *Eoconodontus notchpeakensis*, *Cordylodus proavs* and *Cordylodus caboti Zones* (Ludvigsen, 1982; James and Stevens, 1986; Barnes, 1988; Miller et al., 2014; Azmy, 2018a).

The deposits of the Martin Point section contain only two species of graptolites (*Rhabdinopora flabelliforme* and *Staurograptus dichotomus*) that are found just above the base of the Broom Point Formation (Barnes, 1988). The occurrences of *R.* cf. *praeparabola*, *R.* cf. *parabola*, and *Aletograptus* were documented by Erdtmann (1971) on the top of the Broom Point Member. Trilobites are rare at Martin Point, only *Hungia magnifica* found in the basal beds (Barnes, 1988).

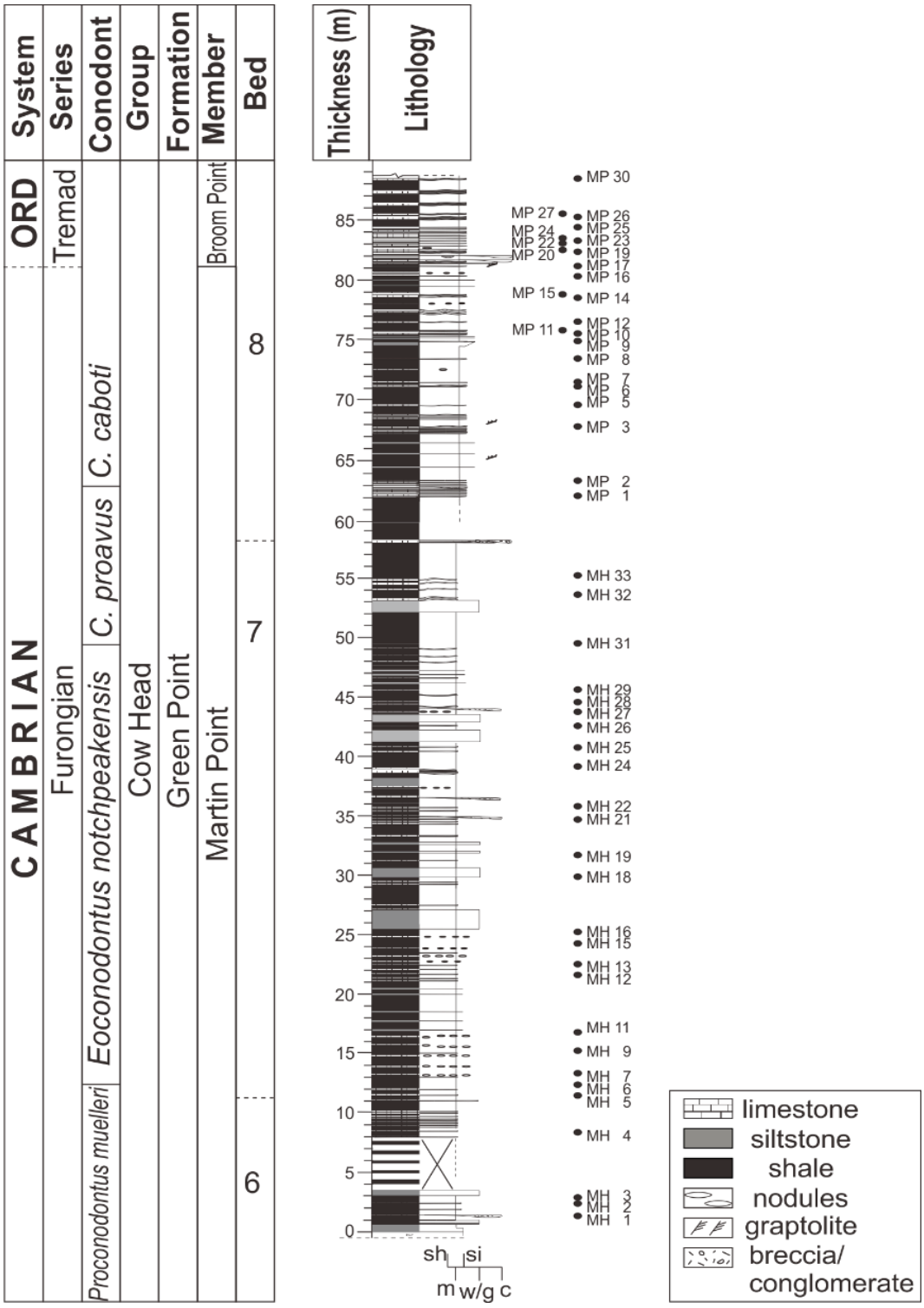


**Figure 1.2** Stratigraphic framework of the investigated Martin Point section in western Newfoundland, Canada, illustrating bed number and detailed measured positions of investigated samples and conodont zonation scheme (Barnes, 1988). Abbreviations: ORD = Ordovician; MH and MP = sample ids; *C. proavus* = *Cordylodus proavus*; *C. caboti* = *Cordylodus caboti*; Tremad = Tremadocian.

## 1.3 Paleoenvironmental Geochemical Proxies

### 1.3.1 Organic C- and N- Isotopes and Total Organic Content (TOC)

Stable isotopes have been found to be reliable proxies of paleoenvironmental changes. In the current study, stable isotopes are applied to understand the changes in primary productivity, which is influenced by the oxygen budget of ocean, light intensity, nutrients, and terrestrial inputs (Bernasconi, 1997; Quan et al., 2008; Herrmann et al., 2012, Quan et al., 2013; Azmy et al., 2015).

Carbon is the primary element in the biosphere and exists in the lithosphere (sedimentary rocks, atmosphere and hydrosphere). Biochemical reactions, such as in plants and bacteria, prefer $^{12}C$ and therefore organic matter becomes variably depleted in $\delta^{13}C$ depending on the degree of primary productivity and photosynthesis (Schidlowski et al., 1984). Accordingly, the range of $\delta^{13}C_{org}$ could identify the type of plant (marine vs. terrestrial) and origin of organic matter (Chi et al., 2013, Bianchi et al., 2018). Therefore, the $\delta^{13}C_{org}$ profile could reflect the abundance in photosphere and the primary productivity changes (Kump et al., 2011; Jiang et al., 2012). The TOC contents can also be used as a proxy of marine organic productivity and degree of terrestrial input as well as eustatic sea-level changes (associated with changes in redox conditions) particularly when combined with corresponding signatures of other geochemical proxies, such as trace elements contents as well as values of C- and N- isotope (Azmy et al., 2015).

Nitrogen is an important nutrient in ecological systems and therefore the $\delta^{14}N$ values are widely used as a proxy of paleoenvironmental redox conditions. The nitrogen isotope cycle is mainly controlled by three processes: nitrogen fixation, nitrification, and

denitrification, which are sensitive to, or dependent on, redox conditions (Falkowski, 1997; Fennel et al., 2005; Quan et al., 2013). The fixation of nitrogen is a conversion of atmospheric $N_2$ into ammonia $NH^{4+}$ by many kinds of bacteria and characterized by an insignificant fractionation of N-isotopes (Quan, 2008). Nitrification is a process that produces nitrate ($NO^{3-}$), which is derived from $NH^{4+}$ released from reduced organic N in oxic conditions (Ward et al., 1982, Yool et al., 2007), which is associated with considerable fractionation of N-isotopes (Casciotti, 2009, 2016). Denitrification is the reduction of nitrate ($NO^{3-}$) to $N_2$ under anoxic conditions and is associated with a significant fractionation that leaves residual sediments enriched in $^{15}N$ (Quan, 2013).

### 1.3.2 Trace Elements

#### 1.3.2.1 Iron and Manganese Geochemistry

Iron (Fe) is the most abundant redox-sensitive element in the geologic past as it interacts with carbon, sulfur, phosphorus, and other trace elements in marine sediments (Raiswell and Canfield, 2012). Under reducing condition, reactive Fe oxides are reduced and buried as Fe(II) sulfides, Fe(II) carbonate and Fe(II) phosphates in different diagenetic environments (Aller et al., 2004; Egger et al., 2015). Under oxic condition, through biogenic or abiogenic oxidation, Fe(II) is oxidized to Fe(III) and forms Fe(III) oxides which play an important part in organic carbon sorption and preservation against microbial degradation in sediment (Ma et al., 2018), especially at pH ~ 8 (seawater pH = 7.5 – 8.4; Pham et al., 2006; Chester and Jickells, 2012). Thus, the concentration of dissolved Fe(II) is low in oxic marine environments. On the other hand, terrigenous

materials in riverine inputs are also a source of Fe(II) and may cause Fe concentrations to increase intensively in marine sediments (Govin et al., 2012).

Manganese (Mn) is also a proxy of redox condition. It is a micronutrient for all organisms and exerts an important influence on photosynthesis (Gavalas and Clark, 1971). Under oxic conditions, Mn mostly exists as soluble Mn(II), which is converted to insoluble Mn oxides or lost by sinking (Sunda et al., 1983; Calvert and Pedersen, 1993) while Mn(II) is oxidized and forms Mn(III, IV) minerals through biotic or abiotic process (Tebo et al., 2004). Under reducing condition, Mn oxides are reduced and the released Mn(II) form Mn-rich sediments, which results in a high concentration of Mn in carbonate (Aguilar and Nealson, 1994).

#### 1.3.2.2 Silicon and Aluminum Geochemistry

Aluminum (Al) and silicon (Si) are proxies of the terrigenous material transported to seawater through riverine fluvial processes (Zhao et al., 2014; Ganai et al., 2018) and are sensitive to climate changes, such as aridity, variation in sea level and continental precipitation (Milliman et al., 1975; Milliman and Syvitski, 1992; Govin et al., 2012). Also, Al is broadly used to calibrate Fe, Mn and Ti concentrations for excluding terrigenous influence (Yarincik et al., 2000; Pattan et al., 2013; Clarkson, 2014) and identify their sources. Generally speaking, the Mn/Al and Fe/Al ratios in the upper continental crust are 0.0075 and 0.44, respectively (Mclennan, 2001). If Mn/Al and Fe/Al ratios are greater than the upper continental crustal values, they indicate the occurrence of unsupported Mn and Fe in the form of Fe-Mn oxy-hydroxides, which reflect dominant oxic conditions (Pattan et al., 2013). On the other hand, if the ratios of Mn/Al and Fe/Al

are under those values, they reflect suboxic-anoxic conditions. Si concentration is widely used to reflect terrigenous influences, and the correlations between $SiO_2$, $Al_2O_3$, $K_2O$ and CaO could indicate sediment origin (Ganai et al., 2017).

#### 1.3.2.3 Strontium Geochemistry

Strontium (Sr) has been used as a proxy to indicate carbonate diagenetic environments and the hydrological cycle changes (Holland et al., 1964, Kinsman, 1969; Banner, 1995). The Sr values exhibit a wide range in diagenetic carbonates, ranging from 20 ppm to 10000 ppm (Gregg and Shelton, 1989; Kimbell and Humphrey, 1994), which are mainly influenced by fluid-rock interaction, subaerial weathering flux from land masses, and submarine hydrothermal flux from oceanic crust (Derry et al., 1992). And sr is well known to be depleted during diagenesis of carbonates, therefore, it could be used to evaluate the degree of carbonate preservation (e.g., Azmy et al., 2001, 2012; Azmy and Lavoie, 2009; Veizer, 1983).

#### 1.3.2.4 Phosphorus Geochemistry

Phosphorus (P) is a significant nutrient for marine ecosystems and has been used as a proxy to reflect biological productivity on geological time scales (e.g. Broecker and Peng, 1982). It is mainly used to reconstruct long-term feedback mechanisms between climate, environment, and ecology (Föllmi, 1996). As to biogeochemical reactions during diagenetic processes, phosphorus occurs in two forms, reactive and non-reactive. The precipitation of reactive P is always mediated by precipitating organic matter (OM) and iron oxides, which have the ability to absorb phosphate ($PO_4^{3-}$). Thus, most phosphate is transferred to the deep ocean in the form of aggregated organic matter or inorganic

phosphate through oxidation, and then reintroduced to the photic zone by upwelling (Defforey and Paytan, 2018; Gao et al., 2018). The non-reactive P is mainly derived from detrital input and only represents a small portion of the total P pool (e.g. Ruttenberg and Berner, 1993; Filippelli and Delanrey, 1996).

#### 1.3.2.5 Nickel Geochemistry

Nickel (Ni), a biologically active element, is widely used to reflect bioproductivity and indicates variations in terrigenous influx (Boyle and Edmond., 1976; Śliwiński et al., 2010; Azmy, 2018a). Earlier studies (Bruland, 1980; Ragsdale, 2009) suggest that Ni is significantly correlated with other major nutrients like phosphate and silica. The Ni content is mainly dominated by two processes: the sorption by Fe-Mn oxides under oxic conditions and the precipitation in sediments coupled with the existence of sulfide under anoxic conditions (e.g. Peacock and Sherman, 2007; Gall et al., 2013; Vance et al., 2016; Ciscato et al., 2018)

## 1.4 Rare Earth Elements (REE)

Rare earth elements (REE) have been used to determine marine environments because the distribution of these elements is sensitive to water depth, salinity and oxygen level (Piepgras and Jacobsen, 1992; Frimmel, 2009; Hua, 2012). Continental crust is the main source of REEs, whereas the riverine input and atmospheric flux are the dominant carriers into ocean (Ryu et al., 2007, Hagedorn et al., 2011). Therefore, REE distributions in marine water is primarily controlled by terrigenous source and transportation mechanisms (Alibo and Nozaki, 2004). Through fluvial transportation, REEs are influenced by the quantity of colloidal particulates (Hannigan et al., 2010). The dissolved

organic carbon (DOC) and pH value also exist partly influence on REE concentration in sediments during deposition process (Gaillardet et al., 2003). Winds can also carry the terrestrial dust containing REEs into marine water (Nozaki, 2001). However, aeolian input mainly influence REE concentrations on the surface of water, the impact of which decreases significantly within water depth (Zhang and Nozaki, 1998; Alibo and Nozaki, 2004). Several other conditions are also suggested to impact the concentration of REE, including erosion of volcanic islands (Sholkovitz and Szymczak, 2000), remineralization of the bottom sediments (Alibo and Nozaki, 2004), hydrothermal fluids (Schmidt et al., 2010) and submarine groundwater discharge (Johannesson et al., 2011).

### 1.5 Cerium (Ce) Anomalies

Cerium (Ce) anomalies have been found to reflect redox conditions due to the variable valence and solubility of Ce under different oxygen levels. Under oxic conditions, Ce(III) is oxidized to Ce(IV) which is less soluble in marine water and becomes absorbed on particle surfaces, leading to negative Ce anomalies in marine carbonates (German and Elderfield, 1990; Bau and Dulski, 1996). However, the Ce anomalies in seawater and marine sediments are complicated and impacted by anomalous abundances of lanthanum (La; Bau and Dulski, 1996). Therefore, the Ce anomaly (Ce/Ce* ratio) is calculated as $[(Ce/Ce^*)_{SN} = Ce_{SN}/(0.5La_{SN} + 0.5Pr_{SN})]$ and is used to eliminate the influence from La enrichment (SN = shale normalized). In anoxic and suboxic environments, Ce(IV) is reduced to Ce(III) which is released and becomes soluble in marine water, resulting in a positive excursion in Ce anomalies (German and Elderfield, 1990). Therefore, when the $Ce/Ce^* > 1$ is a positive anomaly and suggests an oxidized environment, whereas a $Ce/Ce^* < 1$ indicates a reducing condition (Elderfield et

al., 1981; Pattan et al., 2005). Beyond that, Ce/Ce* = 1 may symbolize terrigenous dominated sediment (Nath et al., 1992).

### 1.6 Th/U Ratio

Uranium concentration in marine sediments has been widely used to reflect paleo-redox depositional environments (Algeo and Maynard, 2004; Tribovillard et al., 2006; Algeo and Rowe, 2012; Azmy et al., 2015). Under oxic conditions, uranium ions are in a high-valence state U(VI) and exist as uranyl carbonate complexes $UO_2(CO_3)_3^{4-}$ which are soluble in water. On the contrary, in anoxic or suboxic conditions, reduced U(IV) ions form insoluble uranous fluoride which is absorbed in marine carbonates (Wignall and Twitchett, 1996). Unlike U, Thorium (Th) is not affected by redox conditions and stays in the insoluble Th(IV) state (Anderson et al., 1989). Thus, the Th/U is a reliable paleo-redox proxy, with a Th/U ratio below 2 occurring in reducing marine sediments, between 2 and 7 in oxic marine sediments, and in excess of 7 under intensely oxidizing terrestrial environments (Wignall and Twitchett, 1966).

Although diagenesis may significantly alter the geochemical composition of carbonate through burial history, the micritic to near-micritic carbonate may still retain at least their near-primary contents of Th and U because they are heavy elements and not easily enriched or depleted during diagenesis, (such as Sr, Fe, or Mn), particularly at low water/rock interaction ratios. Accordingly, if the variations of the Th/U in the altered rocks cannot be interpreted for their absolute values, their relative variations across the profile may still reflect changes in redox conditions.

## 1.7 Objectives

(1) to investigate the C- and N- isotope compositions of the organic matter in the lime mudstones interbeds to better understand the control of sea-level change on their signatures, and therefore the potential as paleoredox proxies during the late Cambrian, particularly the HERB Event which is a distinct negative excursion of $\delta^{13}C_{carb}$ during the Late Cambrian. And to reconstruct the global paleoenvironmental changes (climatic and oceanographic) that dominated during that time interval (Ripperdan et al., 1993; Buggisch et al., 2003; Miller et al., 2014; Li et al., 2017) and

(2) to investigate the influence of sea-level changes on the trace element geochemistry of the seawater and consequently changes in terrestrial inputs and primary productivity.

# Chapter 2

# Methodology

A multi-technique approach has been applied to investigate and reconstruct the paleoenvironmental variations across late-Cambrian to early-Ordovician Martin Point carbonates. Fifty-one samples were collected from outcrop at high resolution (sampling intervals as small as 10 cm; Fig. 1.2) mainly from the upper Martin Point Member at Martin Point (49° 40′ 51″ N; 57° 57′ 36″ W) in western Newfoundland (Fig. 1.1). Samples were thin sectioned for petrographic examinations and mirror-image slabs from each thin section were polished for micro-sampling. The slabs were cleaned by deionized water and dried overnight in the oven at 50℃ in order to isolate the finest grained lime mudstone (micrites) from secondary cements and other contaminants. Since Alizarin Red-S could stain aragonite, calcite, witherite, and cerussite, but not stain dolomite, and patassium ferricyanide could precipitate if Turnbull's blue encounters with ferrous iron (Dickson, 1966), thin sections were stained with a mixture of both solutions to differentiate between dolomicrite and lime mudstones. Petrographic analyses (optical microscope and cathodoluminoscope) were used for preliminary evaluation of petrography, which was needed before micro-sampling for geochemical analyses (C- and N- isotope, trace elements and rare earth elements).

## 2.1 Optical Microscopy and Cathodoluminoscopy

Thin sections were observed under a Nikon Eclipse E600POL microscope to select the most micritic (<10 μm) and laminated lime mudstone interbeds in order to avoid the influence from allochthonous clasts, dolomites and recrystallized carbonate.

Guided by the $\delta^{13}C_{carb}$ profile of Azmy (2018a), the most micritic samples were selected at higher resolution (Appendix 1), particularly from the interval that spans the peak of the negative excursion of the HERB event (Figure 2 in Azmy, 2018a), for organic $\delta^{13}C$ and $\delta^{15}N$ and inorganic elemental measurements (Fig. 1.2). Polished thin sections were examined under CL by using a Technosyn 8200 MKII cold cathode instrument operated at 8 kV accelerating voltage and 0.7 mA current.

Cathodoluminescence (CL) is the visible light emitted by solid minerals due to irradiation with cathode rays caused by high-energy electron bombardment. When a crystal is bombarded by electrons loaded with enough energy, the electrons gain energy and move from ground state shells to higher energy counterparts. Because the reached high energy condition is not stable, electrons will be temporarily captured by electron traps. When they attempt to return to ground state, they emit the gained energy (quanta) in the form of photons. The wavelengths of photons emitted by most minerals are within the visible-light range, but emissions can also occur in the ultraviolet and infrared spectra (Boggs and Krinsley, 2006). These electron traps are divided into intrinsic and extrinsic. Intrinsic traps are characteristic of the crystal lattice and extrinsic traps result from impurities, such as the transition elements (rare earth elements-REE), which are the most common source of CL in minerals (Azomani et al., 2013) .Some ions of trace elements like $Mn^{2+}$, $Pb^{2+}$, $Cu^{2+}$, $Zn^{2+}$ and REE are activators which could promote CL in a mineral. On the contrary, other elements such as $Fe^{2+}$, $Ni^{2+}$ and $Co^{2+}$ are common quenchers that inhibit CL (Machel, 1985). However, in carbonates, the intensity of CL could be altered by the ratio of $Mn^{2+}/Fe^{2+}$ (Boggs and Krinsley, 2006). Thus, CL in a mineral is dependent on compositions of minerals, crystal structure and extrinsic elements (Parish and Russell,

2007). It can provide valuable information about the cement phases in order to reconstruct diagenetic history (e.g., Sippel, 1968; Sprunt and Nur, 1979; Burley et al., 1989; Rush and Chafetz, 1990; Machel and Burton, 1991; Machel, 2000), and can allow for a better understanding of the redox conditions of precipitation through Mn and Fe contents of calcite (Frank et al., 1982; Barnaby and Rimstidt, 1989).

The most micritic samples were selected at investigated interval (Appendix 1), particularly from the interval that spans the peak of the negative excursion of the HERB event (See Azmy, 2018a, Fig. 2), for trace element and organic $\delta^{13}C$ and $\delta^{15}N$ measurements (Fig. 1.2).

### 2.2 Trace Elements and Rare Earth Elements

For elemental analysis, 25 samples (10 mg each) were extracted by a slow-speed microdrill under a binocular microscope and were processed in 5 % (v/v) acetic acid for 70 - 80 minutes and measured by an Elan DRC II ICP-MS (Perkin Elmer SCIEX) at Memorial University of Newfoundland to measure major and trace elements including rare earth elements (REEs). The uncertainty is better than 5 % and the results are calibrated to 100 % carbonate basis (e.g. Veizer et al., 1999). The Ce anomaly (Ce/Ce*) was calculated based on the equation $[(Ce/Ce^*)_{SN} = Ce_{SN}/(0.5La_{SN} + 0.5Pr_{SN})]$ (Bau and Dulski, 1996). The REE concentrations were normalized to Post Archean Australian Shale (PAAS; Mclennan, 1989).

### 2.3 Stable C- and N- Isotopes

For TOC and organic C- and N- isotope analysis, ~ 7 to 15 grams of powder were digested in 20 % (v/v) HCl repeatedly to remove carbonates. The remaining residue was separated by centrifugation and decantation and washed with deionized water at least 3 times. Samples were subsequently dried overnight at ~ 40 °C. The $\delta^{13}C_{org}$ values were measured through a Carlo Erba Elemental Analyzer (EA) coupled with a Thermofinnigan DELTA V plus isotope ratio mass spectrometer. The TOC values were calculated from the peak area of the individual analyses based on mass. The results ($\sigma < 0.25$) were calibrated by the standards L-glutamic acid ($\delta^{13}C_{VPDB} = -26.74 \pm 0.06$ ‰ VPDB), SPEX $CaCO_3$ ($\delta^{13}C_{VPDB} = -21.02 \pm 0.10$ ‰ VPDB), Suprapur $CaCO_3$ ($\delta^{13}C_{VPDB} = -40.11 \pm 0.15$ ‰ VPDB) and B2153 low org soil ($\delta^{13}C_{VPDB} = -26.71 \pm 0.24$ ‰ VPDB). For $\delta^{15}N_{org}$, values were measured by a VARIO ISOTOPE CUBE (ELEMENTAR) connected to a Thermofinnigan DELTA V plus isotope ratio mass spectrometer at the isotope laboratory of Memorial University of Newfoundland. The results ($\sigma < 0.15$) were normalized to the standards IAEA-N-1 ($\delta^{15}N_{air} = 0.43 \pm 0.07$ ‰ air), IAEA-N2 ($\delta^{15}N_{air} = 20.32 \pm 0.09$ ‰ air) and B2151 high-organic sediment ($\delta^{15}N_{air} = 4.35 \pm 0.20$ ‰ air).

# Chapter 3

# Results

The investigated Martin Point section spans two main intervals: the HERB event of the late Cambrian (e.g., Miller et al., 2014) and the Cambrian–Ordovician boundary (e.g., Azmy et al., 2014; 2015). Table 3.1 summarizes the statistics of the geochemical results of the investigated Martin Point lime mudstones and the detailed values are listed in Appendix 1. The mean values of the investigated geochemical proxies of both intervals (Table 3.1) are almost comparable although the profiles of most of the proxies show relatively faster and sharper fluctuations during the Cambrian–Ordovician boundary (Azmy et al., 2015) compared to those across the HERB event. The geochemical variations across the Cambrian–Ordovician boundary have been discussed in detail by Azmy et al., (2014, 2015) and therefore the focus of the current study will be on the geochemistry of the carbonates of the interval spanning the HERB event.

## 3.1 Petrography

Petrographic examinations of all samples show that the selected samples are dominated by fabric retentive micritic (< 4 μm) to near-micritic (~ 10 μm) lime mudstones that are occasionally cut by fractures filled with burial cements. They appear dull to non-luminescent under CL (Fig. 3.1 a – b).

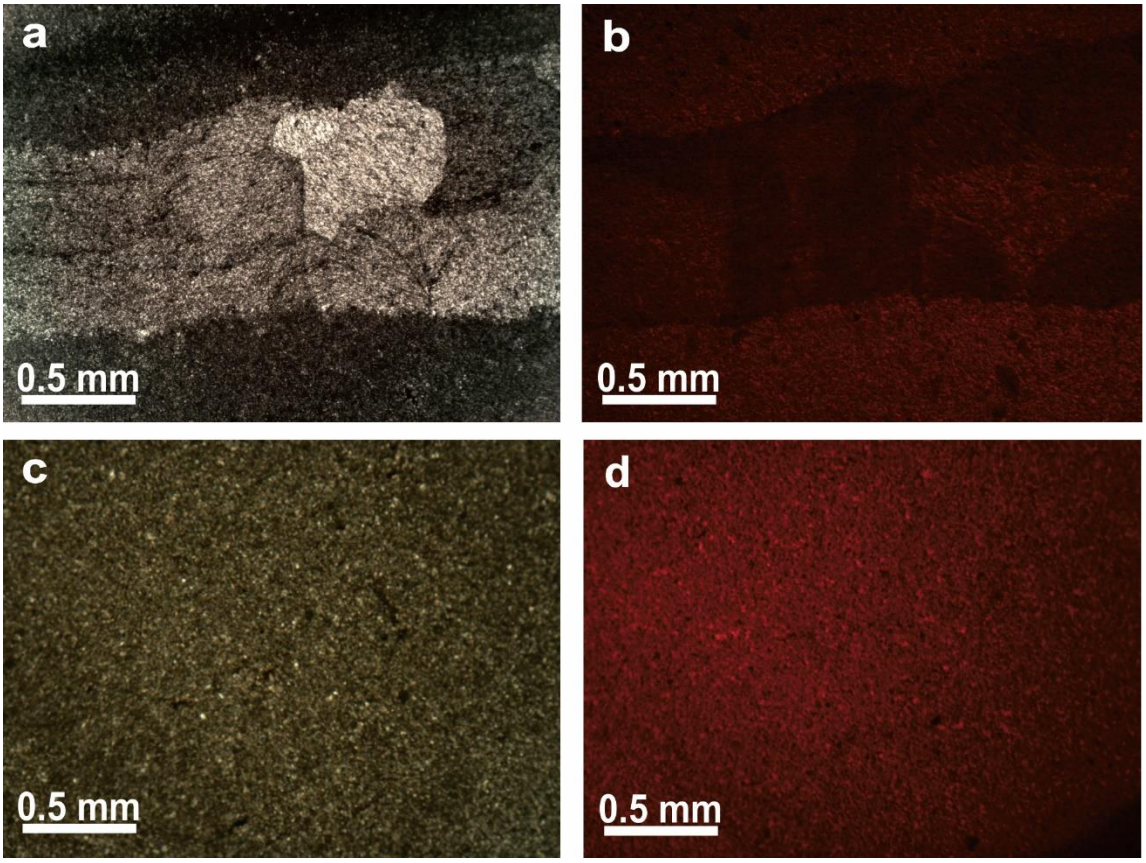


**Figure 3.1** Photomicrographs of the investigated carbonates showing (a) micritic lime mudstones (Sample MP 28) cut by fracture filled with a late burial cement (under plane polarized) and (b) CL image of (a) showing dull to non-CL micritic lime mudstone and cement. (c) micritic lime mudstones (Sample MH 8; under plane polarized) (d) CL image of (c) showing dull luminescence.

### 3.2 Trace Elements and REE

Table 3.1 summarizes the statistics of paleoenvironmental proxies of the investigated samples from Cambrian–Ordovician (Є – O) boundary and HERB intervals such as AL, Si, P, Fe, Mn, Ce/Ce* and REE and the detailed values are listed in Appendix 1. The concentrations of elements have generally comparable mean values throughout the entire section.

**Table 3.1**. Summary of statistics of isotopic and elemental geochemistry for the investigated lime mudstones of the Martin Point section. Ni and Th/U data are produced from Azmy (2018a).

| | $\delta^{13}C_{org}$ (‰ VPDB) | wt. % TOC | $\delta^{15}N_{org}$ (‰ Air) | P (ppm) | Ni (ppm) | Sr (ppm) | Ce/Ce* | Th/U | ΣREE (ppm) | Si (ppm) | Al (ppm) | Mn (ppm) | Fe (ppm) | Mn/Al | Fe/Al |
|---|---|---|---|---|---|---|---|---|---|---|---|---|---|---|---|
| **Entire investigated interval** | | | | | | | | | | | | | | | |
| n | 47 | 47 | 27 | 25 | 25 | 25 | 25 | 24 | 25 | 25 | 25 | 25 | 25 | 25 | 25 |
| **Mean** | **-29.0** | **0.1** | **3.0** | **141.8** | **3.5** | **324.5** | **0.9** | **1.1** | **46.7** | **2563.2** | **1528.8** | **359.8** | **2360.7** | **0.3** | **1.6** |
| Stdev | 0.8 | 0.1 | 1.0 | 40.5 | 1.8 | 192.3 | 0.1 | 1.3 | 23.0 | 1085.7 | 904.4 | 159.5 | 1772.2 | 0.2 | 0.8 |
| Max | -27.1 | 0.7 | 5.0 | 251.9 | 8.5 | 979.8 | 1.0 | 5.1 | 95.1 | 5111.7 | 3546.7 | 648.6 | 6900.3 | 0.9 | 4.5 |
| Min | -30.5 | 0.0 | 0.8 | 85.3 | 1.4 | 151.5 | 0.7 | 0.1 | 18.0 | 1245.7 | 611.0 | 141.6 | 784.9 | 0.1 | 0.4 |
| **Cambrian–Ordovician boundary** | | | | | | | | | | | | | | | |
| n | 11 | 11 | 6 | 8 | 8 | 8 | 8 | 7 | 8 | 8 | 8 | 8 | 8 | 8 | 8 |
| **Mean** | **-28.6** | **0.2** | **2.9** | **141.2** | **2.4** | **257.7** | **0.9** | **0.5** | **42.5** | **2872.0** | **1725.3** | **316.3** | **1974.5** | **0.2** | **1.2** |
| Stdev | 0.7 | 0.1 | 1.1 | 32.0 | 0.6 | 49.0 | 0.1 | 0.2 | 25.8 | 1331.8 | 1144.9 | 195.0 | 1573.0 | 0.2 | 0.4 |
| Max | -27.1 | 0.5 | 4.1 | 180.4 | 3.4 | 301.3 | 0.9 | 0.7 | 79.3 | 5111.7 | 3546.7 | 648.6 | 5594.1 | 0.6 | 1.6 |
| Min | -29.6 | 0.0 | 1.0 | 93.2 | 1.4 | 151.5 | 0.8 | 0.3 | 18.0 | 1393.7 | 633.9 | 141.6 | 905.9 | 0.1 | 0.4 |
| **HERB interval** | | | | | | | | | | | | | | | |
| n | 36 | 36 | 21 | 17 | 17 | 17 | 17 | 17 | 17 | 17 | 17 | 17 | 17 | 17 | 17 |
| **Mean** | **-29.1** | **0.1** | **3.0** | **142.0** | **4.1** | **355.9** | **0.8** | **1.4** | **48.6** | **2417.9** | **1436.3** | **380.2** | **2542.5** | **0.3** | **1.7** |
| Stdev | 0.7 | 0.1 | 1.0 | 44.8 | 1.9 | 226.1 | 0.1 | 1.5 | 22.2 | 960.3 | 790.5 | 141.9 | 1875.8 | 0.2 | 0.8 |
| Max | -27.8 | 0.7 | 5.0 | 251.9 | 8.5 | 979.8 | 1.0 | 5.1 | 95.1 | 4478.2 | 3202.3 | 571.5 | 6900.3 | 0.9 | 4.5 |
| Min | -30.5 | 0.0 | 0.8 | 85.3 | 1.9 | 165.0 | 0.7 | 0.1 | 24.6 | 1245.7 | 611.0 | 150.0 | 784.9 | 0.1 | 1.1 |

The Sr concentrations in the investigated Martin Point succession vary between 152 and 980 ppm and those of Fe and Mn range from 785 to 6900 ppm and from 142 to 649 ppm respectively. The Fe and Mn values have very poor correlation ($R^2$ = 0.01; Fig. 3.2a) and they show weak to poor correlations with those of Sr ($R^2$ = 0.01 and 0.04, respectively; Fig. 3.2b, d). The Al and Si concentrations vary from 611 to 3547 ppm and from 1246 to 5112 ppm, respectively. Although Al poorly correlates with Sr ($R^2$ = 0.13; Fig. 3.2c), it exhibits a strong correlation with those of the Si ($R^2$ = 0.67; Fig. 3.2e).

The mean values of P (141.2 and 142.0 ppm, respectively) and Ce/Ce* (0.9 and 0.8, respectively) between two aimed intervals are nearly the same, whereas the mean values of Ni, Sr, Mn, Fe, Th/U, Mn/Al and Fe/Al from the HERB interval are slightly higher. Additionally, Si and Al counterparts are slightly higher in the Є – O boundary carbonates (Table. 3.1).

Generally speaking, the mean Ce/Ce* and Th/U values of the Є – O boundary carbonates at Martin Point are comparable to those of the counterpart interval in Green Point (Azmy et al., 2014; 2015). However, Mn, Sr, P and ΣREE contents of the Martin Point (316 ± 195, 258 ± 49, 141 ± 32 and 43 ± 26 ppm, respectively) are lower than their counterparts of the Green Point (392 ± 220, 271 ± 74, 413 ± 1165, 67 ± 6 ppm, respectively) although the Al and Si value at Martin Point (1725 ± 1145 and 2872 ± 1332 ppm) is obviously higher than those value at Green Point (1093 ± 1552 and 1918 ± 2493 ppm; Azmy et al., 2014; 2015).

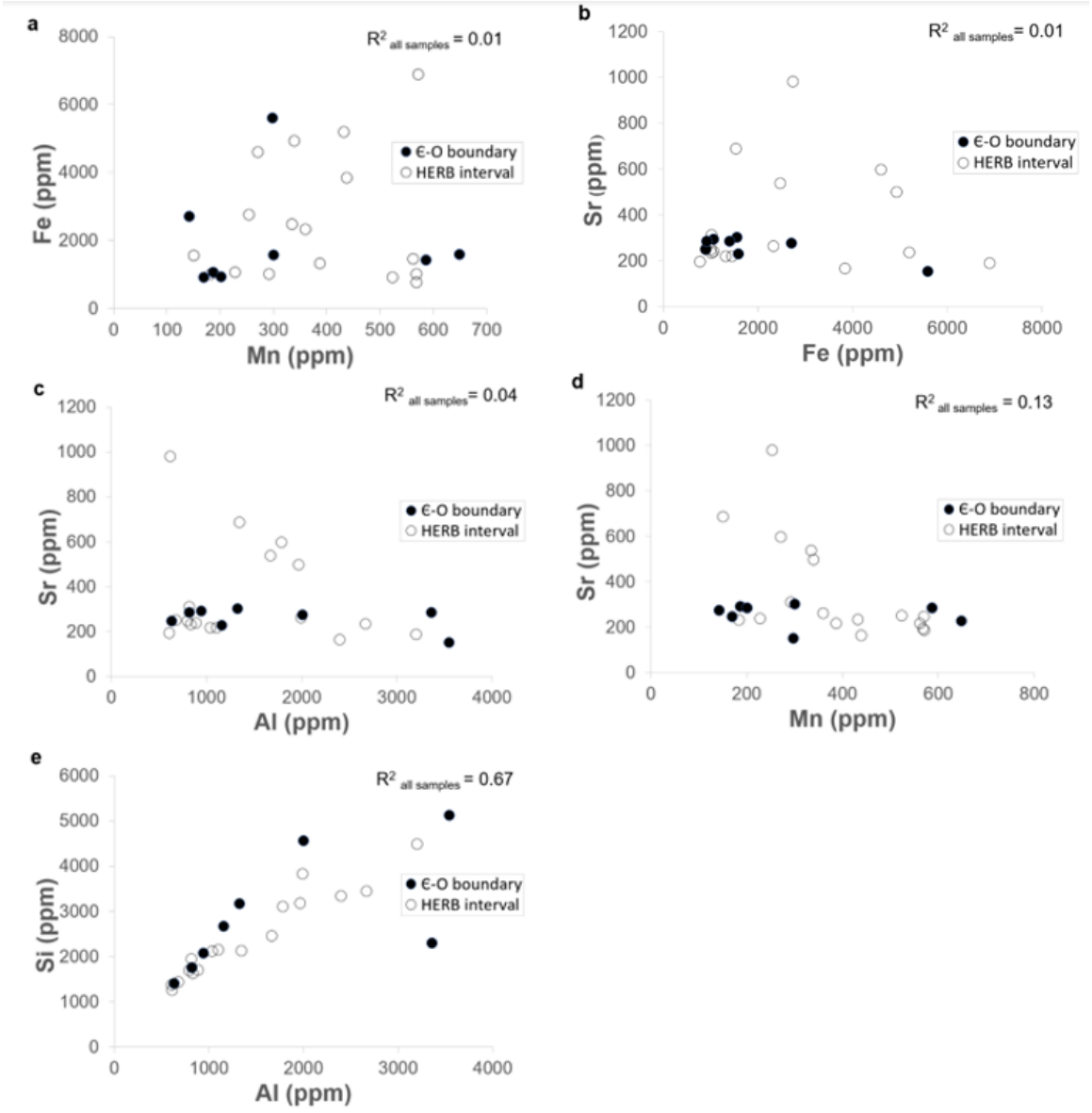


**Figure. 3.2** Scatter diagrams showing insignificant correlations of (a) Mn with Fe, as well as Sr with (b) Fe, (c) AL, and (d) Mn, and significant correlation of (e) Si with Al.

The profiles of the investigated elements (Fig. 3.3) exhibit distinct variations associated with the stratigraphic interval that spans the peak of the HERB event (Azmy, 2018a).

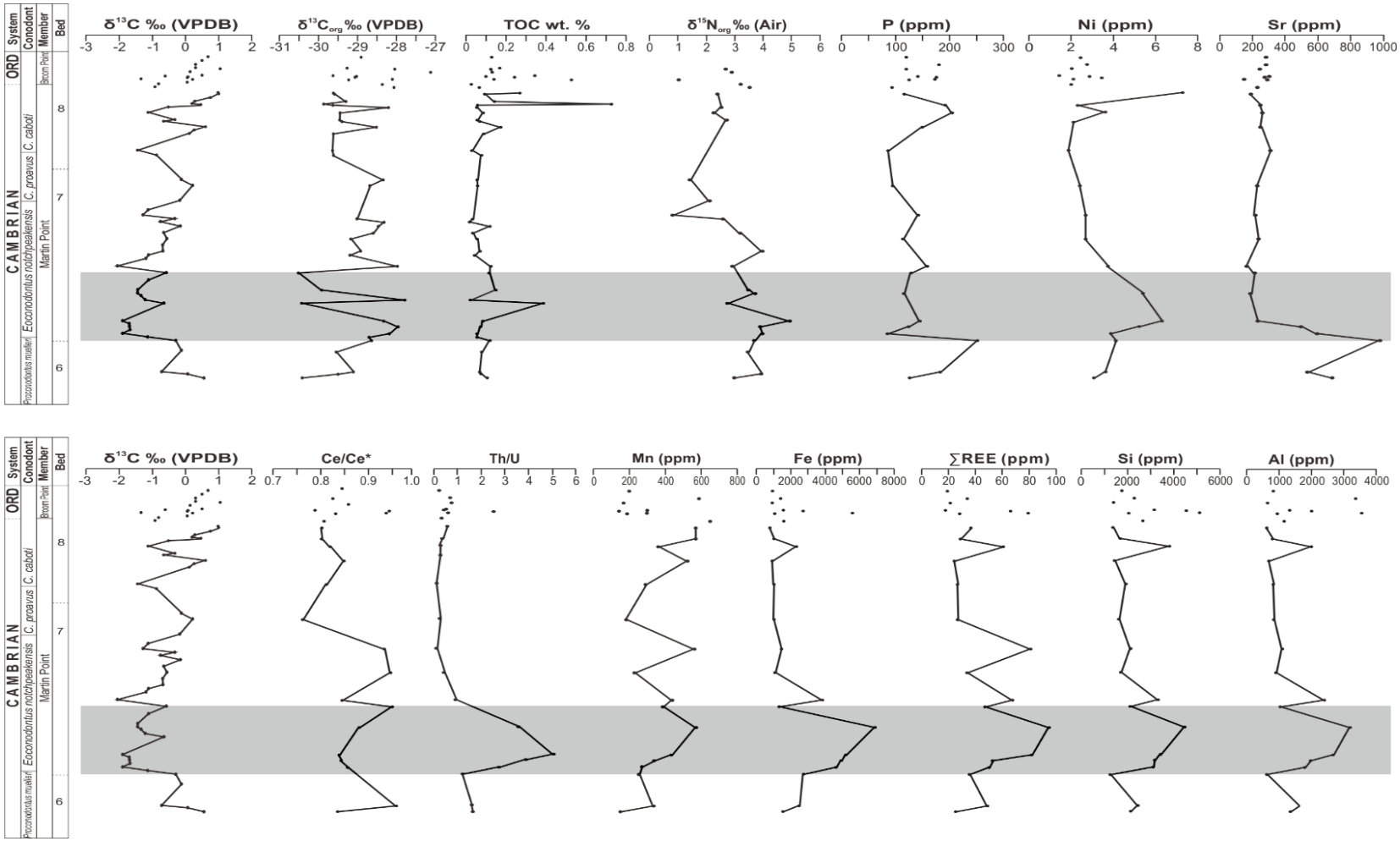


**Figure. 3.3** The profiles of $\delta^{13}C_{carb}$, $\delta^{13}C_{org}$, TOC, $\delta^{15}N_{org}$, P, Ni, Sr, Ce/Ce*, Th/U, Mn, Fe, ΣREE, Si and Al across the HERB event in Martin Point section. The $\delta^{13}C_{carb}$, Th/U and Ni profiles are reproduced from Azmy (2018a). The highlighted horizon (grey band) marks the peak area of the HERB $\delta^{13}C_{carb}$ profile.

### 3.3 Organic C- and N- Isotopes

The total organic content (TOC) of the entire investigated Martin Point section varies between 0.02 and 0.73 wt. % (0.1 ± 0.1 wt. %) and $\delta^{13}C_{org}$ ranges from − 30.5 to − 27.1 ‰ VPDB (− 29.1 ± 0.7 ‰ VPDB; Table 3.1). TOC and $\delta^{13}C_{org}$ exhibit insignificant correlations ($R^2 = 0.11$, Fig. 3.4a). The $\delta^{13}C_{org}$ profile exhibits a positive shift (~ 2 ‰) that correlates with a slight decrease in the TOC (Fig. 3.3), which is also correlated with the HERB $\delta^{13}C_{carb}$ excursion documented by Azmy (2018a) from the same investigated samples.

The $\delta^{15}N_{org}$ values range between + 0.8 ‰ and + 5.0 ‰ (3.0 ± 1.0 ‰ air; Table 3.1), which have a slightly wider spectrum than that documented for the present-day Black Sea sediments (~ 2.5 ‰ to 3.6 ‰; Fry et al., 1991; Çoban-Yıldızetal et al., 2006) and $\delta^{15}N_{org}$ exhibit a general insignificant correlation with TOC ($R^2 = 0.18$; Fig. 3.4b). The $\delta^{15}N_{org}$ profile shows a parallel variation with that of the $\delta^{13}C_{org}$ and also exhibits a comparable positive excursion (~ 2 ‰; Fig. 3.3) associated with the stratigraphic level of the HERB event (Azmy, 2018a). The mean $\delta^{15}N_{org}$ value of the HERB interval of the Martin Point carbonates (3.0 ± 1.0 ‰) is slightly higher than that of the Є – O boundary carbonates (2.9 ± 1.1 ‰) whereas the $\delta^{13}C_{org}$ and TOC values are lower (Table 3.1).

By comparing the signatures of $\delta^{13}C_{org}$, $\delta^{15}N_{org}$ and TOC of the Є – O boundary carbonates from Martin Point with those from their age-equivalent counterparts at the Green Point (GSSP) section (Azmy et al., 2015), the mean values of $\delta^{15}N_{org}$ are nearly equal (2.9 ± 1.1 ‰ at Martin Point vs. 2.8 ± 1.5 ‰ at Green Point), the $\delta^{13}C_{org}$ value at Martin Point (− 28.6 ± 0.7 ‰ of Martin Point here) is slightly lower (− 27.8 ± 1.1 ‰ in

Green Point), whereas the TOC value at Martin Point is remarkably lower (0.2 ± 0.1 wt. % in Martin Point vs. 0.6 ± 0.5 wt. % in Green Point).

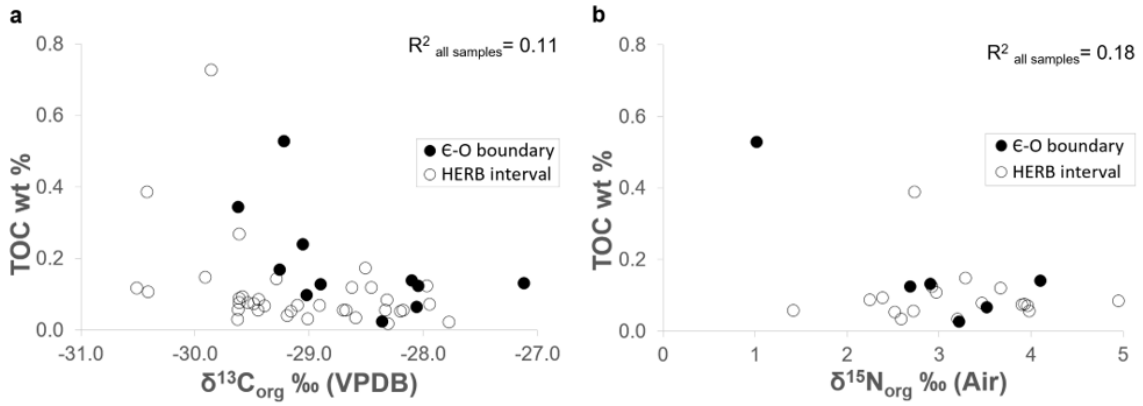


**Figure. 3.4** Scatter diagrams showing insignificant correlations of (a) $\delta^{13}C_{org}$ and (b) $\delta^{15}N_{org}$ with TOC.

# Chapter 4

# Discussion

## 4.1 Diagenetic Influence

The preservation of the investigated samples has been discussed in detail by Azmy (2018a) and is summarized below. Petrographic examination indicated that that the samples are dominated by lime mudstones with almost pristine sedimentary fabrics and insignificant recrystallization (Fig. 3.1). The grain size is mainly micritic to near-micritic (≤ 10 μm), suggesting a high degree of textural preservation and the limestone exhibit dull to no luminescence (Fig. 3.1). Luminescence in carbonates is activated by the enrichment of Mn but, on the contrary, quenched by high concentrations of Fe (Machel and Burton, 1991). Thus, the dull and non-CL images have to be interpreted with caution because they may reflect geochemical preservation or enrichment of Fe by diagenetic alteration (Rush and Chafetz, 1990). However, the investigated lime mudstones are known to have precipitated in a slope setting of lower oxygen compared with that of shallow environment and therefore expected to be relatively more enriched in Fe and/or Mn (Morrison and Brand, 1986; Azmy, 2018a). Therefore, CL is a preliminary evaluation tool that should be combined with other signatures (such as correlation between Sr and $\delta^{13}C_{carb}$) to confirm sample preservation (Brand et al., 2011).

Progressive burial of sediments is associated with an increase in temperature (>50$^{o}$ C), which results in thermal degradation of organic matter and a decrease in the TOC values (Azmy et al., 2015). This is also associated with an increase in $\delta^{15}N_{org}$ and $\delta^{13}C_{org}$ values since $^{12}C$- and $^{14}N$- enriched organic compounds are released from

limestone (e.g. Saino and Hattori, 1980; Popp et al., 1997; Faure and Mensing, 2005;). The $\delta^{13}C_{org}$ values of the Martin Point carbonates show an insignificant correlation ($R^2$ = 0.11) with their TOC (Fig. 3.4a) which argues against the scenario of organic matter degradation and is consistent with the petrographic evidence of preservation of the micritic fabric, thus supporting the preservation of the $\delta^{13}C_{org}$ signatures. Similarly, the poor correlation ($R^2$ = 0.18; Fig. 3.4b) between the $\delta^{15}N_{org}$ and TOC values supports at least near-primary $\delta^{15}N_{org}$ signatures.

Diagenetic alteration through water/rock interactions during burial of carbonates is known to deplete some elements such as Sr but enrich others such as Mn, Fe, and Al. The Sr is poorly correlated with Fe, Al, Mn and $\delta^{13}C_{carb}$ ($R^2$= 0.01, 0.04, 0.13 and 0.0002, respectively; Fig. 3.2b – d, 3.5a), which suggests an insignificant alteration by diagenesis. Microbial lime mudstones have been documented on Paleozoic slope settings at depths down to 300 m (e.g., Della Porta et al., 2003), which suggests that the investigated slope carbonates of the Martin Point section (James and Stevens, 1986; Landing, 2013) might have had contributions from in situ lime muds (James and Stevens, 1986; Landing, 2013; Azmy, 2018a) through microbial mediation (e.g., George, 1999; Della Porta et al., 2003; Bahamonde et al., 2007; Schlager, 2005; Bartley et al., 2015). Slope settings have oxygen-poor (dysoxic) conditions (Azmy, 2018a) compared with those of oxic shallow-water settings and this may explain their enriched Mn and Fe contents (360 ± 160 ppm and 2361 ± 1772 ppm, respectively). Contaminations from hidden microrhombic bacterial pyrite during micro-sampling might have also contributed to the Fe measurements. Thus, Mn and Fe concentrations are not the ideal proxies of diagenesis for slope carbonates, but yet they still exhibit insignificant correlations with their Sr

counterparts in the investigated limestones (Fig. 3.2b – c). Azmy (2018a) indicated that the correlation between the Sr and $\delta^{18}O_{carb}$ values is also poor ($R^2$ = 0.02; Fig. 3.5b), suggesting a high degree of preservation of the geochemical signatures (at least near primary), which is supported by the fabric retention and micritic to near-micritic grain size of the investigated lime mudstones (Fig. 3.1). The strong correlation between Si and Al ($R^2$ = 0.67; Fig. 3.2e) may reflect an influence of terrigenous input possibly during a sea-level drop, which is consistent with the sea-level variations documented by earlier studies (e.g., Miller et al., 2011; Azmy, 2018a)

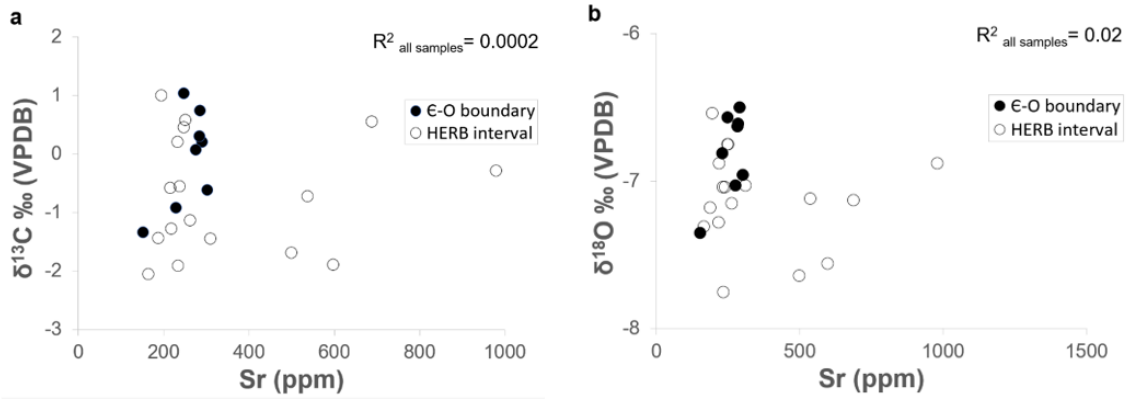


**Figure 3.5** Scatter diagrams, reproduced from Azmy 2018a, showing insignificant correlations of Sr with (a) $\delta^{13}C_{carb}$ and (b) $\delta^{18}O_{carb}$.

### 4.2 Elemental Variation

Variations in eustatic sea-level not only influence the redox conditions and organic productivity but also the input of terrigenous sediments and nutrients in the ocean, which is reflected in the associated changes in the concentrations of trace elements in marine sediments (e.g., Cowan and James, 1993; Wignall and Twitchett, 1996; Kimura et al., 2005; Arnaboldi and Meyers, 2007; Piper and Calvert, 2009; Śliwiński et al., 2010; Dickson et al., 2011). An earlier study (Azmy, 2018a) documented a noticeable negative $\delta^{13}C_{carb}$ excursion (~ 3 ‰), associated with sea-level changes (Miller et al., 2011), that

peaks at the base of the *Eoconodontus notchpeakensis* conodont Zone near the bottom of bed 6 (Fig.3.3). Phosphorus and Ni have been proven to be reliable proxies of bioproductivity whereas Ce/Ce*, Th/U, Fe and Mn contents are used to reflect paleoredox condition (e.g., Hatch and Leventhal, 1992; Wignall and Twickett, 1996; Rue et al., 1997; Morel et al., 2004; Tribovillard et al., 2006; Arnaboldi and Meyers, 2007; Śliwiński et al., 2010). Aluminum and Si reflect the influence of terrestrial input in oceans (e.g., Govin et al., 2012; Zhao and Zheng, 2014). The biodiversity is expected to be lower in the slope settings compared to other deposition environments (James and Stevens, 1986), where the investigated Martin Point carbonates were deposited, particularly near the lower boundary of the photic zone and during the early Paleozoic when the evolution and abundance of shelly marine biota were relatively lower than present day.

Aluminum, Si, and total REE (ΣREE) are enriched in continental crustal rocks and they are therefore proxies of the terrigenous inputs in oceans (e.g., Veizer, 1983; Śliwiński et al., 2010; Tripathy et al., 2014). Their profiles, from the Martin Point section, exhibit parallel positive excursions (Fig. 3.3) that are correlated with the HERB negative $\delta^{13}C$ excursion (Fig. 3.3) documented by Azmy (2018a). The peak of the HERB $\delta^{13}C$ excursion was associated with a sea-level drop (Miller et al., 2014; Azmy, 2018a), which most likely led to enhanced terrigenous input and resulted in enrichment of Al, Si and ΣREE in ocean water and also during precipitation of marine carbonates. Nickel is a micronutrient and also a proxy of bioproductivity and is captured by the organic matter in the water column (e.g., Calvert and Pedersen, 1993; Śliwiński et al., 2010). An earlier study (Azmy, 2018a) indicated that no diagenetic overprint seems to have influenced the

Ni signatures in the investigated Martin Point carbonates (Azmy, 2018a). The Martin Point Ni profile (Azmy, 2018a) shows a positive excursion parallel to those exhibited by Al, Si and ΣREE (Fig. 3.3) and also correlates with the HERB $\delta^{13}C$ excursion, which supports the scenario of increased nutrients through terrigenous inputs during the sea-level drop before it resumed rising.

The concentration of P (141.8 ± 40.5 ppm, Table 3.1; Appendix 1) does not change considerably throughout the investigated interval but the P profile exhibits a relative enrichment (251.9 ppm, MH5, Appendix 1) immediately below the peak of the HERB negative $\delta^{13}C$ excursion (Fig. 3.3) with concentrating decreasing again until they approach the Cambrian–Ordovician boundary. The brief increase in P concentrations at the bottom of the profile is possibly related to an upwelling event (Föllmi, 1996; Gao et al., 2018) since upwelling can be driven not only by ice-cap melting but also by wind and tectonic activities (Anderson et al., 2009). Contributions from falling phosphatic fecal pellets from top of the water column and microaggregates of phosphatic algae (e.g., Azmy et al., 2014) could also explain the enrichment. There is another pulse at the top of the whole profile correlated with enhanced Al, Si and ΣREE input reflecting some influence of terrigenous inputs. This may suggest contributions from detrital organic matter, which is consistent with the parallel increase shown by the TOC profile (Fig. 3.3; Latimer and Filippelli, 2002). Unlike the lime mudstones spanning the Cambrian–Ordovician Boundary in the GSSP section at Green Point, petrographic examinations did not reveal any occurrences of phosphatic algae in the carbonates of the HERB event interval of the current Martin Point study (Azmy et al., 2014).

The Sr profile (Fig. 3.3) shows a maximum value, immediately below the peak of the HERB $\delta^{13}C$ excursion, followed by a distinct decrease, after which values remain approximately unchanged upward. No diagenetic system has been known yet to cause such variations but a change from carbonates dominated by aragonite to those dominated by calcite is suggested as a possible scenario (e.g., Brand, 1991; Sunagawa et al., 2007).

Eustasy influences oxygen levels in the water column, which control the redox proxies (e.g., Ce) by changing their oxidation state and solubility in seawater and consequently their concentrations in marine carbonates (e.g., Webb et al., 2009). The micritic ($\leq 4$ μm) to near-micritic (~ 10 μm) grain size of the investigated carbonates suggests a low water/rock interaction (insignificant alteration) and the Ce concentrations have insignificant correlation ($R^2 = 0.13$) with Sr. Therefore, the Ce values are not significantly impacted by diagenesis and can be utilized to highlight the relative redox variations across the HERB event. The Ce anomaly (Ce/Ce*) has been proven to be a proxy of redox conditions (e.g., Bau and Dulski, 1996; Webb and Kamber, 2000; Azmy et al., 2015). In shallow oxic water, trivalent Ce is oxidized to trivalent Ce and absorbed on particle surfaces and/or form less soluble $Ce^{4+}$ species (Bau and Dulski, 1996) leaving shallow oxic water depleted in Ce. The Ce/Ce* ratios (between 0.7 and 1.0, Table 3.1) of the investigated interval have a poor correlation with Sr ($R^2 = 0.13$), thus suggesting insignificant influence by diagenesis. The Ce/Ce* anomalies at Martin Point are generally < 1 and likely reflect dysoxic (suboxic) conditions (e.g., Webb and Kamber, 2000). The Ce/Ce* profile (Fig. 3.3) shows a negative shift correlated with the peak of the HERB negative $\delta^{13}C$ excursion, which is consistent with the initial sea-level drop that enhanced the oxygenation of water and decreased Ce before it resumed rising.

Th/U ratios have also been known to be reliable proxies for redox conditions (Wignall and Twichett, 1996; Wignall et al., 2007) as they are found to increase with oxidizing conditions because U maintains the soluble $U^{6+}$ higher state of oxidation whereas Th is not affected by changes in redox conditions. An earlier study (Azmy, 2018a) indicated that the Th/U profile of the Martin Point section has a positive shift that correlates with the HERB negative $\delta^{13}C$ excursion, which is consistent with the observed Ce/Ce* shift related to a drop in sea-level and a brief oxygenation.

The relative increases in Mn and Fe concentrations may reflect the variations in redox conditions because both elements are more soluble in their reduced states (Landing and Bruland, 1987) and thus become more enriched in seawater under dysoxic conditions compared with oxic shallow waters. The Mn and Fe concentrations vary from 142 to 649 ppm and 785 to 6900 ppm, respectively (Table 3.1) and their concentrations are higher than those of modern warm shallow-water marine carbonates (Mn = 5.4 – 30 ppm and Fe = 1 – 20 ppm; Ichikuni, 1973; Veizer, 1974; Richter and Füchtbauer, 1978; Lorens, 1981; Brand et al., 2003). This is consistent with their enrichment in the investigated Martin Point slope carbonates (James and Stevens, 1986) and the interpreted dysoxic conditions (e.g., Azmy, 2018a). Meanwhile, the Mn and Fe profiles exhibit correlated positive excursions parallel to those exhibited by the Al, Si and ΣREE (Fig. 3.3), thus reflecting an overprint of terrigenous inputs (e.g., Rao and Adabi, 1992). However, the Mn and Fe concentrations can be normalized by aluminum to eliminate the influence of detrital fraction and be utilized as proxies of redox conditions (Clarkson et al., 2014). The investigated Martin point carbonates have Mn/Al ratios between 0.1 and 0.9 and Fe/Al ratio between 0.4 and 4.5 (Table 3.1), which are considerably higher than those of the

upper continental crust (0.0075 and 0.44, respectively; McLennan, 2001). This may reflect the occurrence of Fe-Mn oxy-hydroxides (Pattan et al., 2013) that cannot form in anoxic environments but require at least dysoxic conditions (cf. Landing et al., 2002; Azmy, 2018a).

The profiles of Al, Si, ΣREE, Fe, Mn, Ni and P show upper positive shifts below the Cambrian–Ordovician boundary at the same stratigraphic level correlated with a negative subpeak on the $\delta^{13}C_{carb}$ profile, thus suggesting an increase in terrigenous inputs around that time likely due to possible a minor drop in sea-level during an overall rise in sea-level.

The mean concentrations of the investigated elemental proxies of the HERB carbonates and those of the Cambrian–Ordovician boundary (Table 3.1) in the Martin Point section are almost comparable (cf. Azmy et al., 2014, 2015) and therefore suggest no dramatic change in the elemental chemistry of the seawater at least through the late Cambrian and the lowermost Ordovician. However, the Sr shows a considerable drop immediately below the peak of the HERB negative $\delta^{13}C_{carb}$ excursion and remains low up-section and thorough the Cambrian–Ordovician boundary. Also, the mean Th/U value of the HERB carbonates (1.4; Table 3.1) is relatively higher than that of the Cambrian–Ordovician carbonates (0.5; Table 3.1), which is consistent with the geochemical evidence of the sea-level drop at the peak of the HERB event and the relative decrease in dysoxic conditions.

### 4.3 Organic C- and N- Isotope

The carbon and nitrogen isotopes of the organic matter have been used as reliable indicators to reflect redox states, terrigenous inputs, bioproductivity and the preservation of organic debris (e.g. Altabet and Francois, 1994; Amon et al., 2003; Çoban-Yıldızetal, 2006; Quan et al., 2008; Yamaguchi et al., 2010; Quan et al., 2013; Azmy et al., 2015;). The TOC values vary between 0.02 and 0.7 wt. % (0.1 ± 0.1 wt. %; Table 3.1), which are significantly lower than those documented for the overlying (younger) carbonates (1.1 ± 1.0 wt. %; Azmy et al., 2015) and shales (0.6 to 5.2 wt. %; Weaver and Macko, 1988) of the Cambrian–Ordovician GSSP boundary at Green Point. This may suggest significant lower organic productivity, at the same slope settings, during the HERB time interval. A drop in sea-level is expected to bring the lower boundary of the photic zone down and enhance primary productivity whereas a sea-level rise results in increased burial of organic matter in the relatively deeper settings and enrichments of $^{12}C$ in buried organic matter.

The peak of the of the HERB negative $\delta^{13}C_{carb}$ excursion is correlated with a positive shift on the $\delta^{13}C_{org}$ profile (Fig. 3.3), thus suggesting contributions from detrital organic matter, which is relatively depleted in $^{12}C$, that overprinted the enhanced primary productivity caused by a sea-level drop particularly when primary productivity was generally low during the Late Cambrian as indicated by the very low TOC values (0.1 ± 0.1 wt. %, Table 3.1). This scenario of increased organic matter is supported by the correlation of distinct enhancements in detrital inputs reflected by the positive shifts in the Al, Si, ΣREE, and Ni profiles (Fig. 3.3).

The TOC profile shows insignificant variations except for a lower positive shift (~ 0.4 %) that correlates with the start of general sea-level rise after the peak of the HERB negative $\delta^{13}C_{carb}$ excursion and an upper shift (0.7 %) close to the Cambrian–Ordovician boundary (Fig. 3.3). Both shifts correlate with negative shifts on the $\delta^{13}C_{org}$ profile (Fig. 3.3) and are associated with positive shifts on the Al, Si, and ΣREE, thus reflecting episodes of relatively higher inputs of detrital organics and fast burial.

The $\delta^{15}N_{org}$ values have been widely used as a proxy to determine organic matter sources and redox states (Yamaguchi et al., 2010; Quan et al., 2013; Ren et al., 2017), but this has to be taken with caution since the ocean N budget is complicated and influenced by several factors, such as the organic nitrogen (ON) from terrigenous fluxes, deterioration of ON, uptake of nitrogen by phytoplankton, N-fixation by cyanobacteria in surface waters, and denitrification. The values of $\delta^{15}N_{org}$ for the Martin Point section vary between 0.8 and 5.0 ‰ (3.0 ± 1.0 ‰; Fig. 3.3; Table 3.1), which is higher than those of terrestrial plants (Drechsler and Stiehl, 1977; Stiehl and Lehmann, 1980) but comparable to those of the modern Black Sea sediments (~ 3 ‰; Quan et al., 2008), thus suggesting at least dysoxic conditions (e.g., Azmy et al., 2015). This also implies that the contribution from terrestrial plants through terrigenous inputs under normal conditions is minimal, which is consistent with low diversity of land plants especially during the earliest Phanerozoic (Late Cambrian) (e.g. Meyers, 1994; Theissen et al., 2003).

Microbial denitrification (reduction of $NO_3^-$ into $N_2$) under oxygen-depleted conditions results in enrichment of $^{15}N$ in organic matter (e.g., Sigman et al., 2009; Cremonese et al., 2013; Quan et al, 2013). The $\delta^{15}N_{org}$ profile of the Martin Point

carbonates (Fig. 3.3) shows a broad positive excursion (~ 2 ‰) that peaks at a stratigraphic level correlated with that of the HERB negative $\delta^{13}C_{carb}$ excursion, which is associated with a sea-level drop. This is opposite to the expected trend but can be attributed to the influence of contributions from detrital organic matter ($^{15}N$-enriched of marine origin) during a sea-level lowstand, which is also consistent with the correlated $\delta^{13}C_{org}$ positive shift.

The sea-level drop might have contributed to the uptake of $^{14}N$ by phytoplankton that would leave seawater relatively more enriched in $^{15}N$ and lead to a positive $\delta^{15}N_{org}$ shift of organic matter (Cline and Kaplan, 1975; Macko et al., 1993; Meyers and Lallier-Vergès, 1999; Talbot and Laerdal, 2000). The short-term sea-level fluctuations inferred from the $\delta^{13}C_{carb}$ subpeaks, the narrow sampling interval (as narrow as 10 cm), and the thinly-bedded carbonate interbeds alternating with shales (Azmy, 2018a) suggest that the enhancement in primary productivity caused by minor drops in sea-level throughout an overall sea-level rise was possibly not enough to overprint the influence of detrital organic matter on the $\delta^{13}C_{org}$ and $\delta^{15}N_{org}$ signatures.

In summary, the stable isotope geochemistry of the carbonates and organic matter, as well as the trace element concentrations of the Martin Point carbonates suggest that the main (first order) trend of sea-level rise during Late Cambrian had a minor distinct sea-level fall associated with the HERB event.

The sea-level fall was associated with recognizable negative $\delta^{13}C_{carb}$ shifts (Azmy 2018a, Fig. 3.3) caused by bringing oxygen-rich shallow water in contact with organic matter that was buried at depth before the sea-level drop. The falling sea-level led to

increased land exposure, which enhanced the input of weathered crustal rocks into the ocean. This is reflected by positive shifts of the Al, Si, Fe, Mn, Ni, ΣREE, and Th/U profiles and a negative shift of the Ce/Ce* profile due to the increase of the concentrations of those crust-enriched elements in the investigated marine carbonates and a relative increase in oxygen level in the top water column. The P profile peaks before the proposed HERB sea-level drop suggesting possible contributions from falling phosphatic fecal pellets or traces of phosphatic algae (e.g., Azmy et al., 2014) that were not detected by regular petrographic examinations of thin sections. On the other hand, the peak at the top of the P profile is associated with positive shifts in the Al, Si, Fe, Mn, Ni, and ΣREE profiles suggesting contributions from weathered material of land sources.

The change in the sea-level impacted the primary productivity and the inputs of recycled organic matter in the weathered material that accordingly led to variations in the TOC budget and C- and N- isotope signatures. These variations were reflected in recognizable shifts on the $\delta^{13}C_{org}$ and $\delta^{15}N_{org}$ profiles.

# Chapter 5

# Conclusion

The petrographic and geochemical examinations prove the preservation of samples at least near-primary trace element signatures and C- and N- isotope compositions of organic matter from the lime mudstone interbeds of the slope rhythmites spanning the Upper Cambrian section at Martin Point, western Newfoundland. The signatures can therefore be utilized as proxies to investigate the changes in redox condition, bioproductivity, and terrigenous input in response to sea-level variations.

The trace element profiles of Al, Si, ΣREE, Fe, Mn, and Ce/Ce* profiles exhibit consistent shifts correlated with the peak of the HERB negative $\delta^{13}C_{carb}$ excursion documented by earlier studies, which is consistent with a sea-level drop, a more oxic depositional environment, and increased contributions from terrigenous inputs.

The associated positive shifts exhibited by Fe and Mn reflect overprinting by terrigenous inputs rather than a change in redox condition, which is consistent with the correlated Ce/Ce* negative shift and the earlier documented positive Th/U shift.

The TOC values (0.1 ± 0.1 wt. %) of the carbonates spanning the HERB interval are significantly lower than those of the overlying Cambrian–Ordovician boundary, thus suggesting significant lower primary productivity. The $\delta^{13}C_{org}$ and $\delta^{15}N_{org}$ profiles show positive shifts correlated with the HERB negative $\delta^{13}C_{carb}$ peak and enhancement in the Al, Si, and ΣREE concentrations, thus suggesting contributions from detrital organic matter during a sea-level drop.

The mean $\delta^{15}N_{org}$ values (3.0 ± 1.0 ‰ air) are consistent with dysoxic conditions and suggest that contributions of detrital organic matter through terrigenous inputs were not from terrestrial plants but rather marine origin.

# Reference

**Acharya**, S.S., Panigrahi, M.K., Gupta, A.K., Tripathy, S., 2015. Response of trace metal redox proxies in continental shelf environment: The Eastern Arabian Sea scenario. Continental Shelf Research. 106, 70–84.

**Aguilar**, C., Nealson, K.H., 1994. Manganese reduction in Oneida Lake, New York: estimates of spatial and temporal manganese flux. Canadian Journal of Fisheries and Aquatic Sciences. 5, 185–196.

**Algeo**, T.J., Maynard, J.B., 2004. Trace element behavior and redox facies in core shales of Upper Pennsylvanian Kansas-type cyclothems. Chemical Geology. 206, 289–318.

**Algeo**, T.J., Rowe, H., 2012. Paleoceanographic applications of trace-metal concentration data. Chemical Geology. 324-325, 6–18.

**Alibo**, D.S., Nozaki, Y., 2004. Dissolved rare earth elements in the eastern Indian Ocean: chemical tracers of the water masses. Deep–Sea Research I. 51, 559–576.

**Aller**, R.C., Heilburun, C., Panzeca, C., Zhu, Z.B., Baltzer, F., 2004. Coupling between sedimentary dynamics, early diagenetic processes, and biogeochemical cycling in the Amazon-Guianas mobile mud belt: coastal French Guiana. Marine Geology. 208, 331–360.

**Altabet**, M.A., Francois, R., 1994. Sedimentary nitrogen isotopic ratio as a recorder for surface ocean nitrate utilization, Global Biogeochemical Cycles. 8(1), 103–116.

**Amon**, R.M.W., Budéus, G., Meon, B., 2003. Dissolved organic carbon distribution and origin in the Nordic Seas: exchanges with the Arctic Ocean and the North Atlantic. Journal of Geophysical Research: Oceans. 108 (C7, 3221).

**Anderson**, R.F., Ali, S., Bradtmiller, L.I., Nielsen, S.H.H., Fleisher, M.Q., Anderson, B.E., Burckle, L.H., 2009. Wind-driven upwelling in Southern Ocean and the deglacial rise in atmospheric $CO_2$. Science, 323, 1443–1448.

**Anderson**, R.F., Fleisher, M.Q., Lehuray, A.P., 1989. Concentration, oxidation state, and particulate flux of uranium in the Black Sea. Geochimica et Cosmochimica Acta. 53, 2215–2224.

**Arnaboldi**, M., Meyers, P.A., 2007. Trace element indicators of increased primary production and decreased water-column ventilation during deposition of latest Pliocene sapropels at five locations across the Mediterranean Sea. Palaeogeography. Palaeoclimatology, Palaeoecology. 249, 425–443.

**Azmy**, K., 2018a. Carbon-isotope stratigraphy of the uppermost Cambrian in eastern Laurentia: implications for global correlation. Geological Magazine. 156, 759–771.

**Azmy**, K., 2018b. Carbon-isotope stratigraphy of the SPICE event (Upper Cambrian) in eastern Laurentia: implications for global correlation and a potential reference section. Geological Magazine published online 30 October 2018. doi:10.1017/S0016756818000638

**Azmy**, K., Kendall, K., Brand, U., Stouge, S., Gordon, G.W., 2015. Redox conditions across the Cambrian Ordovician boundary: elemental and isotopic signatures retained in the GSSP carbonates. Palaeogeography. Paleoclimatology, Palaeoecology. 440, 440–54.

**Azmy**, K., Stouge, S., Brand, U., Bagnoli, G., Ripperdan, R., 2014. High-resolution chemostratigraphy of the Cambrian–Ordovician GSSP in western Newfoundland, Canada: enhanced global correlation tool. Palaeogeography, Palaeoclimatology, Palaeoecology. 409, 135–44.

**Azomani**, E., Azmy, K., Blamey, N., Brand, U., Al-Aasm, I., 2013. Origin of Lower Ordovician dolomites in eastern Laurentia: controls on porosity and implications from geochemistry. Marine and Petroleum Geology. 40, 99–114.

**Bahamonde**, J.R., Meno-Tomé, O.A., Heredia, N., 2007. A Pennsylvanian microbial boundstone-dominated carbonate shelf in a distal foreland margin (Picos de Europa Province, NW Spain). Sedimentary Geology. 198, 167–193.

**Banner**, J.L., 1995. Application of the trace element and isotope geochemistry of strontium to studies of carbonate diagenesis. Sedimentology. 42, 805–824.

**Barnaby**, R. J., Rimstidt, J. D., 1989. Redox conditions of calcite cementation interpreted from Mn and Fe contents of authigenic calcites. Geological Society of America Bulletin. 101, 795-804.

**Barnes**, C.R., 1988. The proposed Cambrian–Ordovician global boundary stratotype and point (GSSP) in western Newfoundland, Canada. Geological Magazine. 125, 381–414.

**Bartley,** J.K., Kah, L.C., Frank, T.D., Lyons, T.W., 2015. Deep-water microbialites of the Mesoproterozoic Dismal Lakes Group: microbial growth, lithification, and implications for coniform stromatolites. Geobiology. 13, 15–32.

**Bau**, M., Dulski, P., 1996. Distribution of yttrium and rare-earth elements in the Penge and Kuruman iron-formations, Transvaal Super group, South Africa. Precambrian Research. 79, 37–55.

**Bernasconi**, S.M., 1997. Carbon and nitrogen isotope variation in sedimenting organic matter in Lake Lugano. Limnology and Oceanography. 42(8), 1755–1765.

**Bianchi**, T.S., Cui, X., Blair, N.E., Burdige, D.J., Eglinton. T.I., Galy, V., 2018. Centers of organic carbon burial and oxidation at the land-ocean interface. Organic Geochemistry. 115, 138-155.

**Boggs**, S., Krinsley, D., 2006. Application of cathodoluminescence imaging to the study of sedimentary rocks. Cambridge University Press, New York.

**Boyle**, S.E., Edmond, J.M., 1976. On the marine geochemistry of nickel. Earth and Planetary Science Letters. 31, 119–128.

**Brand**, U., Logan, A., Bitner, M.A., Griesshaber, E., Azmy, K., Buhl, D., 2011. What is the ideal proxy of Paleozoic seawater? Memoirs of the Association of Australasian Paleontological Society Memoirs. 41, 9–24.

**Brand**, U., Logan, A., Hiller, N., Richardson, J., 2003. Geochemistry of modern brachiopods: applications and implications for oceanography and paleoceanography. Chemical Geology. 198, 305–334.

**Brand**, U., 1991. Strontium isotope diagenesis of biogenic aragonite and low-Mg calcite. Geochimicu et Cosmochimica Acta. 55, 505–513.

**Broecker**, W.S., Peng, T.H., 1982. Tracers in the Sea. Eldigio, Palisades. 690 pp.

**Bruland**, K.W., 1980. Oceanographic distributions of cadmium, zinc, nickel, and copper in the North Pacific. Earth and Planet Science Letter. 47, 176–198.

**Buggisch**, W., Keller, M., Lehnert, O., 2003. Carbon isotope record of Late Cambrian to Early Ordovician carbonates of the Argentine Precordillera. Palaeogeography. Palaeoclimatology. Palaeoecology. 195, 357–73.

**Burley**, S. D., Mullis, J. T., Matter, A., 1989. Timing diagenesis in the Tartan Reservoir (UK North Sea): constraints from combined cathodoluminescence microscopy and fluid inclusion studies. Marine and Petroleum Geology. 6, 98–120.

**Calvert**, S.E., Pedersen, T.F., 1993. Geochemistry of recent oxic and anoxic marine sediments: implications for the geological record. Marine Geology. 113(1), 67–88.

**Casciotti**, K.L., 2009. Inverse kinetic isotope fractionation during bacterial nitrite oxidation. Geochimica et Cosmochimica Acta. 73, 2061–2076.

**Casciotti**, K.L., 2016. Nitrogen and Oxygen Isotopic Studies of the Marine Nitrogen Cycle. Annual Review of Marine Science. 8, 379–407.

**Cawood**, P.A., McCausland, P.J.A., Dunning, G.R., 2001. Opening Iapetus: constraints from Laurentian margin in Newfoundland. Geological Society of America Bulletin. 113, 443–53.

**Chester**, R., Jickells, T., 2012. Marine Geochemistry. DOI: 10.1002/9781118349083.

**Chi**, Y., Fang, X., Song, C., Miao, Y., Teng, X., Han, W., Wu, F., Yang, J., 2013. Cenozoic organic carbon isotope and pollen records from the Xining Basin, NE Tibetan Plateau, and their palaeoenvironmental significance. Palaeogeography, Palaeoclimatology. Palaeoecology. 386, 436–444.

**Ciscato**, E.R., Tomaso, B., Derek, V., 2018. Nickel and its isotopes in organic-rich sediments: implications for oceanic budgets and a potential record of ancient seawater. Earth and Planetary Science Letters. 494, 239–250.

**Clarkson**, M.O., Poulton, S.W., Wood, R.A., 2014. Assessing the utility of Fe/Al and Fe-speciation to record water column redox conditions in carbonate-rich sediments. Chemical Geology. 382, 111–122.

**Cline**, J.D., Kaplan, I.R., 1975. Isotopic fractionation of dissolved nitrate during denitrification in the eastern tropical North Pacific Ocean. Marine Chemistry. 3, 271–299.

**Çoban-Yıldız**, Y., Altabet, M.A., Yılmaz, A., Tuğrul, S., 2006. Carbon and nitrogen isotopic ratios of suspended particulate organic matter (SPOM) in the Black Sea water column. Deep-Sea Research. 53, 1875–1892.

**Cooper**, R.A., Nowlan, G.S., Williams, S.H., 2001. Global Stratotype Section and Point for base of the Ordovician System. Episodes. 24, 19–28.

**Cowan**, C.A., James, N.P., 1993. The interactions of sea level change, terrigenous sediment influx, and carbonate productivity as controls on Upper Cambrian grand cycles

of western Newfoundland, Canada. Geological Society of America Bulletin. 105, 1576–1590.

**Cremonese**, L., Shields-Zhou, G., Struck, U., Ling, H.F., Och, L., Chen, X., Li. D., 2013. Marine biogeochemical cycling during the early Cambrian constrained by a nitrogen and organic carbon isotope study of the Xiaotan section, South China. Precambrian Research. 225, 148–165.

**Defforey**, D., Paytan, A., 2018. Phosphorus cycling in marine sediments: Advances and challenges. Chemical Geology. 499, 1–11.

**Derry**, L.A., Kaufman, A. J., Jacobsen, S.B., 1992. Sedimentary cycles and environmental change in the Late Proterozoic: evidence from stable and radiogenic isotopes. Geochimica et Cosmochimica Acta. 56, 1317–1329.

**Dickson**, J.A.D., 1966. Carbonate identification and genesis as revealed by staining. Journal of Sedimentary Research. 36(2), 491–505.

**Dickson**, A.J, Cohen, A.S., Coe, A.L., 2011. Seawater oxygenation during the Paleocene–Eocene Thermal Maximum. Geology. 40(7), 639–642.

**Drechsler**, M., Stiehl, G., 1977. Stickstoffisotopen variationen in organischen Sedimenten 1. Untersuchungen an humosen Kohlen. Chemie der Erde. 36, 126–138.

**Egger**, M., Jilbert, T., Behrends, T., Rivard, C., Slomp, C.P., 2015. Vivianite is a major sink for phosphorus in methanogenic coastal surface sediments. Geochimica et Cosmochimica Acta. 169, 217–235.

**Elderfield**, H., Hawkeswirth, C.J., Greaves, M.J., Calvert, S.E., 1981. Rare earth element geochemistry of oceanic ferromanganese nodules and associated sediments. Geochimica et Cosmochimica Acta. 45, 513–528.

**Falkowski**, P.G., 1997. Evolution of the nitrogen cycle and its influence on the biological sequestration of $CO_2$ in the ocean. Nature. 387, 272–275.

**Faure**, G., Mensing, T.M., 2005. Isotopes: Principles and Applications. third edition. John Willey and Sons, Inc., Hoboken NJ.

**Fennel**, K., Follows, M., Falkowski, P.G., 2005. The coevolution of the nitrogen, carbon and oxygen cycles in the Proterozoic ocean. American Journal of Science. 305, 526–545.

**Filippelli**, G.M., Delaney, M.L., 1996. Phosphorus geochemistry of equatorial Pacific sediments. Geochimica et Cosmochimica Acta. 60, 1479–1495.

**Föllmi**, K.B., 1996. The phosphorus cycle, phosphogenesis and marine phosphate-rich deposits. Earth-Science Reviews. 40, 55–124.

**Frank**, J. R., Carpenter, A. B., Oglesby, T. W., 1982. Cathodoluminescence and composition of calcite cement in the Taum Sauk Limestone (Upper Cambrian), Southeast Missouri. Journal of Sedimentary Research. 52, 631–638.

**Frimmel**, H. E., 2009. Trace element distribution in Neoproterozoic carbonates as palaeoenvironmental indicator. Chemical Geology. 258(3-4), 338–353.

**Fry**, B., Jannasch, H.W., Molyneaux, S.J., Wirsen, C.O., Muramoto, J.A., King. S., 1991. Stable isotope studies of the carbon, nitrogen and sulfur cycles in the Black Sea and the Cariaco Trench. Deep-Sea Research. 38, 1003–1019.

**Gaillardet**, J., Viers, J., Dupré, B., 2003. Trace elements in river waters. Treatise on geochemistry. 5, 225–272.

**Gall**, L., Williams, H., Siebert, C., Halliday, A., Herrington, R., Hein, J., 2013. Nickel isotopic compositions of ferromanganese crusts and the constancy of deep ocean inputs and continental weathering effects over the Cenozoic. Earth Planet. Sci. Lett. 375, 148–155.

**Ganai**, J.A., Rashid, S.A., Romshoo, S.A., 2018. Evaluation of terrigenous input, diagenetic alteration and depositional conditions of Lower Carboniferous carbonates of Tethys Himalaya, India. Solid Earth Sciences. 3, 33–49.

**Gao**, Y., Zhang, X., Zhang, G., Chen, Kefan., Shen, Y., 2018. Ediacaran negative C-isotopic excursions associated with phosphogenic events: Evidence from South China. Precambrian Research. 307, 218–228.

Gavalas, N.A., Clark, H.E., 1971. On the role of manganese in photosynthesis. Plant Physiology. 47, 139–143.

**George**, A.D., 1999. Deep-water Stromatolites, Canning Basin, Northwestern Australia. PALAIOS. 14, 493–505.

**German**, C.R., Elderfield, H., 1990. Application of the Ce Anomaly as a Paleoredox Indicator: The Ground Rules. Paleoceanography. 5(5), 823–833.

**Govin**, A., Holzwarth, U., Heslop, D., Keeling, L.F., Zabel, M., Mulitza, S., Collins, J.A., Chiessi, C.M., 2012. Distribution of major elements in Atlantic surface sediments (36°N–

49°S): Imprint of terrigenous input and continental weathering. Geochemistry, Geophysics, Geosystems. 13,1525–2027.

**Gregg**, J.M., Shelton K.L., 1989, Minor and trace element distributions in the Bonneterre Dolomite (Cambrian), southeast Missouri — Evidence for possible multiple basin fluid sources and pathways during lead zinc mineralization. Geological Society of America Bulletin. 101, 221–230.

**Hagedorn**, B., Cartwright, I., Raveggi, M., Maas, R. 2011. Rare earth element and strontium geochemistry of the Australian Victorian Alps drainage system: Evaluating the dominance of carbonate vs. aluminosilicate weathering under varying runoff. Chemical Geology. 284, 105–126.

**Halverson,** G.P., Hoffman, P.F., Schrag, D.P., Maloof, A.C., Rice, A.H.N., 2005. Toward a Neoproterozoic composite carbon-isotope record. Geological Society of America Bulletin. 117, 1181–1207.

**Hannigan**, R., Dorval, E., Jones, C., 2010. The rare earth element chemistry of estuarine surface sediments in the Chesapeake Bay. Chemical Geology. 272(1), 20–30.

**Hatch,** J.R., Leventhal, J.S., 1992. Relationship between inferred redox potential of the depositional environment and geochemistry of the Upper Pennsylvanian (Missourian) Stark Shale Member of the Dennis Limestone, Wabaunsee Country, Kansas, U.S.A. Chemical Geology. 99, 65–82.

**Herrmann**, A.D., Kendall, B., Algeo, T.J., Gordon, G.W., Wasylenki, L.E., Anbar, A.D., 2012. Anomalous molybdenum isotope trends in Upper Pennsylvanian euxinic facies:

significance for use of $\delta^{98}$Mo as a global marine redox proxy. Chemical Geology. 324–325, 87–98.

**Holland**, H.D., Holland, J.J., Munoz, J.L., 1964. The coprecipitation of cations with $CaCO_3$ - II. The coprecipitation of $Sr^{2+}$ with aragonite and of $Ca^{2+}$ with strontianite between 90 and 100 ℃. Geochimica et Cosmochimica Acta. 28, 1287–1302.

**Hua**, G., Yuansheng, D., Lian, Z., Jianghai, Y., Hu, H., 2012. Trace and rare earth elemental geochemistry of carbonate succession in the Middle Gaoyuzhuang Formation, Pingquan Section: Implications for Early Mesoproterozoic ocean redox conditions. Journal of Palaeogeography. 2, 209–221.

**Ichikuni,** M., 1973. Partition of strontium between calcite and solution: effect of substitution by manganese. Chemical Geology. 11, 315–319.

**James**, N.P., Stevens, P.K., 1986. Stratigraphy and correlation of the Cambro-Ordovician Cow Head Group, western Newfoundland. Geological Survey of Canada Bulletin. 366, 1–143.

**James**, N.P., Stevens, R.K., Barnes, C.R., Knight, I., 1989. Evolution of a Lower Paleozoic continental margin carbonate platform, northern Canadian Appalachians. The Society of Economic Paleontologists and Mineralogists, Special Publication 44.

**Jiang**, G., Wang, X., Shi, X., Xiao, S., Zhang, S., Dong, J., 2012. The origin of decoupled carbonate and organic carbon isotope signatures in the early Cambrian (ca. 542–520 Ma) Yangtze platform. Earth and Planetary Science Letters. 317–318, 96–110.

**Johannesson**, K.H., Chevis, D.A., Burdige, D.J., Cable, JE., Martin, J. B., Roy, M., 2011. Submarine groundwater discharge is an important net source of light and middle REEs to coastal waters of the Indian River Lagoon, Florida, USA. Geochimica et Cosmochimica Acta. 75(3), 825–843.

**Kimbell**, T.N., Humphrey, J.D., 1994. Geochemistry and crystal morphology of aragonite cements of mixing-zone origin, Barbados, West Indies. Journal of Sedimentary Research. 64, 604–614.

**Kimura**, H., Azmy, K., Yamamuro, M., Zhi-Wen, J., Cizdziel, J.V., 2005. Integrated stratigraphy of the Upper Proterozoic succession in Yunnan of South China: re-evaluation of global correlation and carbon cycle. Precambrian Research. 138, 1–36.

**Kinsman**, D.J.J., 1969. Interpretation of $Sr^{2+}$ concentrations in carbonate minerals and rocks. Journal of Sedimentary Petrology. 39, 486–508.

**Knight,** I., Azmy, K., Greene, M., Lavoie, D., 2007. Lithostratigraphic setting of diagenetic, isotopic, and geochemistry studies of Ibexian and Whiterockian carbonates of the St. George and Table Head groups in western Newfoundland. Current Research Newfoundland and Labrador Department of Natural Resources Geological Survey. 7(1), 55–84.

**Kump**, L.R., Junium, C., Arthur, M.A., Brasier, A., Fallick, A., Melezhik, V.A., Lepland, A., Crne, A.E., Luo, G., 2011. Isotopic evidence for massive oxidation of organic matter following the great oxidation event. Science (New York). 334, 1694–1696.

**Landing**, E., 2007. Ediacaran–Ordovician of east Laurentia – geologic setting and controls on deposition along the New York Promontory. New York State Museum Bulletin. 510.

**Landing**, E., 2012. Time-specific black mudstones and global hyperwarming on the Cambrian–Ordovician slope and shelf of the Laurentia. Palaeogeography, Palaeoclimatology. Palaeoecology. 367–368, 256–272.

**Landing**, E., 2013. The Great American Carbonate Bank in northeast Laurentia: its births, deaths, and linkage to continental slope oxygenation (Early Cambrian–Late Ordovician). American Association of Petroleum Geologists Bulletin. Memoir 98, 451–492.

**Landing**, E., Geyer, G., Bartowski, K.E., 2002. Latest Early Cambrian small shelly fossils, trilobites, and Hatch Hill dysaerobic interval on the east Laurentian continental slope. Journal of Paleontology. 76, 285–303.

**Landing**, E., Webster, M., 2018. Iapetan Rift–Passive Margin Transition in NE Laurentia and Eustatic Control on Continental Slope Oxygenation, Taconic Slate Colors, and Early Paleozoic Climate. Guidebook the Field Trips in New York, Vermont, and Massachusetts.

**Landing**, W.M., Bruland, K.W., 1987. The contrasting biogeochemistry of iron and manganese in the Pacific Ocean. Geochimica et Cosmochimica Act. 51(1), 29–43.

**Latimer**, J.C., Filippelli, G.M., 2002. Eocene to Miocene terrigenous inputs and export production: geochemical evidence from ODP Leg 177, Site 1090. Palaeogeography, Palaeoclimatology, Palaeoecology. 182, 151–164.

**Lavoie**, D., Desrochers, A., Dix, G., Knight, A., Hersi, O.S., 2013. The great carbonate Bank in eastern Canada: an overview. In: Derby, J., Fritz, R., Longcare, S., Morgan, W., Sternbach, C. (Eds.), The Great American Carbonate Bank: The Geology and Economic Resources of Cambrian–Ordovician Sauk Megasequence of Laurentia. American Association of Petroleum Geologists. Memoir 98, 499–524.

**Li**, D., Zhang, X., Chen, K., Zhang, G., Chen, X., Huang, W., Peng,S., Shen, Y., 2017. High-resolution Cisotope chemostratigraphy of the uppermost Cambrian stage (Stage 10) in South China: implications for defining the base of Stage 10 and palaeoenvironmental change. Geological Magazine. 1, 1–12.

**Ling**, H.F., Chen, X., Li, D., Wang, D., Shields-Zhou, G.A., Zhu, M.Y., 2011. Cerium anomaly variations in Ediacaran–earliest Cambrian carbonates from the Yangtze Gorges area, South China: implications for oxygenation of coeval shallow seawater. Precambrian Research. 225, 110–127.

**Lorens**, R.B., 1981. Sr, Cd, Mn and Co distribution coefficients in calcite as a function of calcite precipitation rate. Geochimica et Cosmochimica Acta. 45, 553–561.

**Ludvigsen**, R., 1982. Upper Cambrian and Lower Ordovician trilobite biostratigraphy of the Rabbitkettle Formation, western District of Mackenzie. Royal Ontario Museum, Life Sciences Division. pp. 188.

**Ma**, W.W., Zhu, M.X., Yang, G.P., Li, T., 2018. Iron geochemistry and organic carbon preservation by iron (oxyhydr) oxides in surface sediments of the East China Sea and the south Yellow Sea. Journal of Marine Systems. 178, 62–74.

**Machel**, H.G., 1985. Facies and diagenesis of the Upper Devonian Nisku Formation in the subsurface of Alberta. McGill University, Montreal. pp. 392.

**Machel**, H. G., 2000. Application of cathodoluminescence to carbonate diagenesis. In: Pagle, M., Barbin, V., Balnc, P., Ohnenstetter, D., (Eds.), Cathodoluminescence in geosciences. Springer, Berlin Heidelberg. pp. 271–301.

**Machel**, H.G., Burton, E.A., 1991. Factors governing cathodoluminescence in calcite and dolomite, and their implications for studies of carbonate diagenesis. Luminescence Microscopy and Spectroscopy, Qualitative and Quantitative Applications. SEPM Short Course. 25, 37–57.

**Macko**, S.A., Engel, M.H., Parker, P.L., 1993. Early diagenesis of organic matter in sediments: assessment of mechanisms and preservation by the use of isotopic molecular approaches. Organic Geochemistry. pp. 211–224.

**McLennan**, S.B., 1989. Rare earth elements in sedimentary rocks. Influence of provenance and sedimentary processes. Mineralogical Society of America, Washington. pp, 169-200.

**McLennan**, S.M., 2001. Relationships between the trace element composition of sedimentary rocks and upper continental crust. Geochemistry, Geophysics, Geosystems. 2(4).

**Meyers**, P.A., 1994. Preservation of elemental and isotopic source identification of sedimentary organic matter. Chemical Geology. 144, 289–302.

**Meyers**, P.A., Lallier-Vergès, E., 1999. Lacustrine sedimentary organic matter records of Late Quaternary paleoclimates. Journal of Paleolimnology. 21, 345–372.

**Miller**, J.F., Evans, K.R., Freeman, R.L., Ripperdan, R.L., Taylor, J.F., 2011. Proposed stratotype for the base of the Lawsonian Stage (Cambrian Stage 10) at the first appearance datum of *Econodontus notchpeakensis* (Miller) in the house Range, Utah, USA. Bulletin of Geosciences. 86, 595–620.

**Miller**, J.F., Repetski, J.E., Nicoll, R.S., Nowlan, G., Ethington, R.L., 2014. The conodont *Iapetognathus* and its value for defining the base of the Ordovician System. Geologiska Foreningens i Stockholm Forhandlingar. 136, 185–188.

**Milliman**, J. D., Syvitski, J.P.M., 1992. Geomorphic/tectonic control of sediment discharge to the ocean: The importance of small mountainous rivers. The Journal of Geology. 100, 525–544.

**Milliman**, J. D., Summerhayes, C.P., Barretto, H.T., 1975. Quaternary sedimentation on the Amazon continental margin: A model. Geological Society of America Bulletin. 86, 610–614.

**Morel**, F.M.M., Milligan, A.J., Saito, M.A., 2004. Marine bioinorganic chemistry: the role of trace metals in the oceanic cycles of major nutrients. The Oceans and Marine Geochemistry, Treatise on Geochemistry. 6, 113–143.

**Morrison,** J.O., Brand, U., 1986. Geochemistry of recent marine invertebrates. Geoscience Canada. 13, 237–253.

**Murphy**, A.E., Sageman, B.B., Hollander, D.J., Lyons, D.J., Brett, C.E., 2000. Black shale deposition and faunal overturn in the Devonian Appalachian Basin: clastic starvation, seasonal water-column mixing, and efficient biolimiting nutrient recycling. Paleoceanography. 15, 280–291.

**Nakada**, R., Takahashi, Y., Tanimizu, M., 2013. Isotopic and speciation study on cerium during its solid–water distribution with implication for Ce stable isotope as a paleo-redox proxy. Geochimica et Cosmochimica Acta. 103, 49–62.

**Nath**, B.N., Roelandts, I., Sudhakar, M., Pluger, W., 1992. Rare earth element patterns of the Central Indian Basin sediment related to their lithology. Geophysical Research Letters. 19, 1197–2000.

**Parish**, C.M., Russell, P.E., 2007. Scanning Cathodoluminescence Microscopy. Advance in Imaging and Electron Physics. 147.

**Pattan**, J.N., Pearce, N.J.G., Mislankar, P.G., 2005. Constraints in using cerium anomaly of bulk sediments as an indicator of paleo bottom water redox environment: a case study from the Central Indian Ocean Basin. Chemical Geology. 221, 260–278.

**Pattan**, J.N., Mir, I.A., Parthiban, G., Karapurkar, S.G., Matta, V.M., Naidu, P.D., Naqvi, S.W.A., 2013. Coupling between suboxic condition in sediments of the western Bay of Bengal and southwest monsoon intensification: a geochemical study. Chemistry Geology. 343, 55–66.

**Peacock**, C.L., Sherman, D.M., 2007. Sorption of Ni by birnessite: equilibrium controls on Ni in seawater. Chemical Geology. 238, 94–106.

**Pham**, A.N., Rose, A.L., Feitz, A.J., Waite, T.D., 2006. Kinetics of Fe (III) precipitation in aqueous solutions at pH 6.0–9.5 and 25 ℃. Geochimica et cosmochimica Acta. 70, 640–650.

**Piepgras**, D.J., Jacobsen, S.B., 1992. The behavior of rare earth elements in seawater: Precise determination of variations in the North Pacific water column. Geochimica et Cosmochimica Acta. 56, 1851–1862.

**Piper**, D.Z., Calvert, S.E., 2009. A marine biogeochemical perspective on black shale deposition. Earth Science Reviews. 95, 63–96.

**Popp**, B.N., Parekh, P., Tilbrook, B., Bidigare, R.R., Laws, E.A., 1997. Organic carbon $\delta^{13}C$ variations in sedimentary rocks as chemostratigraphic and paleoenvironmental tools. Palaeogeography, Palaeoclimatology, Palaeoecology. 132, 119–132.

**Della Porta**, G., Kenter, J.A.M., Bahamonde, J.R., Immenhauser, A., Villa, E., 2003. Microbial Boundstone Dominated Carbonate Slope (Upper Carboniferous, N Spain): Microfacies, Lithofacies Distribution and Stratal Geometry. Facies. 49, 195–207.

**Quan**, T.M., Van de Schootbrugge, B., Field, M.P., Rosenthal, Y., Falkowski, P.G., 2008. Nitrogen isotope and trace metal analyses from the Mingolsheim core (Germany): evidence for redox variations across the Triassic–Jurassic boundary. Global Biogeochemistry Cycles. 22.

**Quan**, T.M., Wright, J.D., Falkowski, P.G., 2013. Co-variation of nitrogen isotopes and redo states through glacial–interglacial cycles in the Black Sea. Geochimica et Cosmochimica Acta. 112, 305–320.

**Ragsdale**, S.W., 2009. Nickel-based enzyme systems. Journal of Biological Chemistry. 284, 18571–18575.

**Raiswell**, R., Canfield, D.E., 2012. The iron biogeochemical cycle past and present. Geochemical Prospective. 1, 1–220.

**Rao**, C.P., Adabi, M.H., 1992. Carbonate minerals, major and minor elements and oxygen and carbon isotopes and their variation with water depth in cool, temperate carbonates, western Tasmania, Australia. Marine Geology. 103, 249–272.

**Ren**, H., Sigman, D.M., Martínez-Garcíac, A., Anderson, R.F., Chen, M., Ravelo, A.C., Straub, M., Wong, G.T.F., Haug, G.H., 2017. Impact of glacial/interglacial sea level change on the ocean nitrogen cycle. the National Academy of Sciences of the United States of America. 114(33), 6759–6766

**Richter**, D.K., Füchtbauer, H., 1978. Ferroan calcite replacement indicates former magnesian calcite skeletons. sedimentology. 25, 843–860.

**Ripperdan**, R.L., Magaritz, M., Kirschvink, J. L., 1993. Carbon isotope and magnetic polarity evidence for non-depositional events within the Cambrian–Ordovician boundary section at Dayangcha. Jilin Province, China. Geological Magazine. 130, 443–52.

**Rue**, E.L., Smith, G.J., Cutter, G.A., 1997. The response of trace element redox couples to suboxic conditions in the water column. Deep-sea Research I. 44, 113–434.

**Rush**, P.F., Chafetz, H.S., 1990. Fabric retentive, non-luminescent brachiopods as indicators of original $\delta^{13}C$ and $\delta^{18}O$ compositions: a test. Journal of Sedimentary Research. 60, 968–981.

**Ruttenberg**, K.C., Berner, R.A., 1993. Authigenic apatite formation and burial in sediments from non-upwelling continental margin environments. Geochimica et Cosmochimica Acta. 57, 991–1007.

**Ryu**, J.S., Lee, K.S., Lee, S.G., Lee, D., and Changd H.W., 2007. Seasonal and spatial variations of rare earth elements in rain waters, river waters and total suspended particles in air in South Korea. Journal of Alloys and Compounds. 437, 344–350.

**Saino**, T., Hattori, A., 1980. $^{15}N$ natural abundance in oceanic suspended particulate matter. Nature. 283, 752–754.

**Schidlowski**, M., Matzigkeit, U., Krumbein, W.E., 1984. Superheavy organic carbon from hypersaline microbil mats: assimatory pathway and geochemical implications. Naturwisesenschaften. 71, 303–308.

**Schlager**, W., 2005. Carbonate Sedimentology and Sequence Stratigraphy. SEPM Concepts in Sedimentology and Paleontology. 8, 200.

**Schmidt**, K., Garbe–Schönberg, D., Bau, M., Koschinsky, A., 2010. Rare earth element distribution in> 400 C hot hydrothermal fluids from 5S, MAR: The role of anhydrite in controlling highly variable distribution patterns. Geochimica et Cosmochimica Acta. 74(14), 4058–4077.

**Schuchert**, C., Dunbar, C.O., 1934. Stratigraphy of western Newfoundland. Geological society of America., Washington, D.C.

**Sholkovitz**, E.R., Szymczak, R., 2000. The estuarine chemistry of rare earth elements: comparison of the Amazon, Fly, Sepik and the Gulf of Papua systems. Earth and Planetary Science Letters. 179(2), 299–309.

Sigman, D.M., Karsh, K.L., Casciotti, K.L., 2009. Ocean process tracers: Nitrogen isotopes in the ocean. Encyclopedia of ocean science. Elsevier. Amsterdam. pp. 4138–4153.

**Sippel**, R. F., 1968. Sandstone petrology, evidence from luminescence petrography. Journal of Sedimentary Research. 38, 530–554.

**Śliwiński**, M.G., Whalen, M.T., Day, J., 2010. Trace element variations in the Middle Frasnian punctata zone (Late Devonian) in the western Canada sedimentary Basin—changes in oceanic bioproductivity and paleoredox spurred by a pulse of terrestrial afforestation? Geologica Belgica. 4, 459–482.

**Sprunt**, E.S., Nur, A., 1979. Microcracking and healing in granites: new evidence from cathodoluminescence. Science. 205, 495–497.

**Stiehl**, G., Lehmann, M., 1980. Isotopenvariationen des Stickstoffs humoser und bituminöser natürlicher organischer Substanzen. Geochmica et cosmochimica Acta. 44, 1737–1746.

**Sunagawam**, U., Takahashi, Y., Imai, H., 2007. Strontium and aragonite-calcite precipitation. Journal of Mineralogical and Petrological Sciences. 102, 174─181.

**Sunda**, W.G., Huntsman, S.A., Harvey, G.R., 1983. Photoreduction of manganese oxides in seawater and its geochemical and biological implications. Nature. 301, 20.

**Talbot**, M.R., Laerdal, T., 2000. The lake Pleistocene–Holocene paleolimnology of Late Victoria East Africa based upon elemental and isotopic analyses of sedimentary organic matter. Journal of Paleolimnology. 23, 141–164.

**Tebo**, B.M., Bargar, J.R., Clement, B.G., Dick, G.J., Murray, K.J., Parker, D., Veity, R., Webb, S.M., 2004. Biogenic manganese oxides: properties and mechanisms of formation. Annual Reviews of Earth Planetary Science. 32, 287–328.

**Terfelt**, F., Bagnoli, G., Stouge, S., 2012. Re-evaluation of the conodont *Iapetognathus* and implications for the base of the Ordovician System GSSP. Lethaia. 45, 227–237.

**Terfelt**, F., Eriksson, M.E., Schmitz, B., 2014. The Cambrian–Ordovician transition in dysoxic facies in Baltica—diverse faunas and carbon isotope anomalies. Palaeogeography, Palaeoclimatology, Palaeoecology. 394, 59–73.

**Theissen**, K.M., Dunbar, R.B., Cooper, A.K., 2003. Stable isotopic measurements of sedimentary organic matter and N. *Pachyderma* (S.) from Site 1166, Prydz Bay continental shelf. Proceedings of the Ocean Drilling Program, Scientific Results. 188, 1–11.

**Towe**, K.M., 1991. Aerobic carbon cycling and cerium oxidation: Significance for Archean oxygen levels and banded iron-formation deposition. Palaeogeography, Palaeoclimatology, Palaeoecology. 97, 113–123.

**Tribovillard**, N., Algeo, T.J., Lyons, T., Riboulleau, A., 2006. Trace metals as paleoredox and paleoproductivity proxies: an update. Chemical Geology. 232, 12–32.

**Tripathy**, G.R., Singh, S.K., Ramaswamy, V., 2014. Major and trace element geochemistry of Bay of Bengal sediments: Implications to provenances and their controlling factors. Palaeogeography, Palaeoclimatology, Palaeoecology. 397, 20–30.

**Vance**, D., Little, S.H., Archer, C., Cameron, V., Andersen, M.B., Rijkenberg, M.J.A., Lyons, T.W., 2016. The oceanic budgets of nickel and zinc isotopes: the importance of sulfidic environments as illustrated by the Black Sea. Philos. Philosophical Transactions of the Royal Society A: Mathematical, Physical and Engineering Sciences. 374, 20150294.

**Veizer**, J., 1974. Chemical diagenesis of belemnite shells and possible consequences for paleotemperature determinations: Neues Jahrb. Geology and Palaontology, Abh 145, 279–305.

**Veizer**, J., 1983. Chemical diagenesis of carbonates. Society of Economic Paleontologists and Mineralogists (SEPM), Stable Isotope in Sedimentary geology (SC10), Short Course Notes. 10, III–1–III–100.

**Veizer**, J., Ala, D., Azmy, K., Bruckschen, P., Bruhn, F., Buhl, D., Carden, G., Diener, A., Ebneth, S., Goddris, Y., Jasper, T., Korte, C., Pawellek, F., Podlaha, O., Strauss, H., 1999. $^{87}Sr/^{86}Sr$, $\delta^{18}O$ and $\delta^{13}C$ evolution of Phanerozoic seawater. Chemical Geology. 161, 59–88.

**Ward**, B.B., Olson, R.J., Perry, M.J., 1982. Microbial nitrification rates in the primary nitrite maximum off Southern California. Deep-Sea Research. 29, 247–55.

**Weaver**, F.J., Macko, S.A., 1988. Source rocks of western Newfoundland. Organic Geochemistry. 13, 411–421.

**Webb**, G.E., Nothdurft, L.D., Kamber, B.S., Kloprogge, J.T., Zhao, J.X., 2009. Rare earth element geochemistry of scleractinian coral skeleton during meteoric diagenesis: a sequence through neomorphism of aragonite to calcite. Sedimentology. 56, 1433–1463.

**Webb**, G.E., Kamber, B.S., 2000. Rare Earth elements in Holocene reefal microbialites: a new shallow seawater proxy. Geochimicu et Cosmochimica Acta. 64, 1557–1565.

**Wignall**, P.B., Twitchett, R.J., 1996. Oceanic anoxia and the end Permian mass extinction. Science. 272, 1155–1158.

**Wignall**, P.B., Zonneveld, J.P., Newton, R.J., Amor, K., Sephton, M.A., Hartley, S., 2007. The end Triassic mass extinction record of Williston Lake, British Columbia. Palaeogeography, Palaeoclimatology, Palaeoecology. 253, 385–406.

**Wilson**, J.L., Medlock, P.L., Fritz, R.D., Canter, K.L., Geesaman, R.G., 1992. A review of Cambro-Ordovician breccias in North America. Paleokarst, Karst-Related Diagenesis and Reservoir Development. Permian Basin Section, Society of Economic Paleontologists and Mineralogists (SEPM). 92(33), 19–29.

**Yamaguchi**, K.E., Ogurim, K., Ogawa, N.O., Sakai, S., Hirano, S., Kitazato, H., Ohkouchi, N., 2010. Geochemistry of modern carbonaceous sediments overlain by a water mass showing photic zone anoxia in the saline meromictic Lake Kai-ike, southwest

Japan: I. Early diagenesis of organic carbon, nitrogen, and phosphorus. Palaeogeography, Palaeoclimatology, Palaeoecology. 294, 72–82.

**Yarincik**, K.M., Murray, R.W., Lyons, T.W., Peterson, L.C., Haug, G.H., 2000. Oxygenation history of bottom waters in the Cariaco Basin, Venezuela, over the past 578,000 years: results from redox-sensitive metals (Mo, V, Mn and Fe). Paleoceanography. 15, 593–604.

**Yool**, A., Martin, A.P., Fernandez, C., Clark, D.R., 2007. The significance of nitrification for oceanic new production. Nature. 447, 999–1002.

**Zhang**, J., Nozaki, Y., 1998. Behavior of rare earth elements in seawater at the ocean margin: A study along the slopes of the Sagami and Nankai troughs near Japan. Geochimica et Cosmochimica Acta. 62(8), 1307–1317.

**Zhao**, M.Y., Zheng, Y.F., 2014. Marine carbonate records of terrigenous input into Paleotethyan seawater: Geochemical constraints from Carboniferous limestones. Geochimica et Cosmochimica Acta. 141, 508–531.

**Appendix.** Isotopic and elemental compositions of Martin Point carbonates. The $\delta^{13}C_{carb}$, Th/U and Ni data are from Azmy (2018). Trace elements and rare earth elements concentrations in ppm.

| Sample id | $\delta^{13}C_{carb}$ (‰ VPDB) | $\delta^{13}C_{org}$ (‰ VPDB) | TOC wt. % | $\delta^{15}N_{org}$ (‰ Air) | $CaCO_3$ wt. % | $MgCO_3$ wt. % | Al | Si | Fe | Mn | Sr | P | Ni | Th | U |
|---|---|---|---|---|---|---|---|---|---|---|---|---|---|---|---|
| **Cambrian-Ordovician boundary** | | | | | | | | | | | | | | | |
| **MP16** | -0.9 | -28.06 | 0.07 | 3.52 | 98.7 | 1.3 | 1158.1 | 2663.1 | 1598.3 | 648.6 | 228.9 | 93.2 | 2.0 | 0.53 | 1.56 |
| **MP17** | -0.8 | -28.36 | 0.03 | 3.22 | | | | | | | | | | | |
| **MP18** | 0.1 | | | | | | | | | | | | | | |
| **MP19** | 0.2 | -29.22 | 0.53 | 1.02 | 98.6 | 1.4 | 945.6 | 2061.7 | 1072.8 | 186.8 | 290.8 | 125.4 | 2.1 | 0.49 | 0.80 |
| **MP20** | -1.3 | -28.1 | 0.14 | 4.11 | 96.3 | 3.7 | 3546.7 | 5111.7 | 5594.1 | 297.2 | 151.5 | 173.1 | 3.4 | | |
| **MP21** | 0.1 | | | | | | | | | | | | | | |
| **MP22** | 0.1 | -29.06 | 0.24 | | 98.3 | 1.7 | 2004.4 | 4551.5 | 2714.9 | 141.6 | 274.5 | 175.3 | 2.9 | 0.70 | 1.65 |
| **MP23** | -0.6 | -29.02 | 0.10 | | 98.3 | 1.7 | 1326.8 | 3160.3 | 1567.6 | 300.6 | 301.3 | 141.7 | 1.4 | 0.32 | 0.63 |
| **MP24** | 0.5 | -29.62 | 0.34 | | | | | | | | | | | | |
| **MP25** | 0.1 | -27.12 | 0.13 | 2.91 | | | | | | | | | | | |
| **MP26** | 1.0 | -28.04 | 0.12 | 2.69 | 99.0 | 1.0 | 633.9 | 1393.7 | 905.9 | 168.9 | 247.2 | 119.5 | 2.0 | 0.24 | 0.32 |
| **MP27** | 0.3 | -29.26 | 0.17 | | | | | | | | | | | | |
| **MP28** | 0.3 | | | | 98.8 | 1.2 | 3364.3 | 2289.6 | 1413.7 | 586.2 | 283.0 | 180.4 | 2.8 | 0.24 | 0.35 |
| **MP29** | 0.5 | | | | | | | | | | | | | | |
| **MP30** | 0.7 | -28.9 | 0.13 | | 98.9 | 1.1 | 822.7 | 1744.3 | 928.4 | 200.9 | 284.3 | 120.6 | 2.4 | 0.22 | 0.83 |
| **HERB interval** | | | | | | | | | | | | | | | |
| **MH1** | 0.6 | -30.41 | 0.11 | 2.98 | 98.5 | 1.5 | 1346.5 | 2119.8 | 1545.8 | 150.0 | 687.4 | 125.9 | 3.1 | 0.58 | 0.35 |
| **MH2** | 0.1 | -29.49 | 0.07 | 3.93 | | | | | | | | | | | |
| **MH3** | -0.7 | -29.10 | 0.07 | | 98.6 | 1.4 | 1668.1 | 2446.5 | 2477.9 | 335.1 | 536.4 | 182.6 | 3.6 | 0.66 | 0.41 |
| **MH4** | -0.1 | -29.54 | 0.08 | 3.47 | | | | | | | | | | | |
| **MH5** | -0.3 | -28.63 | 0.12 | 3.67 | 98.2 | 1.8 | 613.6 | 1245.7 | 2747.4 | 253.4 | 979.8 | 251.9 | 4.1 | 0.24 | 0.19 |
| **MH6** | -1.1 | -28.70 | 0.06 | | | | | | | | | | | | |

| | | | | | | | | | | | | | | | |
|---|---|---|---|---|---|---|---|---|---|---|---|---|---|---|---|
| **MH7** | -1.9 | -28.18 | 0.06 | 3.99 | 98.5 | 1.5 | 1785.1 | 3097.6 | 4603.7 | 271.4 | 596.4 | 85.3 | 3.9 | 0.61 | 0.22 |
| **MH8** | -1.7 | | | | | | | | | | | | | | |
| **MH9** | -1.7 | -27.95 | 0.07 | 3.91 | 98.4 | 1.6 | 1966.6 | 3164.6 | 4932.1 | 338.9 | 498.2 | 123.4 | 5.2 | 0.85 | 0.22 |
| **MH10** | -1.7 | | | | | | | | | | | | | | |
| **MH11** | -1.9 | -28.32 | 0.08 | 4.95 | 98.2 | 1.8 | 2672.2 | 3433.0 | 5200.6 | 433.0 | 233.5 | 145.3 | 6.3 | 2.15 | 0.43 |
| **MH12** | -0.7 | -30.42 | 0.39 | 2.74 | | | | | | | | | | | |
| **MH13** | -1.2 | -27.78 | 0.02 | | | | | | | | | | | | |
| **MH14** | -1.3 | | | | | | | | | | | | | | |
| **MH15** | -1.4 | | | 3.72 | 97.9 | 2.1 | 3202.3 | 4478.2 | 6900.3 | 571.5 | 186.9 | 115.2 | 5.4 | 1.19 | 0.33 |
| **MH16** | -1.4 | -29.91 | 0.15 | 3.29 | | | | | | | | | | | |
| **MH17** | -1.1 | | | | | | | | | | | | | | |
| **MH18** | -0.6 | -30.51 | 0.12 | | 98.9 | 1.1 | 1037.7 | 2102.2 | 1325.6 | 386.8 | 216.4 | 128.5 | 8.5 | 0.55 | 1.98 |
| **MH19** | -2.1 | -27.97 | 0.12 | 2.93 | 97.2 | 2.8 | 2399.7 | 3329.4 | 3851.7 | 438.2 | 165.0 | 158.6 | 3.7 | 0.88 | 0.97 |
| **MH20** | -1.2 | | | | | | | | | | | | | | |
| **MH21** | -1.1 | -29.19 | 0.04 | | | | | | | | | | | | |
| **MH22** | -0.7 | -28.91 | 0.07 | 3.97 | | | | | | | | | | | |
| **MH23** | -0.7 | | | | | | | | | | | | | | |
| **MH24** | -0.6 | -29.16 | 0.05 | | 98.9 | 1.1 | 891.7 | 1697.8 | 1073.5 | 227.9 | 237.7 | 113.4 | 2.7 | 0.39 | 0.94 |
| **MH25** | -0.7 | -28.59 | 0.03 | 3.20 | | | | | | | | | | | |
| **MH26** | -0.2 | -28.46 | 0.12 | | | | | | | | | | | | |
| **MH27** | -0.8 | -28.31 | 0.02 | | | | | | | | | | | | |
| **MH28** | -0.3 | -29.01 | 0.03 | 2.59 | | | | | | | | | | | |
| **MH29** | -1.3 | | | 0.81 | 98.8 | 1.2 | 1103.2 | 2135.0 | 1465.3 | 562.0 | 217.8 | 142.1 | 2.7 | 0.43 | 3.57 |
| **MH30** | -1.1 | | | | | | | | | | | | | | |
| **MH31** | -0.2 | | | 2.13 | | | | | | | | | | | |
| **MH32** | 0.2 | -28.68 | 0.06 | 1.42 | 98.7 | 1.3 | 833.1 | 1621.1 | 1026.9 | 183.4 | 231.3 | 94.4 | 2.4 | 0.23 | 0.95 |
| **MH33** | -0.1 | -28.33 | 0.05 | | | | | | | | | | | | |

| | | | | | | | | | | | | | | | |
|---|---|---|---|---|---|---|---|---|---|---|---|---|---|---|---|
| **MP1** | -0.9 | -29.61 | 0.08 | | | | | | | | | | | | |
| **MP2** | -1.5 | -29.63 | 0.03 | | 98.8 | 1.2 | 819.7 | 1938.1 | 1027.4 | 291.5 | 310.1 | 85.9 | 1.9 | 0.14 | 0.82 |
| **MP3** | 0.1 | -29.61 | 0.09 | | | | | | | | | | | | |
| **MP4** | 0.3 | | | | | | | | | | | | | | |
| **MP5** | 0.6 | -28.51 | 0.17 | | 99.0 | 1.0 | 680.8 | 1431.7 | 904.2 | 523.1 | 249.9 | 150.1 | 2.1 | 0.21 | 1.60 |
| **MP6** | -0.7 | -29.39 | 0.07 | | | | | | | | | | | | |
| **MP7** | -0.3 | -29.45 | 0.06 | 2.72 | | | | | | | | | | | |
| **MP8** | -1.1 | -29.44 | 0.09 | 2.25 | 97.3 | 2.7 | 1991.9 | 3821.4 | 2335.6 | 360.3 | 262.2 | 205.2 | 3.6 | 0.58 | 2.14 |
| **MP9** | -0.5 | -28.2 | 0.05 | 2.52 | | | | | | | | | | | |
| **MP10** | 0.5 | -29.62 | 0.06 | | 98.9 | 1.1 | 794.1 | 1680.8 | 1018.9 | 569.0 | 247.5 | 191.4 | 2.3 | 0.27 | 0.75 |
| **MP11** | 0.2 | -29.86 | 0.73 | | | | | | | | | | | | |
| **MP12** | 0.3 | -29.29 | 0.14 | | | | | | | | | | | | |
| **MP13** | 0.8 | | | | | | | | | | | | | | |
| **MP14** | 1.0 | -29.58 | 0.09 | 2.39 | 99.0 | 1.0 | 611.0 | 1362.0 | 784.9 | 568.5 | 193.6 | 115.8 | 7.3 | 1.49 | 2.63 |
| **MP15** | 1.0 | -29.61 | 0.27 | | | | | | | | | | | | |

| Sample id | La | Ce | Pr | Nd | Sm | Eu | Gd | Tb | Dy | Ho | Er | Tm | Yb | Lu | ΣREE |
|---|---|---|---|---|---|---|---|---|---|---|---|---|---|---|---|
| **Cambrian–Ordovician boundary** | | | | | | | | | | | | | | | |
| **MP16** | 18.587 | 28.191 | 3.455 | 12.738 | 2.171 | 0.507 | 1.979 | 0.334 | 1.859 | 0.432 | 1.159 | 0.187 | 0.950 | 0.149 | 72.7 |
| **MP17** | | | | | | | | | | | | | | | |
| **MP18** | | | | | | | | | | | | | | | |
| **MP19** | 7.082 | 11.070 | 1.320 | 5.418 | 0.875 | 0.238 | 0.675 | 0.146 | 0.746 | 0.164 | 0.340 | 0.088 | 0.261 | 0.071 | 28.5 |
| **MP20** | 17.908 | 33.406 | 3.770 | 14.952 | 2.489 | 0.523 | 1.900 | 0.294 | 1.814 | 0.341 | 0.971 | 0.124 | 0.729 | 0.103 | 79.3 |
| **MP21** | | | | | | | | | | | | | | | |
| **MP22** | 15.910 | 28.042 | 2.916 | 11.336 | 1.992 | 0.478 | 1.630 | 0.202 | 1.625 | 0.342 | 0.927 | 0.130 | 0.690 | 0.104 | 66.3 |
| **MP23** | 4.662 | 6.870 | 0.855 | 3.083 | 0.679 | 0.113 | 0.604 | 0.076 | 0.440 | 0.126 | 0.278 | 0.051 | 0.145 | 0.036 | 18.0 |
| **MP24** | | | | | | | | | | | | | | | |
| **MP25** | | | | | | | | | | | | | | | |
| **MP26** | 5.182 | 8.817 | 1.082 | 3.840 | 0.674 | 0.185 | 0.440 | 0.078 | 0.569 | 0.118 | 0.268 | 0.044 | 0.214 | 0.044 | 21.6 |
| **MP27** | | | | | | | | | | | | | | | |
| **MP28** | 8.355 | 13.555 | 1.713 | 6.130 | 0.978 | 0.273 | 0.864 | 0.143 | 0.858 | 0.206 | 0.587 | 0.060 | 0.390 | 0.082 | 34.2 |
| **MP29** | | | | | | | | | | | | | | | |
| **MP30** | 4.974 | 7.801 | 0.900 | 3.518 | 0.599 | 0.104 | 0.504 | 0.081 | 0.445 | 0.102 | 0.200 | 0.024 | 0.168 | 0.024 | 19.4 |
| **HERB interval** | | | | | | | | | | | | | | | |
| **MH1** | 6.008 | 10.341 | 1.358 | 4.872 | 0.857 | 0.185 | 0.636 | 0.094 | 0.560 | 0.113 | 0.296 | 0.045 | 0.219 | 0.042 | 25.6 |
| **MH2** | | | | | | | | | | | | | | | |
| **MH3** | 11.272 | 20.795 | 2.207 | 8.624 | 1.247 | 0.287 | 1.347 | 0.190 | 1.175 | 0.297 | 0.901 | 0.125 | 0.618 | 0.093 | 49.2 |
| **MH4** | | | | | | | | | | | | | | | |
| **MH5** | 10.516 | 13.294 | 1.779 | 6.843 | 0.988 | 0.241 | 0.826 | 0.119 | 0.646 | 0.138 | 0.328 | 0.041 | 0.166 | 0.050 | 36.0 |
| **MH6** | | | | | | | | | | | | | | | |
| **MH7** | 12.797 | 20.602 | 2.378 | 9.035 | 1.425 | 0.297 | 1.148 | 0.167 | 1.029 | 0.211 | 0.578 | 0.090 | 0.504 | 0.052 | 50.3 |
| **MH8** | | | | | | | | | | | | | | | |
| **MH9** | 13.000 | 21.667 | 2.696 | 9.777 | 1.575 | 0.304 | 1.175 | 0.170 | 1.050 | 0.222 | 0.602 | 0.066 | 0.441 | 0.075 | 52.8 |

| | | | | | | | | | | | | | | | |
|---|---|---|---|---|---|---|---|---|---|---|---|---|---|---|---|
| **MH10** | | | | | | | | | | | | | | | |
| **MH11** | 20.912 | 33.001 | 3.900 | 14.833 | 2.421 | 0.564 | 1.947 | 0.323 | 1.671 | 0.414 | 0.915 | 0.207 | 0.692 | 0.181 | 82.0 |
| **MH12** | | | | | | | | | | | | | | | |
| **MH13** | | | | | | | | | | | | | | | |
| **MH14** | | | | | | | | | | | | | | | |
| **MH15** | 24.479 | 38.829 | 4.118 | 15.740 | 2.340 | 0.612 | 2.252 | 0.407 | 2.488 | 0.617 | 1.469 | 0.271 | 1.266 | 0.254 | 95.1 |
| **MH16** | | | | | | | | | | | | | | | |
| **MH17** | | | | | | | | | | | | | | | |
| **MH18** | 10.396 | 19.648 | 2.185 | 8.109 | 1.562 | 0.328 | 1.277 | 0.260 | 1.415 | 0.315 | 0.764 | 0.142 | 0.727 | 0.131 | 47.3 |
| **MH19** | 17.033 | 26.614 | 3.055 | 12.135 | 1.958 | 0.453 | 1.878 | 0.280 | 1.765 | 0.433 | 1.116 | 0.184 | 0.849 | 0.132 | 67.9 |
| **MH20** | | | | | | | | | | | | | | | |
| **MH21** | | | | | | | | | | | | | | | |
| **MH22** | | | | | | | | | | | | | | | |
| **MH23** | | | | | | | | | | | | | | | |
| **MH24** | 8.172 | 14.037 | 1.402 | 5.926 | 0.976 | 0.227 | 0.830 | 0.122 | 0.904 | 0.156 | 0.494 | 0.061 | 0.404 | 0.081 | 33.8 |
| **MH25** | | | | | | | | | | | | | | | |
| **MH26** | | | | | | | | | | | | | | | |
| **MH27** | | | | | | | | | | | | | | | |
| **MH28** | | | | | | | | | | | | | | | |
| **MH29** | 19.051 | 33.114 | 3.470 | 14.506 | 2.320 | 0.539 | 2.158 | 0.354 | 2.422 | 0.538 | 1.338 | 0.199 | 1.192 | 0.177 | 81.4 |
| **MH30** | | | | | | | | | | | | | | | |
| **MH31** | | | | | | | | | | | | | | | |
| **MH32** | 7.432 | 10.254 | 1.269 | 4.647 | 0.797 | 0.200 | 0.632 | 0.097 | 0.675 | 0.114 | 0.326 | 0.055 | 0.253 | 0.047 | 26.8 |
| **MH33** | | | | | | | | | | | | | | | |
| **MP1** | | | | | | | | | | | | | | | |
| **MP2** | 7.506 | 10.631 | 1.171 | 4.643 | 0.637 | 0.158 | 0.576 | 0.094 | 0.600 | 0.150 | 0.314 | 0.049 | 0.315 | 0.049 | 26.9 |
| **MP3** | | | | | | | | | | | | | | | |

| | | | | | | | | | | | | | | | |
|---|---|---|---|---|---|---|---|---|---|---|---|---|---|---|---|
| **MP4** | | | | | | | | | | | | | | | |
| **MP5** | 5.987 | 9.678 | 1.147 | 4.628 | 0.740 | 0.190 | 0.683 | 0.104 | 0.605 | 0.111 | 0.392 | 0.051 | 0.296 | 0.029 | 24.6 |
| **MP6** | | | | | | | | | | | | | | | |
| **MP7** | | | | | | | | | | | | | | | |
| **MP8** | 15.212 | 23.592 | 2.872 | 11.569 | 2.070 | 0.425 | 1.662 | 0.212 | 1.455 | 0.311 | 0.797 | 0.094 | 0.547 | 0.091 | 60.9 |
| **MP9** | | | | | | | | | | | | | | | |
| **MP10** | 7.329 | 11.216 | 1.411 | 5.629 | 0.891 | 0.210 | 0.615 | 0.115 | 0.701 | 0.147 | 0.375 | 0.051 | 0.251 | 0.052 | 29.0 |
| **MP11** | | | | | | | | | | | | | | | |
| **MP12** | | | | | | | | | | | | | | | |
| **MP13** | | | | | | | | | | | | | | | |
| **MP14** | 9.136 | 13.698 | 1.676 | 6.153 | 1.112 | 0.457 | 1.010 | 0.308 | 1.046 | 0.408 | 0.671 | 0.309 | 0.564 | 0.275 | 36.8 |
| **MP15** | | | | | | | | | | | | | | | |

# Chapter 6

## Paper published on Geological Journal

# Paleoenvironmental changes in slope carbonates across the Late Cambrian–Early Ordovician in western Newfoundland

Luyi Wang, Karem Azmy

Department of Earth Sciences, Memorial University of Newfoundland, St John's, Newfoundland

A1B 3X5, Canada

Correspondence

Luyi Wang, Department of Earth Sciences, Memorial University of Newfoundland, St John's, Newfoundland A1B 3X5, Canada. Email: luyiw@mun.ca

**ABSTRACT**

The Martin Point section (western Newfoundland, Canada) spans the uppermost Cambrian Broom Point and Martin Point members of the Green Point Formation (upper Furongian). The investigated interval (~ 90 m) consists of rhythmites of thinly-bedded marine carbonates (lime mudstones) alternating with green and black shale and thin conglomerate beds. Samples were extracted from the micritic carbonates and their preservation was evaluated by multiple petrographic and geochemical examinations. The $\delta^{13}C_{org}$ profile exhibits a positive shift (~ 2 ‰) associated with the globally well documented negative $\delta^{13}C_{carb}$ HERB (Hellnmaria – Red Tops Boundary) excursion and correlated with similar distinct shifts in the Al, Si, and ΣREE components, thus suggesting contributions from detrital organic matter relatively depleted in $^{12}C$ induced likely by an eustatic sea-level drop and enhancement of terrigenous inputs. Similarly, the $\delta^{15}N_{org}$ variations are consistent with the proposed sea-level drop. This is also correlated with positive shifts on the Fe and Mn profiles reflecting the overprint of terrigenous inputs rather than redox conditions.

KEYWORDS elemental proxies, HERB event, organic C- and N- isotope, redox condition, rhythmites, Upper Furongian, Western Newfoundland (Canada)

# 1 INTRODUCTION

The geochemistry of well-preserved carbonates has been a useful tool to better understand the paleoenvironmental conditions that prevailed during the Earth's history (e.g., Halverson, Hoffman, Schrag, Maloof & Rice, 2005; Śliwiński, Whalen & Day, 2010; Veizer et al., 1999; Wignall & Twitchett, 1996). Therefore, primary/near primary signatures are the essential factors to reconstruct the paleoenvironmental conditions.

Global sea-level variations during the late Cambrian not only influenced seawater redox condition and primary productivity (e.g., Azmy, Kendall, Brand, Stouge, & Gordon, 2015; Landing, 2012, 2013; Terfelt, Bagnoli, & Stouge, 2012; Terfelt, Eriksson, & Schmitz, 2014), but also altered the continental inputs and subsequently the contents of trace elements in marine deposits, which caused the change in P, Si, Al, U, Ni, and REE contents (e.g., Arnaboldi & Meyers, 2007; Murphy, Sageman, Hollander, Lyons, & Brett, 2000; Piper & Calvert, 2009; Wignall & Twitchett, 1996; Wignall et al., 2007). The increase of oxygen level in seawater is associated with oxidation of organic matter and consequently variations in the $\delta^{13}C$ of carbonates and in total organic content (TOC) and C- and N- isotope compositions of the organic matter (e.g., Kump et al., 2011; Quan, van de Schootbrugge, Field, Rosenthal, & Falkowski, 2008). Changes in redox conditions can be reflected by the uranium concentrations and Ce-anomalies of marine carbonates (e.g., Azmy et al., 2015; Bau & Dulski, 1996; Ling et al., 2011; Nakada, Takahashi & Tanimizu, 2013; Towe, 1991). The investigated interval of Martin Point consists of slope deposits of rhythmites of mainly alternating thinly-bedded lime mudstones and shales that were deposited under dysoxic (suboxic) conditions (e.g., Azmy et al., 2015; Azmy,

2018; James & Stevens, 1986; Landing, Geyer, & Bartowski, 2002; Landing, 2013). The main objectives of this study are:

(1) to investigate the C- and N- isotope compositions of the organic matter in the lime mudstone interbeds to better understand the control of sea-level changes on their signatures as paleoredox proxies during the late Cambrian, particularly the HERB event (Azmy, 2018; Landing, Westrop & Adrain, 2011; Miller, Evans, Freeman, Ripperdan & Taylor, 2011;) and reconstruct the global paleoenvironmental changes (climatic and oceanographic) that prevailed during that time interval (Buggisch, Keller & Lehnert, 2003; Li et al., 2017; Miller, Repetski, Nicoll, Nowlan & Ethington, 2014; Ripperdan, Magaritz & Kirschvink, 1993) and

(2) to investigate the influence of sea-level changes on trace element geochemistry of the seawater and consequently those carbonates caused by changes in terrestrial inputs and primary productivity.

## 2 GEOLOGICAL SETTING

The carbonates of the Martin Point Member constitute the lower part of the Green Point Formation, a part of the Cow Head Group, in western Newfoundland (within the northeast Canadian Appalachians), where they were deposited on the eastern Laurentian Margin (Figure 1; James, Stevens, Barnes & Knight, 1989). The Laurentian Plate was formed by an active rifting around ca. 570 Ma, experienced the continued rifting along the Iapetan margin at 540-535 Ma that continued into the late early Cambrian (ca. 520 Ma) and locally into the Middle Cambrian (Cawood, McCausland & Dunning, 2001; Landing, 2012, 2013; Landing & Webster, 2018), and then developed a pre-platform shelf covered by clastic sediments (James et al., 1989). During the late Cambrian, a major sea-level rising resulted in the thick transgressive carbonate deposits (Landing, 2007; Wilson, Medlock, Fritz, Canter & Geesaman, 1992) that were swept off the shelf to form the on-slope Cow Head Group. The outcrops of the Green Point Formation are extensive along western Newfoundland and well exposed at Martin Point, but also occur at Western Brook Pond and St. Pauls Inlet (Figure 1; Schuchert & Dunbar, 1934).

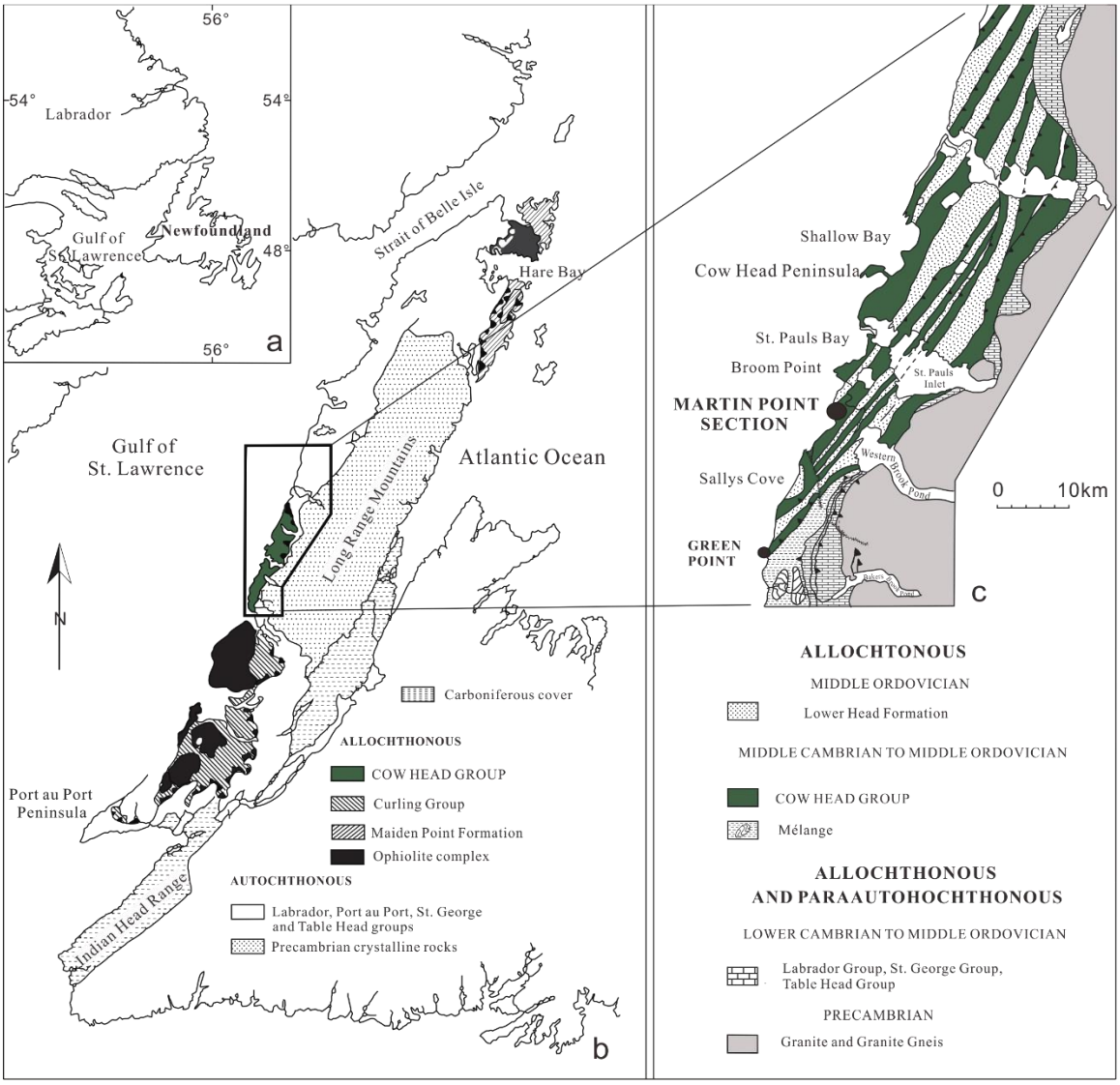


**Figure 1**. Map of the research area showing the surface geology and the location of the Martin Point section (49° 40′ 51″ N; 57° 57′ 36″ W) in western Newfoundland, Canada (modified from Cooper et al. 2001).

# 3 STRATIGRAPHY

## 3.1 Lithostratigraphy

James and Stevens (1986) have discussed in detail the lithostratigraphy of Martin Point section (Figure 2), which is a part of the Green Point Formation of the Cow Head Group. The Green Point Formation includes the Upper Cambrian Martin Point Member and the overlying lowermost Ordovician Broom Point Member. The Martin Point Member consists of 80–100 m of rhythmites of thinly-bedded green and black shale, interspersed with siltstone, alternating with ribbon limestone (micritic to near-micritic) and thin conglomerate interbeds may also occasionally occur. The lime mudstone interbeds may occur isolated or combined with shale counterparts, which are up to 20 cm thick. The conglomerate beds consist of shallow-water carbonate clasts that were transported into the deeper-water environments along the slope of the Laurentian margin (James & Stevens, 1986). The Broom Point Member is ~ 80 m thick and dominated by ribbon to parted limestone with few siltstone, sandstone, conglomerate and red shales. The limestone interbeds of the Broom Point Member are thicker and better developed than those in the Martin Point Member and mostly lime mudstone with fine-grained peloidal calcarenite. Some of the limestone is replaced by brown weathering nodular to bedded chert (James & Stevens, 1986).

## 3.2 Biostratigraphy

The faunal occurrences in the Martin Point section are limited compared to their counterparts of the same age in other sections. The investigated section has conodont Zone (Figure 2) that include, in ascending order, the *Proconodontus muelleri*,

*Eoconodontus notchpeakensis*, *Cordylodus proavus* and *Cordylodus caboti* zones (Azmy, 2018; Barnes, 1988; Ludvigsen, 1982; James & Stevens, 1986; Miller et al., 2014).

The deposits of the Martin Point section have recorded only two species of graptolites (*Rhabdinopora flabelliforme* and *Staurograptus dichotomus*) that were found just above the base of the Broom Point Formation (Barnes, 1988). The occurrences of *R.* cf. *praeparabola*, *R.* cf. *parabola*, and *Aletograptus* were documented by Erdtmann (1971) on the top of the Broom Point Member, but trilobites are rare at Martin Point, only *Hungia magnifica* is found in the basal beds (Barnes, 1988).

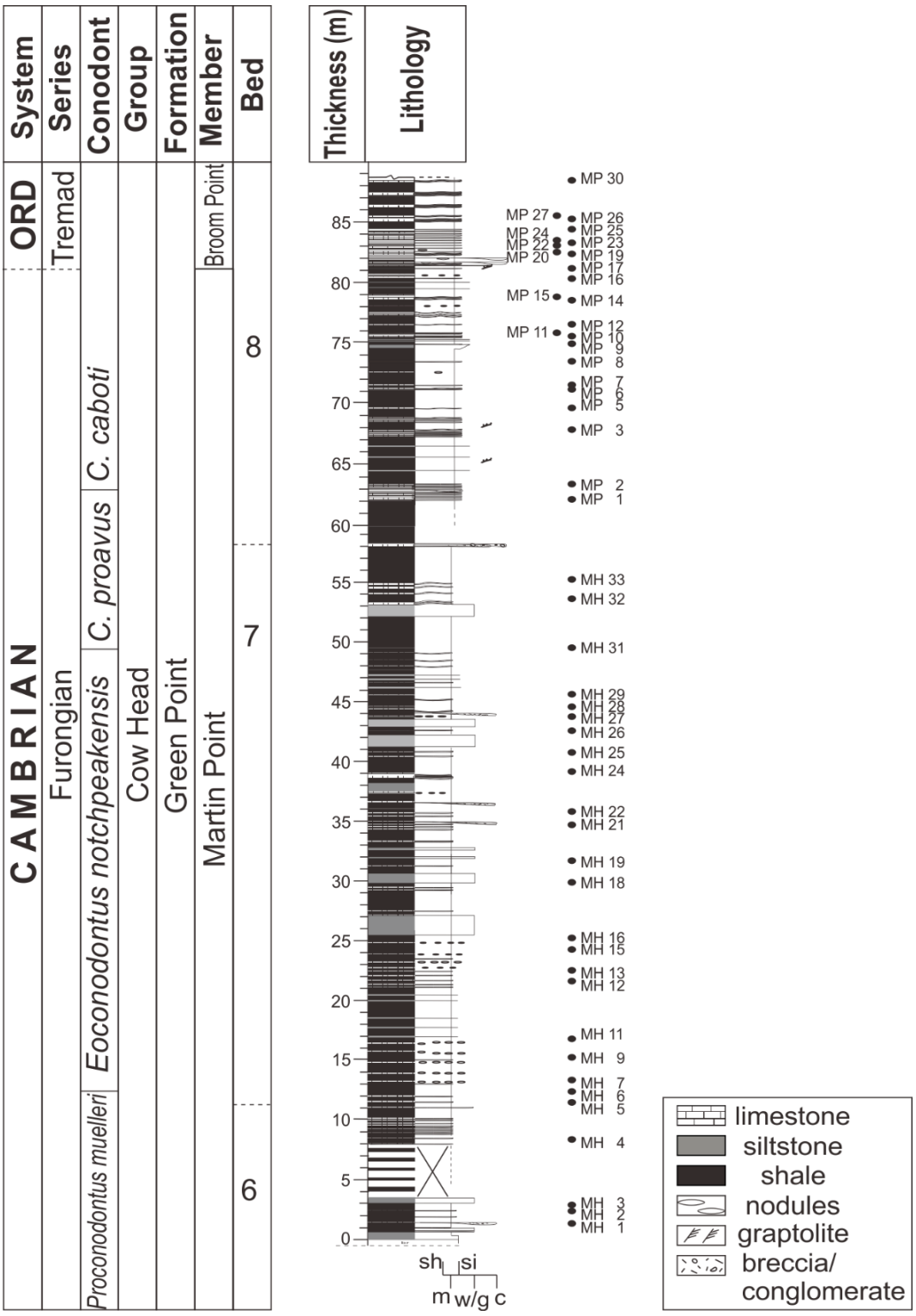


**Figure 2**. Stratigraphic framework of the investigated Martin Point section in western Newfoundland, Canada, illustrating bed number and detailed measured positions of samples and conodont zonation scheme (Barnes, 1988). Abbreviations: *C. proavus* = *Cordylodus proavus*; *C. caboti* = *Cordylodus caboti*; Tremad = Tremadocian.

# 4 METHODOLOGY

## 4.1 Sample preparation

Fifty-one samples were collected at high resolution (sampling intervals as small as 10 cm; Figure 2) mainly from the upper Martin Point Member at the Martin Point (49° 40′ 51″ N; 57° 57′ 36″ W) in western Newfoundland (Figure 1). The samples were taken from the most micritic (< 10 μm) and laminated lime mudstone interbeds to avoid the influence from allochthonous clasts, dolomites and recrystallized carbonate. Thin sections were cut and stained with Alizarin Red-S and potassium ferricyanide solutions (Dickson, 1966) to differentiate between dolomicrite and lime mudstones.

Cathodoluminescence (CL) observations were performed by a Technosyn 8200 MKII cold cathode instrument operated at 8 kV accelerating voltage and 0.7 mA current. Mirror-image slabs of each thin section were polished for micro-sampling. Polished slabs were washed with deionized water to remove contaminants associated with processing and dried overnight in oven at 40 ℃. Sample powder was extracted from the most micritic spots by a microdrill under a binocular microscope for geochemical analyses.

The most micritic samples were selected at close interval (Appendix 1 –See Supplementary material), particularly from the interval that spans the peak of the negative excursion of the HERB event (See Azmy, 2018, Figure 2), for organic $\delta^{13}C$ and $\delta^{15}N$ and trace element measurements (Figure 2).

## 4.2 Isotope analysis

For TOC and organic C- and N-isotope analysis, ~ 7 to 15 grams of powder were digested in 20 % (v/v) HCl repeatedly to remove carbonates. The remaining residue was separated by centrifugation and decantation and washed by deionized water for at least 3 times. It was subsequently dried overnight at ~ 40 °C. The $\delta^{13}C_{org}$ values were measured through a Carlo Erba Elemental Analyzer (EA) coupled with a Thermofinnigan DELTA V plus isotope ratio mass spectrometer. The TOC values were calculated from the peak area of the individual analyses based on mass. The results ($\sigma < 0.25$) were calibrated by the standards L-glutamic acid ($\delta^{13}C_{VPDB}$ = -26.74 ± 0.06 ‰ VPDB), SPEX $CaCO_3$ ($\delta^{13}C_{VPDB}$ = -21.02 ± 0.10 ‰ VPDB), Suprapur $CaCO_3$ ($\delta^{13}C_{VPDB}$ = -40.11 ± 0.15 ‰ VPDB) and B2153 low org soil ($\delta^{13}C_{VPDB}$ = -26.71 ± 0.24 ‰ VPDB). The $\delta^{15}N_{org}$ values were measured by VARIO ISOTOPE CUBE (ELEMENTAR) connected to a Thermofinnigan DELTA V plus isotope ratio mass spectrometer at the isotope laboratory of Memorial University of Newfoundland. The results ($\sigma < 0.15$) were normalized to the standards IAEA-N-1 ($\delta^{15}N_{air}$ = 0.43 ± 0.07 ‰ air), IAEA-N2 ($\delta^{15}N_{air}$ = 20.32 ± 0.09 ‰ air) and B2151 high-organic sediment ($\delta^{15}N_{air}$ = 4.35 ± 0.20 ‰ air).

### 4.3 Element analysis

For elemental analysis, 25 samples (10 mg each) were extracted by a slow-speed microdrill and processed in 5 % (v/v) acetic acid for 70 ─ 80 mins and measured by an Elan DRC II ICP-MS (Perkin Elmer SCIEX) at Memorial University of Newfoundland to measure major and trace elements including rare earth elements (REEs). The uncertainty is better than 5 % and the results are calibrated to 100 % carbonate basis (e.g., Veizer et al., 1999). The Ce anomaly (Ce/Ce*) was calculated based on the equation [$(Ce/Ce^*)_{SN} = Ce_{SN}/(0.5La_{SN} + 0.5Pr_{SN})$] (Bau & Dulski, 1996). The REE concentrations were normalized to Post Archean Australian Shale (PAAS; McLennan, 1989).

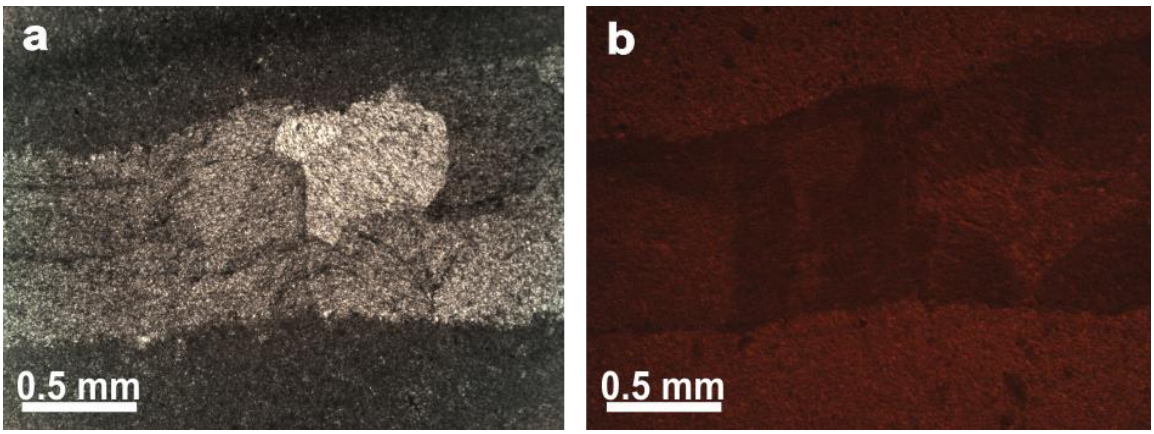


**Figure 3**. Photomicrographs of the investigated carbonates showing (a) micritic lime mudstones (Sample MP 28) cut by a fracture filled with a late burial cement and (b) CL image of (a) showing dull to non-CL micritic lime mudstone and cement. Detail in text.

**Table 1**. Summary of statistics of isotopic and elemental geochemistry of the investigated lime mudstones of the Martin Point section. Th/U and Ni datum are reproduced from Azmy (2018).

| | $\delta^{13}C_{org}$ (‰VPDB) | wt. % TOC | $\delta^{15}N_{org}$ (Air) | P (ppm) | Ni (ppm) | Sr (ppm) | Ce/Ce* | Th/U | ΣREE (ppm) | Si (ppm) | Al (ppm) | Mn (ppm) | Fe (ppm) | Mn/Al | Fe/Al |
|---|---|---|---|---|---|---|---|---|---|---|---|---|---|---|---|
| **Cambrian–Ordovician boundary** | | | | | | | | | | | | | | | |
| **n** | **11** | **11** | **6** | **8** | **8** | **8** | **8** | **7** | **8** | **8** | **8** | **8** | **8** | **8** | **8** |
| **Mean** | **-28.6** | **0.2** | **2.9** | **141.2** | **2.4** | **257.7** | **0.9** | **0.5** | **42.5** | **2872.0** | **1725.3** | **316.3** | **1974.5** | **0.2** | **1.2** |
| **Stdev** | **0.7** | **0.1** | **1.1** | **32.0** | **0.6** | **49.1** | **0.1** | **0.2** | **25.8** | **1331.8** | **1144.9** | **195.0** | **1573.0** | **0.2** | **0.4** |
| **Max** | **-27.1** | **0.5** | **4.1** | **180.4** | **3.4** | **301.3** | **0.9** | **0.7** | **79.3** | **5111.7** | **3546.7** | **648.6** | **5594.1** | **0.6** | **1.6** |
| **Min** | **-29.6** | **0.0** | **1.0** | **93.2** | **1.4** | **151.5** | **0.8** | **0.3** | **18.0** | **1393.7** | **633.9** | **141.6** | **905.9** | **0.1** | **0.4** |
| **HERB interval** | | | | | | | | | | | | | | | |
| **n** | **36** | **36** | **21** | **17** | **17** | **17** | **17** | **17** | **17** | **17** | **17** | **17** | **17** | **17** | **17** |
| **Mean** | **-29.1** | **0.1** | **3.0** | **142.0** | **4.1** | **355.9** | **0.8** | **1.4** | **48.6** | **2417.9** | **1436.3** | **380.2** | **2542.5** | **0.3** | **1.7** |
| **Stdev** | **0.7** | **0.1** | **1.0** | **44.8** | **1.9** | **226.1** | **0.1** | **1.5** | **22.1** | **960.2** | **790.5** | **141.9** | **1875.8** | **0.3** | **0.9** |
| **Max** | **-27.8** | **0.7** | **5.0** | **251.9** | **8.5** | **979.8** | **1** | **5.1** | **95.1** | **4478.2** | **3202.3** | **571.5** | **6900.3** | **0.9** | **4.5** |
| **Min** | **-30.5** | **0.0** | **0.8** | **85.5** | **1.9** | **165.0** | **0.7** | **0.1** | **24.6** | **1245.7** | **611.0** | **150.0** | **784.9** | **0.1** | **1.1** |

## 5 RESULTS

Petrographic examinations illustrate that the selected samples are dominated by micritic (< 4 μm) to near-micritic (~ 10 μm) lime mudstone and are dull to non-luminescent under CL (Figure 3a─b). Table 1 summarizes the statistics of geochemical results of the investigated Martin Point lime mudstones and the detailed values are listed in the Supplementary material. The investigated Martin Point section spans the HERB event of the late Cambrian (e.g., Buggisch et al., 2003; Miller et al., 2014) and the Cambrian–Ordovician boundary (e.g., Azmy, Stouge, Brand, Bagnoli & Ripperdan, 2014; Azmy et al., 2015). The mean values of the investigated geochemical proxies of both intervals (Table 1) are almost comparable although the profiles of most of the proxies show relatively faster and sharper fluctuations during the Cambrian–Ordovician boundary (Azmy et al., 2015) compared to those across the HERB event. The geochemical variations across the Cambrian–Ordovician boundary have been discussed in detail by Azmy et al. (2014, 2015) and therefore the focus of the current study will be on the geochemistry of the carbonates of the interval spanning the HERB event.

The total organic contents (TOC; 0.1 ± 0.1 wt. %) vary between 0.02 and 0.7 wt. % and their $\delta^{13}C_{org}$ values (-29.1 ± 0.7 ‰ VPDB) range from -30.5 to -27.8 ‰ (VPDB; Table 1). They exhibit insignificant correlations ($R^2 = 0.129$, Figure 4a). The $\delta^{13}C_{org}$ profile exhibits a positive shift (~ 2 ‰) that correlates with a slight decrease in the TOC contents (Figure 5 all profiles). These variations are correlated with the peak of the HERB $\delta^{13}C_{carb}$ excursion (Figure 5) documented by Azmy (2018) from the same investigated samples.

The $\delta^{15}N_{org}$ values (3.0 ± 1.0 ‰ air) range between +0.8 ‰ and +5.0 ‰ (Table 1), which have a slightly wider spectrum than that documented for the present-day Black Sea sediments (~2.5 ‰ to 3.6 ‰; Çoban-Yıldızetal, Altabet , Yılmaz & Tuğrul, 2006; Fry et al., 1991) and they exhibit a general insignificant correlation with their TOC counterparts ($R^2 = 0.004$; Figure 4b). The $\delta^{15}N_{org}$ profile shows a parallel variation with that of the $\delta^{13}C_{org}$ and also exhibits a comparable positive excursion (~ 2 ‰; Figure 5) associated with the stratigraphic level of the HERB event (Azmy, 2018).

The Sr concentrations vary between 165 and 980 ppm and their profile shows distinct decrease (Figure 5) above the peak of the HERB $\delta^{13}C_{carb}$ excursion documented by Azmy (2018).

The concentrations of other paleoenvironmental proxies (e.g., Acharya, Panigrahi, Gupta, & Tripathy, 2015; Pattan et al., 2013; Śliwiński et al., 2010) such as Al, Si, P, Fe, Mn, Ce/Ce* and REE, are summarized in Table 1 and their profiles (Figure 5) exhibit distinct variations associated with the stratigraphic interval that spans the peak of the HERB event (Azmy, 2018).

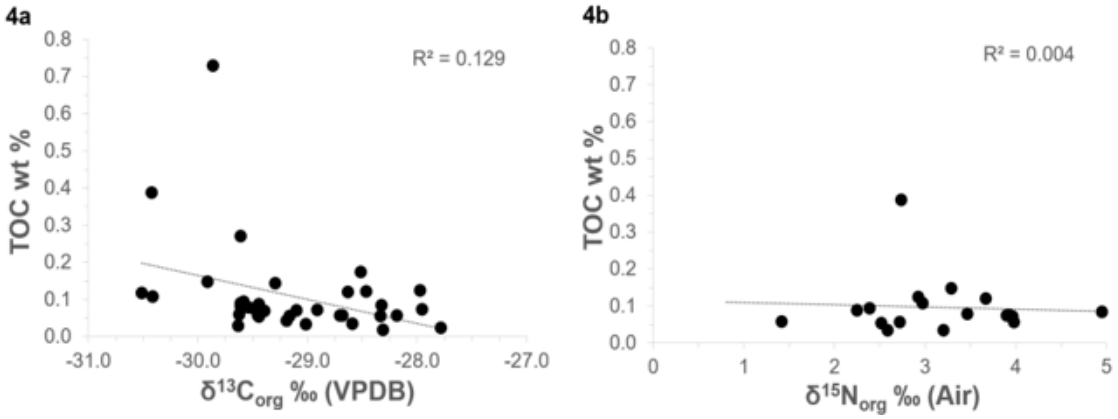


**Figure 4** Scatter diagrams showing insignificant correlations of (a) $\delta^{13}C_{org}$ and (b) $\delta^{15}N_{org}$ with TOC spanning the HERB event.

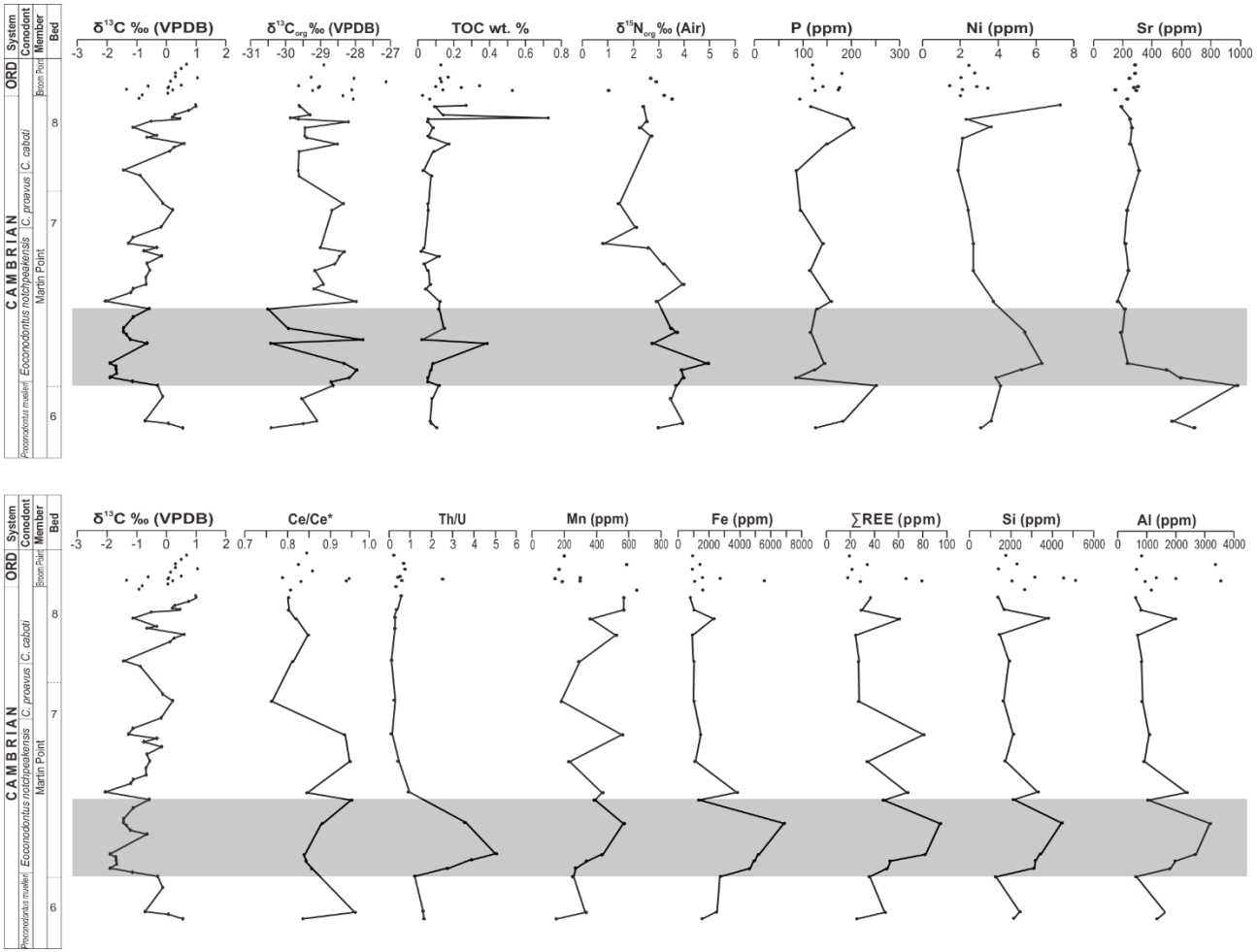


**Figure 5** The profiles of $\delta^{13}C_{carb}$, $\delta^{13}C_{org,}$ TOC, $\delta^{15}N_{org,}$ P, Ni, Sr, Ce/Ce*, Th/U, Mn, Fe, ΣREE, Si and Al across the HERB event in Martin Point section. The $\delta^{13}C_{carb}$, Th/U and Ni profiles are reproduced from Azmy (2018). The highlighted horizon (grey band) marks the peak area of the HERB $\delta^{13}C_{carb}$ profile.

# 6 DISCUSSION

## 6.1 Diagenetic influence

The preservation of the investigated samples has been discussed in detail by Azmy (2018) and is summarized below. The petrographic examination indicated that the samples are dominated by lime mudstones with almost pristine sedimentary fabrics and insignificant recrystallization (Figure 3). The grain size is mainly micritic to near-micritic (≤ 10 μm), suggesting a high degree of textural preservation and they exhibit dull to no luminescence (Figure 3). Luminescence in carbonates is activated by the enrichment of Mn, but, on the contrary, quenched by high concentrations of Fe (Machel & Burton, 1991). Thus, the dull and non-CL images have to be interpreted with caution because they may reflect geochemical preservation or enrichment of Fe by diagenetic alteration (Rush & Chafetz, 1990). However, the investigated lime mudstones are known to have precipitated on a slope setting of lower oxygen than shallow water and sediments are therefore expected to be relatively more enriched in Fe and/or Mn (Azmy, 2018; Morrison & Brand, 1986). Thus, CL is a preliminary evaluation tool that should be combined with others to confirm sample preservation (Brand et al., 2011).

Progressive burial of sediments is associated with an increase in temperature (> 50 °C), which results in thermal degradation of organic matter and a decrease in the TOC values. This is also associated with an increase in $\delta^{15}N_{org}$ and $\delta^{13}C_{org}$ values since $^{12}C$- and $^{14}N$- enriched organic compounds are released (e.g., Faure & Mensing, 2005; Popp, Parekh, Tilbrook, Bidigare & Laws, 1997; Saino & Hattori, 1980). The $\delta^{13}C_{org}$ values of the Martin Point carbonates show an insignificant correlation ($R^2 = 0.129$) with their

TOC counterparts (Figure 4a) that argues against the scenario of organic matter degradation and is consistent with the petrographic evidence of preservation of the micritic fabric, thus supporting the preservation of the $\delta^{13}C_{org}$ signatures. Similarly, the very poor correlation ($R^2 = 0.004$; Figure 4b) between the $\delta^{15}N_{org}$ and TOC values support at least near-primary $\delta^{15}N_{org}$ signatures.

Diagenetic alteration, through water/rock interactions, during the burial history of carbonates is known to deplete some elements such as Sr but enrich others such as Mn, Fe, and Al. The Sr has poor correlation with Mn, Fe and Al ($R^2 = 0.317$, 0.011 and 0.028, respectively; Figure 6a─c), which suggests an insignificant alteration by diagenesis. Microbial lime mudstones have been documented on Paleozoic slope settings at depths down to 300 m (e.g., Della Porta, Kenter, Bahamonde, Immenhauser & Villa, 2003), which suggests that the investigated slope carbonates of the Martin Point section (James & Stevens, 1986; Landing, 2013) might have had contributions from in situ lime muds (Azmy, 2018; James & Stevens, 1986; Landing, 2013) through microbial mediation (e.g., Bahamonde, Meno-Tomé & Heredia, 2007; Bartley, Kah, Frank & Lyons, 2015; Della Porta et al. 2003; George, 1999). The slope settings have oxygen-poor (dysoxic) conditions (Azmy, 2018) compared with those of oxic shallow-water settings and this may explain their enriched Mn and Fe contents (380 ± 142 ppm and 2543 ± 1876 ppm, respectively). Contaminations from hidden microrhombic bacterial pyrite during microsampling might have also contributed to the Fe contents. Thus, Mn and Fe contents are not the ideal proxies of diagenesis for slope carbonates, but yet they still exhibit insignificant correlations with their Sr counterparts in the investigated limestones (Figure 6a─b). The strong correlation between Si and Al ($R^2 = 0.922$; Figure 6d) may reflect an

influence of terrigenous input possibly during a sea-level drop, which is consistent with the sea-level variations documented by earlier studies (e.g., Azmy, 2018; Miller et al., 2011).

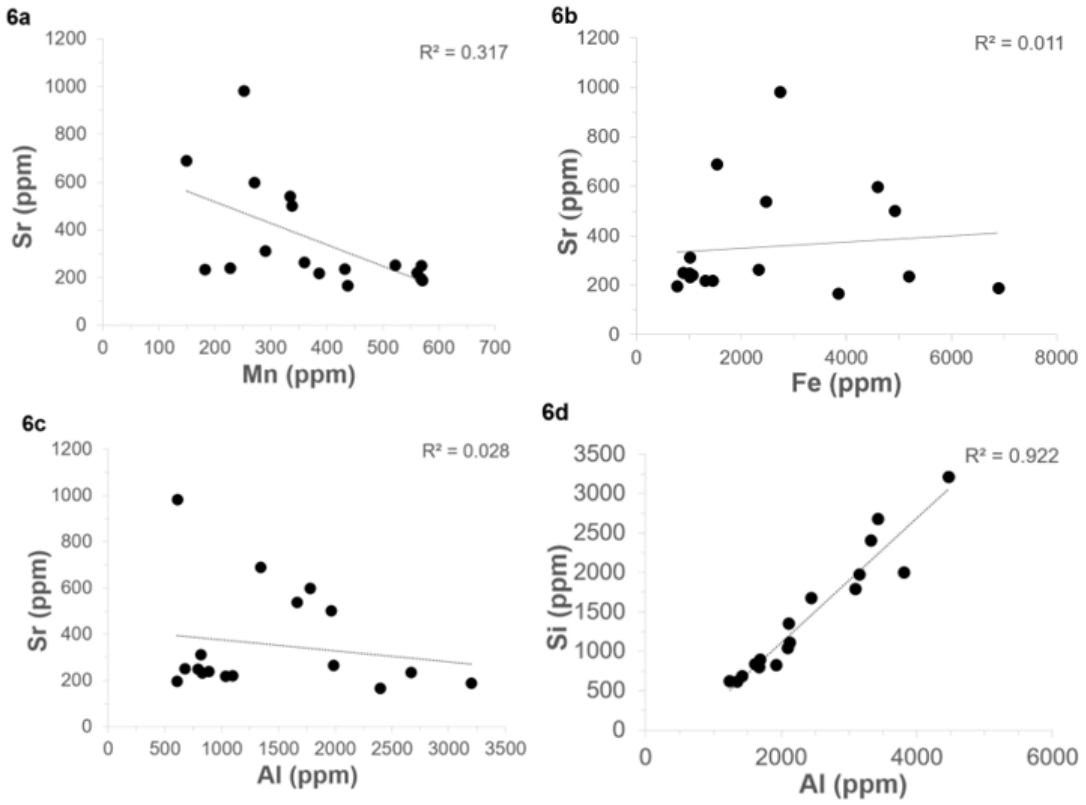


**Figure 6** Scatter diagrams showing insignificant correlations of Sr with (a) Mn, (b) Fe, and (c) Al and (d) Si with Al spanning the HERB event.

### 6.2 Elemental variation

Variations in eustatic sea-level do not influence only the redox conditions and organic productivity but also the input of terrigenous sediments and nutrients in ocean, which is reflected in the associated changes in the concentrations of trace elements in marine sediments (e.g., Arnaboldi & Meyers, 2007; Cowan & James, 1993; Dickson, Cohen & Coe, 2011; Kimura, Azmy, Yamamuro, Zhi-Wen & Cizdziel, 2005; Piper & Calvert,

2009; Śliwiński et al., 2010; Wignall & Twitchett, 1996). An earlier study (Azmy, 2018) documented a noticeable negative $\delta^{13}C_{carb}$ excursion (~ 3 ‰), associated with sea-level changes (Miller et al., 2011), that peaks at the base of the *Eoconodontus notchpeakensis* conodont Zone, which is near the bottom of bed 6 (Figure 5). Phosphorus and Ni have been proven to be reliable proxies of bioproductivity, whereas Ce/Ce*, Th/U, Fe and Mn contents are used for determining paleoredox condition (e.g., Arnaboldi & Meyers, 2007; Hatch & Leventhal, 1992; Morel, Milligan & Saito, 2004; Rue, Smith & Cutter, 1997; Śliwiński et al., 2010; Tribovillard, Algeo, Lyons & Riboulleau, 2006; Wignall & Twichett, 1996). Al and Si reflect the influence of terrestrial input in oceans (e.g., Govin et al., 2012; Zhao & Zheng, 2014). The biodiversity, particularly of shelly organisms, is expected to be lower on the slope settings (James & Stevens, 1986). Al, Si and total REE (ΣREE) are enriched in the crustal rocks and they are therefore proxies of the terrigenous inputs in oceans (e.g., Śliwiński et al. 2010; Tripathy, Singh & Ramaswamy, 2014; Veizer, 1983). Their profiles, from the Martin Point section, exhibit parallel positive excursions (Figure 5) that are correlated with the HERB negative $\delta^{13}C$ excursion (Figure 5) documented by Azmy (2018). The peak of the HERB $\delta^{13}C$ excursion was associated with a sea-level drop (Azmy, 2018; Miller et al., 2014), which most likely led to enhancement in the terrigenous inputs and resulted in enrichment of the Al, Si and ΣREE in ocean water and also during precipitation of the marine carbonates. Nickel is a micronutrient and also a proxy of bioproductivity and it is captured by the organic matter in the water column (e.g., Calvert & Pedersen, 1993; Śliwiński et al., 2010). An earlier study (Azmy, 2018) indicated that no diagenetic overprint influenced the Ni signatures in the investigated Martin Point carbonates. The Martin Point Ni profile (Azmy, 2018)

shows a positive excursion parallel to those exhibited by AL, Si and ΣREE counterparts (Figure 5) and also correlated with the HERB $\delta^{13}C$ excursion, which supports the scenario of increase of nutrients through terrigenous inputs during the sea-level drop before it resumed rising.

The concentrations of P (142 ± 45 ppm, Table 1; Appendix 1) do not change considerably throughout the investigated interval. However, the P profile exhibits a relative enrichment (252 ppm, MH5, Appendix 1) at a level immediately below the peak of the HERB negative $\delta^{13}C$ excursion (Figure 5), but the concentrations decrease again until they approach the Cambrian–Ordovician boundary. The brief increase in P concentrations at the bottom of the profile is possibly related to an upwelling event (Föllmi, 1996; Gao et al., 2018) since upwelling can be driven not only by ice-cap melting but also by wind and tectonic activities (Anderson et al., 2009). Contributions from falling phosphatic fecal pellets from top of the water column and microaggregates of phosphatic algae (e.g., Azmy et al., 2014) could be also possible. However, there is another pulse at the top of the profile correlated with enhancement in the input of Al, Si and ΣREE, which reflects some influence of terrigenous inputs. This may suggest contributions from detrital organic matter, which is consistent with the parallel increase shown by the TOC profile (Figure 5; Latimer & Filippelli, 2002). Unlike the lime mudstones spanning the Cambrian–Ordovician Boundary in the GSSP section at Green Point, petrographic examinations did not reveal any occurrences of phosphatic algae in the carbonates of the HERB event interval of the current study (Azmy et al., 2014).

The Sr contents (Figure 5) show a maximum value within the profile, immediately below the peak of the HERB $\delta^{13}C$ excursion, followed by a distinctive decrease and values remain approximately unchanged upward. No diagenetic system has been known yet to cause such consistent variations, but a change from carbonates dominated by aragonite to those by calcite is suggested to be a possible scenario since aragonite is known to have much higher contents of Sr relative to calcite (e.g., Brand, 1991; Sunagawa, Takahashi & Imai, 2007).

Eustasy influences the oxygen levels in water column, which controls the redox proxies (e.g., Ce) by changing their oxidation state and solubility in seawater and concequently their concentrations in marine carbonates (e.g., Webb, Nothdurft, Kamber, Kloprogge & Zhao, 2009). The micritic ($\leq$ 4 μm) to near-micritic (~ 10 μm) grain size of the investigated carbonates suggest a low water/rock interaction (insignificant alteration) and the Ce concentrations have insignificant correlation ($R^2 = 0.084$) with their Sr counterparts. Therefore, the Ce values are not significantly impacted by diagenesis and can be utilized at least to highlight the relative redox variations across the HERB event. The Ce anomaly (Ce/Ce*) has been proven to be a proxy of redox conditions (e.g., Azmy et al., 2015; Bau & Dulski, 1996; Webb & Kamber, 2000). In shallow oxic water, trivalent Ce is oxidized to tetravalent Ce and absorbed on particle surfaces and/or form less soluble $Ce^{4+}$ species (Bau & Dulski, 1996) to leave shallow oxic water depleted in Ce. The Ce/Ce* ratios (between 0.7 and 1.0, Table 1) of the investigated interval have a poor correlation with their Sr counterparts ($R^2 = 0.1$), thus suggesting insignificant influence by diagenesis. The Ce/Ce* are generally < 1 and likely reflect dysoxic (suboxic) conditions (e.g., Webb & Kamber, 2000). The Ce/Ce* profile (Figure 5) shows

a negative shift correlated with the peak of the HERB negative $\delta^{13}C$ excursion, which is consistent with the initial sea-level drop that enhanced the oxygenation of water and decrease of Ce before it resumed rising.

Th/U ratios have been also known to be a reliable proxy for redox conditions (Wignall & Twichett, 1996; Wignall et al., 2007) and found to increase with oxidizing conditions, because U maintains the soluble $U^{6+}$ higher state of oxidation, whereas Th is not affected by changes in redox conditions. An earlier study (Azmy, 2018) indicated that the Th/U profile of the Martin Point section has a positive shift that correlates with the HERB negative $\delta^{13}C$ excursion, which is consistent with the negative Ce/Ce* shift caused by a drop in sea-level and a brief oxygenation that relatively decreased the dysoxic conditions.

The relative changes in Mn and Fe concentrations may reflect the variations in redox conditions because both elements are more soluble in their reduced states (Landing & Bruland, 1987) and thus become more enriched in seawater under dysoxic conditions compared with oxic shallow waters. The Mn and Fe contents vary from 150 to 572 ppm and 785 to 6900 ppm, respectively (Table 1) and their concentrations are higher than those of modern warm shallow-water marine carbonates (Mn = 5.4 ─ 30 ppm and Fe = 1 ─ 20 ppm; Brand, Logan, Hiller & Richardson, 2003; Ichikuni, 1973; Lorens, 1981; Richter & Füchtbauer, 1978; Veizer, 1974), which is consistent with their enrichment in the investigated Martin Point carbonates of slope settings (James & Stevens, 1986) and the suggested dysoxic conditions (e.g., Azmy, 2018). Meanwhile, the Mn and Fe profiles exhibit correlated positive excursions parallel to those exhibited by the Al, Si and ΣREE (Figure 5), thus reflecting an overprint by the influence of terrigenous inputs (e.g., Rao &

Adabi, 1992). However, the Mn and Fe concentrations can be normalized by Al to eliminate the influence of detrital fraction and be utilized as proxies of redox condition (Clarkson, Poulton & Wood, 2014). The investigated Martin point carbonates have Mn/Al ratios between 0.1 and 0.9 and Fe/Al ratio between 1.1 and 4.5 (Table 1), which are considerably higher than those of the upper continental crust (0.0075 and 0.44, respectively; McLennan, 2001). This may reflect the occurrence of the Fe-Mn oxy-hydroxides (Pattan et al., 2013) that cannot form in anoxic environment but at least dysoxic conditions (cf. Azmy, 2018; Landing et al., 2002).

The profiles of Al, Si, ΣREE, Fe, Mn, Ni and P show upper positive shifts below the Cambrian–Ordovician boundary at the same stratigraphic level correlated with a negative subpeak on the $\delta^{13}C_{carb}$ profile, thus suggesting an increase in terrigenous inputs around that time likely due to possible a minor drop in sea-level along its main trend of rising.

The mean concentrations of the investigated elemental proxies of the HERB carbonates and those of the Cambrian–Ordovician boundary (Table 1) in the Martin Point section are almost comparable (cf. Azmy et al., 2014, 2015) and therefore suggest no dramatic change in the elemental chemistry of the seawater at least through the late Cambrian and the lowermost Ordovician. However, the Sr shows an exceptional considerable drop at a level immediately below the peak of the HERB negative $\delta^{13}C_{carb}$ excursion that remains low almost unchanged up-section and thorough the Cambrian–Ordovician boundary. Also, the mean Th/U value of the HERB Carbonates (1.4; Table 1) is relatively higher than that of the Cambrian–Ordovician counterparts (0.5; Table 1),

which is consistent with the geochemical evidence of the sea-level drop at the peak of the HERB event and the relative decrease in dysoxic conditions.

### 6.3 Organic C- and N- isotope

The carbon and nitrogen isotopes of organic matter have been used as reliable indicators to reflect redox states, terrigenous inputs, bioproductivity and the preservation of organic debris (e.g., Altabet & Francois, 1994; Amon & Mean, 2003; Azmy et al. 2015; Çoban-Yıldızetal et al., 2006; Quan et al., 2008; Quan, Wright & Falkowski, 2013; Yamaguchi et al., 2010). The TOC values vary between 0.02 and 0.7 wt. % (0.1 ± 0.1 wt. %; Table 1), which are significantly lower than those documented for the overlying (younger) carbonates of the Cambrian–Ordovician GSSP boundary at Green Point (1.1 ± 1.0 wt. %; Azmy et al. 2015) and also shales (0.6 to 5.2 wt. %; Weaver & Macko, 1988). This may generally suggest significant lower organic productivity, at the same slope settings, during the HERB time interval. A drop in sea-level is expected to bring the photic zone lower boundary down and enhance primary productivity, whereas a sea-level rise results in more burial of organic matter in the relatively deeper settings and enrichments of $^{12}C$ in buried organic matter.

However, the peak of the of the HERB negative $\delta^{13}C_{carb}$ excursion is correlated with a positive shift on the $\delta^{13}C_{org}$ profile (Figure 5), thus suggesting contributions from detrital organic matter, which is relatively depleted in $^{12}C$, that overprinted the enhancement of primary productivity caused by sea-level drop, particularly when primary productivity was generally low during the Late Cambrian, as indicated by the very low TOC values (0.1 ± 0.1 wt. %, Table 1). The scenario of detrital organic matter is

supported by the correlated distinct enhancement in detrital inputs reflected by the positive shifts on the profiles of Al, Si, ΣREE, and Ni (Figure 5).

This is also consistent with the TOC profile that shows almost insignificant variations except for a lower positive shift (~ 0.4 wt. %) that correlates with the start of general sea-level rise after the peak of the HERB negative $\delta^{13}C_{carb}$ excursion and an upper shift (0.7 wt. %) close to the Cambrian–Ordovician boundary (Figure 5). Both shifts correlate with negative shifts on the $\delta^{13}C_{org}$ profile (Figure 5) and associated with positive shifts on the Al, Si, and ΣREE, thus reflecting episodes of exceptional relative higher input of detrital organics and fast burial.

The $\delta^{15}N_{org}$ values have been widely used as a proxy to determine the organic matter sources and redox states (Quan et al., 2013; Ren et al., 2017; Yamaguchi et al., 2010), but this has to be taken with caution since the ocean N budget is complicated and influenced by several factors, such as the organic nitrogen (ON) from terrigenous fluxes, deterioration of ON, uptake of nitrogen by phytoplankton, N-fixation by cyanobacteria in surface waters, and denitrification. The values of $\delta^{15}N_{org}$ of the Martin Point section vary between 0.8 and 5.0 ‰ (3.0 ± 1.0 ‰; Figure 5; Table 1), which is higher than those of the terrestrial plants (Drechsler & Stiehl, 1977; Stiehl & Lehmann, 1980) but comparable to those of the modern Black Sea sediments (~ 3 ‰; Quan et al., 2008), thus suggesting at least dysoxic conditions (e.g., Azmy et al., 2015). This also implies that the contribution from terrestrial plants through terrigenous inputs is minimal, which is consistent with low diversity of land plants especially during the earliest Phanerozoic (Late Cambrian) (e.g., Meyers, 1994; Theissen, Dunbar & Cooper, 2003).

Microbial denitrification (reduction of $NO_3^-$ into $N_2$) under oxygen-depleted conditions results in enrichment of $^{15}N$ in organic matter (e.g., Cremonese et al., 2013; Quan et al., 2013; Sigman, Karsh & Casciotti, 2009). The $\delta^{15}N_{org}$ profile of the Martin Point carbonates (Figure 5) shows a broad positive excursion (~ 2 ‰) that peaks at a stratigraphic level correlated with that of the HERB negative $\delta^{13}C_{carb}$ counterpart, which is associated with sea-level drop. This is opposite to the expected trend but can be attributed to the influence of contributions from detrital organic matter ($^{15}N$-enriched of marine origin) during a sea-level lowstand, which is also consistent with the correlated $\delta^{13}C_{org}$ positive shift.

The drop of sea-level might have contributed with the uptake of $^{14}N$ by phytoplankton that would leave seawater relatively more enriched in $^{15}N$ and lead to positive $\delta^{15}N_{org}$ of organic matter (Cline & Kaplan, 1975; Macko, Engel & Parker, 1993; Meyer & Lallier-Vergès, 1999; Talbot & Laerdal, 2000). The short-term fluctuations of the sea-level inferred from the $\delta^{13}C_{carb}$ subpeaks, narrow sampling interval (as narrow as 10 cm), and thinly-bedded carbonate interbeds alternating with shales (Azmy, 2018) suggest that the enhancement in primary productivity caused by minor drops in sea-level throughout the main rising trend was possibly not enough to overprint the influence of detrital organic matter on the $\delta^{13}C_{org}$ and $\delta^{15}N_{org}$ signatures.

In summary, the stable isotope geochemistry of carbonates (Azmy, 2018) and organic matter and trace element contents of the Martin point carbonates suggest that the main (first order) trend of sea-level rise during Late Cambrian had a lower distinct sea-

level fall associated with the HERB event and an upper minor counterpart immediately below the Cambrian–Ordovician boundary.

The sea-level falling was associated with recognizable negative $\delta^{13}C_{carb}$ shifts (Azmy 2018, Figure 5) caused by bringing oxygen-rich shallow water in contact with organic matter that was buried at depth before the sea-level drop. The falling sea-level led to more exposure of land, which enhanced the inputs of weathered crustal rocks into the ocean. This is reflected by positive shifts on the Al, Si, Fe, Mn, Ni, ΣREE, and Th/U profiles and a negative counterpart on the Ce*/Ce profile due to the increase of the concentrations of those crust-enriched elements in the investigated marine carbonates and a relative increase in oxygen level in the top water column. The P profile peaks before the proposed HERB sea-level drop suggesting contributions possibly from falling phosphatic fecal pellets or traces of phosphatic algae (e.g., Azmy et al., 2014) that were not detected by regular petrographic examinations of thin sections. On the other hand, the peak at the top of the P profile is associated with positive shifts in the Al, Si, Fe, Mn, Ni, and ΣREE profiles suggesting contributions from weathered material of land sources.

The change in the sea-level impacted the primary productivity and the inputs of recycled organic matter in the weathered material that accordingly led to variations in the TOC budget and C- and N-isotope signatures. These variations were reflected in recognizable shifts on the $\delta^{13}C_{org}$ and $\delta^{15}N_{org}$ profiles.

# 7 CONCLUSIONS

The petrographic and geochemical examinations prove the preservation of at least near-primary trace element signatures and C- and N-isotope compositions of organic matter of the lime mudstone interbeds of the slope rhythmites spanning the Upper Cambrian section at Martin Point, western Newfoundland. The signatures can be utilized as proxies to investigate the changes in redox condition, bioproductivity, and terrigenous input in response to sea-level variations.

The trace element profiles of Al, Si, ΣREE, Fe, Mn, and Ce/Ce* profiles exhibit consistent shifts correlated with the peak of the HERB negative $\delta^{13}C_{carb}$ excursion documented by earlier studies, which is consistent with a sea-level drop, a change in relative dysoxic conditions, and contributions from terrigenous inputs.

The associated positive shifts exhibited by the Fe and Mn reflect the overprint by the terrigenous input rather than redox condition, which is consistent with the correlated Ce/Ce* negative shift and the earlier documented positive Th/U shift.

The TOC values (0.1 ± 0.1 wt. %) of the carbonates spanning the HERB interval are significantly lower than those of the overlying Cambrian–Ordovician boundary, thus suggesting significant lower primary productivity. The $\delta^{13}C_{org}$ and $\delta^{15}N_{org}$ profiles show positive shifts correlated with the HERB negative $\delta^{13}C_{carb}$ peak and enhancement in the Al, Si, and ΣREE concentrations, thus suggesting contributions from detrital organic matter during a sea-level drop.

The mean $\delta^{15}N_{org}$ values (3.0 ± 1.0 ‰ air) are consistent with dysoxic conditions and suggest that contributions of detrital organic matter through terrigenous inputs were not from terrestrial plants but rather marine origin.

**ACKNOWLEDGEMENTS**

The authors wish to thank an anonymous reviewer and Dr. Ed Landing for their constructive reviews. Also, the efforts of Ian Somerville (editor) are much appreciated. Special thanks for Dr. Svend Stouge for his help in the field work. This project was supported by funding (to Karem Azmy) from the Petroleum Exploration Enhancement Program (PEEP), NL, Canada.

## REFERENCES


Acharya, S.S., Panigrahi, M.K., Gupta, A.K., & Tripathy, S. (2015). Response of trace metal redox proxies in continental shelf environment: The Eastern Arabian Sea scenario. *Continental Shelf Research, 106,* 70–84.

Altabet, M.A., & Francois, R. (1994). Sedimentary nitrogen isotopic ratio as a recorder for surface ocean nitrate utilization. *Global Biogeochemical Cycles, 8*(1), 103–116.

Amon, R.M.W., & Meon, B. (2004). The biogeochemistry of dissolved organic matter and nutrients in two large Arctic estuaries and potential implications for our understanding of the Arctic Ocean system. *Marine Chemistry, 92,* 311–330.

Anderson, R.F., Ali, S., Bradtmiller, L.I., Nielsen, S.H.H., Fleisher, M.Q., Anderson, B.E., & Burckle, L.H. (2009). Wind-driven upwelling in Southern Ocean and the deglacial rise in atmospheric $CO_2$. *Science,* 323, 1443–1448.

Arnaboldi, M., & Meyers, P.A. (2007). Trace element indicators of increased primary production and decreased water-column ventilation during deposition of latest Pliocene sapropels at five locations across the Mediterranean Sea. *Palaeogeography, Palaeoclimatology, Palaeoecology, 249,* 425–443.

Azmy, K. (2018). Carbon-isotope stratigraphy of the uppermost Cambrian in eastern Laurentia: implications for global correlation. *Geological Magazine,* 156, 759–771.

Azmy, K., Kendall, K., Brand, U., Stouge, S., & Gordon, G.W. (2015). Redox conditions across the Cambrian–Ordovician boundary: elemental and isotopic signatures retained in the GSSP carbonates. *Palaeogeography, Palaeoclimatology, Palaeoecology, 440,* 440–54.

Azmy, K., Stouge, S., Brand, U., Bagnoli, G., & Ripperdan, R. (2014). High-resolution chemostratigraphy of the Cambrian–Ordovician GSSP in western Newfoundland, Canada: enhanced global correlation tool. *Palaeogeography, Palaeoclimatology, Palaeoecology, 409,* 135–44.

Bahamonde, J.R., Meno-Tomé, O.A., & Heredia, N. (2007). A Pennsylvanian microbial boundstone-dominated carbonate shelf in a distal foreland margin (Picos de Europa Province, NW Spain). *Sedimentary Geology, 198,* 167–193

Barnes, C.R. (1988). The proposed Cambrian–Ordovician global boundary stratotype and point (GSSP) in western Newfoundland, Canada. *Geological Magazine, 125,* 381–414.

Bartley, J.K., Kah, L.C., Frank, T.D., & Lyons, T.W. (2015). Deep-water microbialites of the Mesoproterozoic Dismal Lakes Group: microbial growth, lithification, and implications for coniform stromatolites. *Geobiology, 13,* 15–32.

Bau, M., & Dulski, P. (1996). Distribution of yttrium and rare-earth elements in the Penge and Kuruman iron-formations, Transvaal Super group, South Africa. *Precambrian Research, 79,* 37–55.

Brand, U. (1991). Strontium isotope diagenesis of biogenic aragonite and low-Mg calcite. *Geochimicu et Cosmochimica Acta, 55,* 505–513.

Brand, U., Logan, A., Bitner, M.A., Griesshaber, E., Azmy, K., & Buhl, D. (2011). What is the ideal proxy of Paleozoic seawater? *Memoirs of the Association of Australasian Paleontological Society Memoirs, 41,* 9–24.

Brand, U., Logan, A., Hiller, N., & Richardson, J. (2003). Geochemistry of modern brachiopods: applications and implications for oceanography and paleoceanography. *Chemical Geology, 198,* 305–334.

Buggisch, W., Keller, M., & Lehnert, O. (2003). Carbon isotope record of Late Cambrian to Early Ordovician carbonates of the Argentine *Precordillera. Palaeogeography, Palaeoclimatology, Palaeoecology, 195,* 357–73.

Calvert, S.E., & Pedersen, T.F. (1993). Geochemistry of recent oxic and anoxic marine sediments: implications for the geological record. *Marine Geology, 113*(1), 67–88.

Cawood, P.A., McCausland, P.J.A., & Dunning, G.R. (2001). Opening Iapetus: constraints from Laurentian margin in Newfoundland. *Geological Society of America Bulletin, 113,* 443–453.

Clarkson, M.O., Poulton, S.W., & Wood, R.A. (2014). Assessing the utility of Fe/Al and Fe-speciation to record water column redox conditions in carbonate-rich sediments. *Chemical Geology, 382,* 111–122.

Cline, J.D., & Kaplan, I.R. (1975). Isotopic fractionation of dissolved nitrate during denitrification in the eastern tropical North Pacific Ocean. *Marine Chemistry, 3,* 271–299.

Çoban-Yıldız, Y., Altabet, M.A., Yılmaz, A., & Tuğrul, S. (2006). Carbon and nitrogen isotopic ratios of suspended particulate organic matter (SPOM) in the Black Sea water column. *Deep-Sea Research, 53,* 1875–1892.

Cooper, R.A., Nowlan, G.S., & Williams, S.H. (2001). Global Stratotype Section and Point for base of the Ordovician System. *Episodes, 24,* 19–28.

Cowan, C.A., & James, N.P. (1993). The interactions of sea level change, terrigenous sediment influx, and carbonate productivity as controls on Upper Cambrian grand cycles of western Newfoundland, Canada. *Geological Society of America Bulletin, 105,* 1576–1590.

Cremonese, L., Shields-Zhou, G., Struck, U., Ling, H.F., Och, L., Chen, X., & Li, D. (2013). Marine biogeochemical cycling during the early Cambrian constrained by a nitrogen and organic carbon isotope study of the Xiaotan section, South China. *Precambrian Research, 225,* 148–165.

Della Porta, G., Kenter, J.A.M., Bahamonde, J.R., Immenhauser, A., & Villa, E. (2003). Microbial Boundstone Dominated Carbonate Slope (Upper Carboniferous, N Spain): Microfacies, Lithofacies Distribution and Stratal Geometry. *Facies, 49,* 195–207.

Dickson, J.A.D. (1966). Carbonate identification and genesis as revealed by staining. *Journal of Sedimentary Research, 36*(2), 491–505.

Dickson, A.J., Cohen, A.S., & Coe, A.L. (2011). Seawater oxygenation during the Paleocene–Eocene Thermal Maximum. *Geology, 40*(7), 639–642.

Drechsler, M., & Stiehl, G. (1977). Stickstoffisotopen variationen in organischen Sedimenten 1. Untersuchungen an humosen Kohlen. *Chemie der Erde, 36,* 126–138.

Erdtmann, B.D. (1971). Ordovician graptolite zones of western Newfoundland in relation to paleogeography of the North Atlantic. *Geological Society of America Bulletin, 82,* 1509–1528.

Faure, G., & Mensing, T.M. (2005). Isotopes: Principles and Applications. third edition. John Willey and Sons, Inc., *Hoboken NJ.*

Föllmi, K.B. (1996). The phosphorus cycle, phosphogenesis and marine phosphate-rich deposits. *Earth-Science Reviews, 40,* 55–124.

Fry, B., Jannasch, H.W., Molyneaux, S.J., Wirsen, C.O., Muramoto, J.A., & King, S. (1991). Stable isotope studies of the carbon, nitrogen and sulfur cycles in the Black Sea and the Cariaco Trench. *Deep-Sea Research, 38,* 1003–1019.

Gao, Y., Zhang, X., Zhang, G., Chen, K., & Shen, Y. (2018). Ediacaran negative C-isotopic excursions associated with phosphogenic events: Evidence from South China. *Precambrian Research, 307,* 218–228.

George, A.D. (1999). Deep-water Stromatolites, Canning Basin, Northwestern Australia. *PALAIOS, 14,* 493–505.

Govin, A., Holzwarth, U., Heslop, D., Keeling, L.F., Zabel, M., Mulitza, S., Collins, J.A., & Chiessi, C.M. (2012). Distribution of major elements in Atlantic surface sediments (36°N–49°S): Imprint of terrigenous input and continental weathering. *Geochemistry, Geophysics, Geosystems, 13,* 1525–2027.

Halverson, G.P., Hoffman, P.F., Schrag, D.P., Maloof, A.C., & Rice, A.H.N. (2005). Toward a Neoproterozoic composite carbon-isotope record. *Geological Society of America Bulletin, 117,* 1181–1207.

Hatch, J.R., & Leventhal, J.S. (1992). Relationship between inferred redox potential of the depositional environment and geochemistry of the Upper Pennsylvanian (Missourian) Stark Shale Member of the Dennis Limestone, Wabaunsee Country, Kansas, U.S.A. *Chemical Geology, 99,* 65–82.

Ichikuni, M. (1973). Partition of strontium between calcite and solution: effect of substitution by manganese. *Chemical Geology, 11,* 315–319.

James, N.P., & Stevens, P.K. (1986). Stratigraphy and correlation of the Cambro-Ordovician Cow Head Group, western Newfoundland. *Geological Survey of Canada, 366,* 1–143.

James, N.P., Stevens, R.K., Barnes, C.R., & Knight, I. (1989). Evolution of a Lower Paleozoic continental margin carbonate platform, northern Canadian Appalachians. *The Society of Economic Paleontologists and Mineralogists, Special Publication, 44.*

Kimura, H., Azmy, K., Yamamuro, M., Zhi-Wen, J., & Cizdziel, J.V. (2005). Integrated stratigraphy of the Upper Proterozoic succession in Yunnan of South China: re-evaluation of global correlation and carbon cycle. *Precambrian Research, 138,* 1–36.

Kump, L.R., Junium, C., Arthur, M.A., Brasier, A., Fallick, A., Melezhik, V.A., Lepland, A., Crne, A.E., & Luo, G. (2011). Isotopic evidence for massive oxidation of organic matter following the great oxidation event. *Science (New York), 334,* 1694–1696.

Landing, E. (2007). Ediacaran–Ordovician of east Laurentia – geologic setting and controls on deposition along the New York Promontory. *New York State Museum Bulletin, 510.*

Landing, E. (2012). Time-specific black mudstones and global hyperwarming on the Cambrian–Ordovician slope and shelf of the Laurentia. *Palaeogeography, Palaeoclimatology, Palaeoecology, 367–368,* 256–272.

Landing, E. (2013). The Great American Carbonate Bank in northeast Laurentia: its births, deaths, and linkage to continental slope oxygenation (Early Cambrian–Late Ordovician). *American Association of Petroleum Geologists Bulletin, Memoir, 98,* 451–492.

Landing, E., Geyer, G., & Bartowski, K.E. (2002). Latest Early Cambrian small shelly fossils, trilobites, and Hatch Hill dysaerobic interval on the east Laurentian continental slope. *Journal of Paleontology, 76,* 285–303.

Landing, E., & Webster, M. (2018). Iapetan Rift–Passive Margin Transition in NE Laurentia and Eustatic Control on Continental Slope Oxygenation, Taconic Slate Colors, and Early Paleozoic Climate. *Guidebook the Field Trips in New York, Vermont, and Massachusetts.*

Landing, E., Westrop, S.R., & Adrain, J.M. (2011). The Lawsonian Stage – the *Eoconodontus notchpeakensis* (Miller, 1969) FAD and HERB carbon isotope excursion define a globally correlatable terminal Cambrian stage. *Bulletin of Geosciences, 86,* 621–640.

Latimer, J.C., & Filippelli, G.M. (2002). Eocene to Miocene terrigenous inputs and export production: geochemical evidence from ODP Leg 177, Site 1090. *Palaeogeography, Palaeoclimatology, Palaeoecology, 182,* 151–164.

Landing, W.M., & Bruland, K.W. (1987). The contrasting biogeochemistry of iron and manganese in the Pacific Ocean. *Geochimica et Cosmochimica Acta, 51*(1), 29–43.

Li, D., Zhang, X., Chen, K., Zhang, G., Chen, X., Huang, W., Peng, S., & Shen, Y. (2017). High-resolution C-isotope chemostratigraphy of the uppermost Cambrian stage

(Stage 10) in South China: implications for defining the base of Stage 10 and palaeoenvironmental change. *Geological Magazine, 1,* 1–12.

Ling, H.F., Chen, X., Li, D., Wang, D., Shields-Zhou, G.A., & Zhu, M.Y. (2011). Cerium anomaly variations in Ediacaran–earliest Cambrian carbonates from the Yangtze Gorges area, South China: implications for oxygenation of coeval shallow seawater. *Precambrian Research, 225,* 110–127.

Lorens, R.B. (1981). Sr, Cd, Mn and Co distribution coefficients in calcite as a function of calcite precipitation rate. *Geochimica et Cosmochimica Acta, 45,* 553–561.

Ludvigsen, R. (1982). Upper Cambrian and Lower Ordovician trilobite biostratigraphy of the Rabbitkettle Formation, western District of Mackenzie. *Royal Ontario Museum, Life Sciences Division, pp.* 188.

Machel, H.G., & Burton, E.A. (1991). Factors governing cathodoluminescence in calcite and dolomite, and their implications for studies of carbonate diagenesis. Luminescence Microscopy and Spectroscopy, Qualitative and Quantitative Applications. *SEPM Short Course, 25,* 37–57.

Macko, S.A., Engel, M.H., & Parker, P.L. (1993). Early diagenesis of organic matter in sediments: assessment of mechanisms and preservation by the use of isotopic molecular approaches. *Organic Geochemistry, pp.* 211–224.

McLennan, S.B. (1989). Rare earth elements in sedimentary rocks. Influence of provenance and sedimentary processes. *Mineralogical Society of America, Washington, pp,* 169-200.

McLennan, S.M. (2001). Relationships between the trace element composition of sedimentary rocks and upper continental crust. *Geochemistry, Geophysics, Geosystems 2(4).*

Meyers, P.A. (1994). Preservation of elemental and isotopic source identification of sedimentary organic matter. *Chemical Geology, 144,* 289–302.

Meyers, P.A., & Lallier-Vergès, E. (1999). Lacustrine sedimentary organic matter records of Late Quaternary paleoclimates. *Journal of Paleolimnology, 21,* 345–372.

Miller, J.F., Evans, K.R., Freeman, R.L., Ripperdan, R.L., & Taylor, J.F. (2011). Proposed stratotype for the base of the Lawsonian Stage (Cambrian Stage 10) at the first appearance datum of *Econodontus notchpeakensis* (Miller) in the house Range, Utah, USA. *Bulletin of Geosciences, 86,* 595–620.

Miller, J.F., Repetski, J.E., Nicoll, R.S., Nowlan, G., & Ethington, R.L. (2014). The conodont *Iapetognathus* and its value for defining the base of the Ordovician System. *Geologiska Foreningens i Stockholm Forhandlingar, 136,* 185–188.

Morel, F.M.M., Milligan, A.J., & Saito, M.A. (2004). Marine bioinorganic chemistry: the role of trace metals in the oceanic cycles of major nutrients. *The Oceans and Marine Geochemistry, Treatise on Geochemistry, 6,* 113–143.

Morrison, J.O., & Brand, U. (1986). Geochemistry of recent marine invertebrates. *Geoscience Canada, 13,* 237–253.

Murphy, A.E., Sageman, B.B., Hollander, D.J., Lyons, D.J., & Brett, C.E. (2000). Black shale deposition and faunal overturn in the Devonian Appalachian basin: clastic starvation, seasonal water-column mixing, and efficient biolimiting nutrient recycling. *Paleoceanography, 15,* 280–291.

Nakada, R., Takahashi, Y., & Tanimizu, M. (2013). Isotopic and speciation study on cerium during its solid–water distribution with implication for Ce stable isotope as a paleo-redox proxy. *Geochimica et Cosmochimica Acta, 103,* 49–62.

Pattan, J.N., Mir, I.A., Parthiban, G., Karapurkar, S.G., Matta, V.M., Naidu, P.D., & Naqvi, S.W.A. (2013). Coupling between suboxic condition in sediments of the western Bay of Bengal and southwest monsoon intensification: a geochemical study. *Chemistry Geology, 343,* 55–66.

Piper, D.Z., & Calvert, S.E. (2009). A marine biogeochemical perspective on black shale deposition. *Earth Science Reviews, 95,* 63–96.

Popp, B.N., Parekh, P., Tilbrook, B., Bidigare, R.R., & Laws, E.A. (1997). Organic carbon $\delta^{13}C$ variations in sedimentary rocks as chemostratigraphic and paleoenvironmental tools. *Palaeogeography, Palaeoclimatology, Palaeoecology, 132,* 119–132.

Quan, T.M. van de Schootbrugge, B., Field, M.P., Rosenthal, Y., & Falkowski, P.G. (2008). Nitrogen isotope and trace metal analyses from the Mingolsheim core (Germany): evidence for redox variations across the Triassic–Jurassic boundary. *Global Biogeochemistry Cycles, 22.*

Quan, T.M., Wright, J.D., & Falkowski, P.G. (2013). Co-variation of nitrogen isotopes and redo states through glacial–interglacial cycles in the Black Sea. *Geochimica et Cosmochimica Acta, 112,* 305–320.

Rao, C.P., & Adabi, M.H. (1992). Carbonate minerals, major and minor elements and oxygen and carbon isotopes and their variation with water depth in cool, temperate carbonates, western Tasmania, Australia. *Marine Geology, 103,* 249–272.

Ren, H., Sigman, D.M., Martínez-Garcíac, A., Anderson, R.F., Chen, M., Ravelo, A.C., Straub, M., Wong, G.T.F., & Haug, G.H. (2017). Impact of glacial/interglacial sea level change on the ocean nitrogen cycle. *The National Academy of Sciences of the United States of America, 114*(33), 6759–6766.

Richter, D.K., & Füchtbauer, H. (1978). Ferroan calcite replacement indicates former magnesian calcite skeletons. *Sedimentology, 25,* 843–860.

Ripperdan, R.L., Magaritz, M., & Kirschvink, J. L. (1993). Carbon isotope and magnetic polarity evidence for non-depositional events within the Cambrian–Ordovician boundary section at Dayangcha. Jilin Province, China. *Geological Magazine, 130,* 443–52.

Rue, E.L., Smith, G.J., & Cutter, G.A. (1997). The response of trace element redox couples to suboxic conditions in the water column. *Deep-sea Research I, 44,* 113–434.

Rush, P.F., & Chafetz, H.S. (1990). Fabric retentive, non-luminescent brachiopods as indicators of original $\delta^{13}C$ and $\delta^{18}O$ compositions: a test. *Journal of Sedimentary Research, 60,* 968–981.

Saino, T., & Hattori, A. (1980). $^{15}N$ natural abundance in oceanic suspended particulate matter. *Nature, 283,* 752–754.

Schuchert, C., & Dunbar, C.O. (1934). Stratigraphy of western Newfoundland. Geological society of America., Washington, D.C.

Sigman, D.M., Karsh, K.L., & Casciotti, K.L. (2009). Ocean process tracers: Nitrogen isotopes in the ocean. Encyclopedia of ocean science. *Elsevier, Amsterdam, pp.* 4138–4153.

Śliwiński, M.G., Whalen, M.T., & Day, J. (2010). Trace element variations in the Middle Frasnian punctata zone (Late Devonian) in the western Canada sedimentary Basin-changes in oceanic bioproductivity and paleoredox spurred by a pulse of ter

restrial afforestation? *Geologica Belgica, 4,* 459–482.

Stiehl, G., & Lehmann, M. (1980). Isotopenvariationen des Stickstoffs humoser und bituminÖser natürlicher organischer Substanzen. *Geochmica et cosmochimica Acta, 44,* 1737–1746.

Sunagawam, U., Takahashi, Y., & Imai, H. (2007). Strontium and aragonite-calcite precipitation. *Journal of Mineralogical and Petrological Sciences, 102,* 174─181.

Talbot, M.R., & Laerdal, T. (2000). The lake Pleistocene–Holocene paleolimnology of Lake Victoria East Africa based upon elemental and isotopic analyses of sedimentary organic matter. *Journal of Paleolimnology, 23,* 141–164.

Terfelt, F., Bagnoli, G., & Stouge, S. (2012). Re-evaluation of the conodont *Iapetognathus* and implications for the base of the Ordovician System GSSP. *Lethaia, 45,* 227–237.

Terfelt, F., Eriksson, M.E., & Schmitz, B. (2014). The Cambrian–Ordovician transition in dysoxic facies in Baltica—diverse faunas and carbon isotope anomalies. *Palaeogeography, Palaeoclimatology, Palaeoecology, 394,* 59–73.

Theissen, K.M., Dunbar, R.B., & Cooper, A.K. (2003). Stable isotopic measurements of sedimentary organic matter and N. Pachyderma (S.) from Site 1166, Prydz Bay continental shelf. *Proceedings of the Ocean Drilling Program, Scientific Results, 188,* 1–11.

Towe, K.M. (1991). Aerobic carbon cycling and cerium oxidation: Significance for Archean oxygen levels and banded iron-formation deposition. *Palaeogeography, Palaeoclimatology, Palaeoecology, 97,* 113–123.

Tribovillard, N., Algeo, T.J., Lyons, T., & Riboulleau, A. (2006). Trace metals as paleoredox and paleoproductivity proxies: an update. *Chemical Geology, 232,* 12–32.

Tripathy, G.R., Singh, S.K., & Ramaswamy, V. (2014). Major and trace element geochemistry of Bay of Bengal sediments: Implications to provenances and their controlling factors. *Palaeogeography, Palaeoclimatology, Palaeoecology, 397,* 20–30.

Veizer, J. (1974). Chemical diagenesis of belemnite shells and possible consequences for paleotemperature determinations: Neues Jahrb. *Geology and Palaontology Abh, 145,* 279–305.

Veizer, J. (1983). Chemical diagenesis of carbonates. Society of Economic Paleontologists and Mineralogists (SEPM), Stable Isotope in Sedimentary geology (SC10). *Short Course Notes, 10,* III–1–III–100.

Veizer, J., Ala, D., Azmy, K., Bruckschen, P., Bruhn, F., Buhl, D., Carden, G., Diener, A., Ebneth, S., Goddris, Y., Jasper, T., Korte, C., Pawellek, F., Podlaha, O., & Strauss, H. (1999). $^{87}Sr/^{86}Sr$, $\delta^{18}O$ and $\delta^{13}C$ evolution of Phanerozoic seawater. *Chemical Geology, 161,* 59–88.

Weaver, F.J., & Macko, S.A. (1988). Source rocks of western Newfoundland. *Organic Geochemistry, 13,* 411–421.

Webb, G.E., & Kamber, B.S. (2000). Rare Earth elements in Holocene reefal microbialites: a new shallow seawater proxy. *Geochimicu et Cosmochimica Acta, 64,* 1557–1565.

Webb, G.E., Nothdurft, L.D., Kamber, B.S., Kloprogge, J.T., & Zhao, J.X. (2009). Rare earth element geochemistry of scleractinian coral skeleton during meteoric diagenesis: a sequence through neomorphism of aragonite to calcite. *Sedimentology, 56,* 1433–1463.

Wignall, P.B., & Twitchett, R.J. (1996). Oceanic anoxia and the end Permian mass extinction. *Science, 272,* 1155–1158.

Wignall, P.B., Zonneveld, J.P., Newton, R.J., Amor, K., Sephton, M.A., & Hartley, S. (2007). The end Triassic mass extinction record of Williston Lake, British Columbia. *Palaeogeography, Palaeoclimatology, Palaeoecology, 253,* 385–406.

Wilson, J.L., Medlock, P.L., Fritz, R.D., Canter, K.L., & Geesaman, R.G. (1992). A review of Cambro-Ordovician breccias in North America. Paleokarst, Karst-Related Diagenesis and Reservoir Development. *Permian Basin Section, Society of Economic Paleontologists and Mineralogists (SEPM), 92(33),* 19–29.

Yamaguchi, K.E., Ogurim, K., Ogawa, N.O., Sakai, S., Hirano, S., Kitazato, H., & Ohkouchi, N. (2010). Geochemistry of modern carbonaceous sediments overlain by a water mass showing photic zone anoxia in the saline meromictic Lake Kai-ike, southwest Japan: I. Early diagenesis of organic carbon, nitrogen, and phosphorus. *Palaeogeography, Palaeoclimatology, Palaeoecology, 294,* 72–82.

Zhao, M.Y., & Zheng, Y.F. (2014). Marine carbonate records of terrigenous input into Paleotethyan seawater: Geochemical constraints from Carboniferous limestones. *Geochimica et Cosmochimica Acta, 141*, 508–531.